



Originally published as:

Torsvik, T. H., Van der Voo, R., Preeden, U., Mac Niocaill, C., Steinberger, B., Doubrovine, P. V., van Hinsbergen, D. J. J., Domeier, M., Gaina, C., Tovher, E., Meert, J. G., McCausland, P. J., Cocks, L. R. M. (2012): Phanerozoic polar wander, paleogeography and dynamics. - Earth-Science Reviews, 114, 3-4, 325-368

DOI: [10.1016/j.earscirev.2012.06.007](https://doi.org/10.1016/j.earscirev.2012.06.007)

1

2

Phanerozoic Polar Wander, Palaeogeography and Dynamics

3

4 Trond H. Torsvik ^{a,b,c,d*}, Rob Van der Voo ^{e,a}, Ulla Preeden ^f, Conall Mac Niocaill ^g, Bernhard
5 Steinberger ^{h,a,b}, Pavel V. Doubrovine ^{a,b}, Douwe J.J. van Hinsbergen ^{a,b}, Mathew Domeier ^e,
6 Carmen Gaina ^{a,b}, Eric Tohver ⁱ, Joseph G. Meert ^j, Phil J. A. McCausland ^k, L. Robin M. Cocks ^l

7

8

9 ^aCenter for Advanced Study, Norwegian Academy of Science and Letters, Drammensveien 78, 0271 Oslo, Norway

10 ^bCenter for Physics of Geological Processes (PGP), University of Oslo, Sem Sælands vei 24, NO-0316 Oslo, Norway
t.h.torsvik@geo.uio.no; d.v.hinsbergen@fys.uio.no; paveld@fys.uio.no; carmen.gaina@geo.uio.no

11 ^cGeodynamics, Geological Survey of Norway, Leiv Eirikssons vei 39, 7491 Trondheim, Norway

12 ^dSchool of Geosciences, University of the Witwatersrand, WITS 2050 Johannesburg, South Africa

13 ^eDepartment of Earth and Environmental Sciences, University of Michigan, Ann Arbor, MI 48109-1005, USA
voo@umich.edu; domeier@umich.edu

14 ^fDepartment of Geology, University of Tartu, Ravila 14A, 50411 Tartu, Estonia; ulla.preeden@ut.ee

15 ^gDepartment of Earth Sciences, South Parks Road, Oxford OX1 3AN, UK; conallm@earth.ox.ac.uk

16 ^hHelmholtz Centre Potsdam, GFZ German Research Centre for Geosciences, Section 2.5, Geodynamic Modelling,
17 Helmholtzstrasse 6, H6 117, 14467 Potsdam, Germany; bstein@gfz-potsdam.de

18 ⁱSchool of Earth and Environment, University of Western Australia, 35 Stirling Highway, Crawley, WA 6009,
19 Australia; etohver@cyclene.uwa.edu.au

20 ^jDepartment of Geological Sciences, 355 Williamson Hall, University of Florida, Gainesville FL 32611, USA;
21 jmeert@ufl.edu

22 ^kDepartment of Earth Sciences, University of Western Ontario, London, ON, N6A 5B7, Canada;
23 pmccausl@uwo.ca

24 ^lDepartment of Palaeontology, The Natural History Museum, London SW7 5BD, U.K.; r.rocks@nhm.ac.uk

32 **Keywords:**

33 Phanerozoic

34 Palaeomagnetism

35 Apparent Polar Wander

36 Palaeogeography

37 True Polar Wander

42

43 ABSTRACT

44 A significant number of new palaeomagnetic poles have become available since the last time
45 a compilation was made (assembled in 2005, published in 2008) to indicate to us that a new
46 and significantly expanded set of tables with palaeomagnetic results would be valuable, with
47 results coming from the Gondwana cratonic elements, Laurentia, Baltica/Europe, and Siberia.
48 Following the Silurian Caledonian Orogeny, Laurentia's and Baltica's apparent polar wander
49 paths (APWPs) can be merged into a Laurussia path, followed in turn by a merger of the
50 Laurussia and Siberia data from latest Permian time onward into a Laurasian combined path.
51 Meanwhile, after about 320 Ma, Gondwana's and Laurussia/Laurasia's path can be combined
52 into what comes steadily closer to the ideal of a Global Apparent Polar Wander Path
53 (GAPWaP) for late Palaeozoic and younger times. Tests for True Polar Wander (TPW)
54 episodes are now feasible since Pangaea fusion and we identify four important episodes of
55 Mesozoic TPW between 250 and 100 Ma. TPW rates are in the order of 0.45-0.8°/M.y. but
56 cumulative TPW is nearly zero since the Late Carboniferous. With the exception of a few
57 intervals where data are truly scarce (e.g., 390–340 Ma), the palaeomagnetic database is
58 robust and allows us to make a series of new palaeogeographic reconstructions from the Late
59 Cambrian to the Palaeogene.

60

61

62

63 * Corresponding author at: PGP, University of Oslo, PO Box 1048, N-0316 Oslo, Norway

64 t.h.torsvik@geo.uio.no

65 1. Introduction

66 Since the advent of the understanding of plate tectonics, Earth scientists have wanted to know
67 where the continents lay in past ages, partly from curiosity, but partly so as to understand
68 biodiversity, climate change and where best to search for natural resources. The chief tool in
69 deciphering palaeogeography has been and remains palaeomagnetism, the study of the Earth's
70 magnetic field preserved in rocks. The Earth's ancient magnetic field has provided one of the
71 most fundamental markers used to document the motion of the continents and evolution of the
72 Earth. Changes in ancient magnetic polarity at irregular intervals are recorded in the surface
73 rock record, and over some fifty years, palaeomagnetic data have been used to create the
74 geomagnetic time scale, to firmly document seafloor spreading, to validate plate tectonics,
75 and to reconstruct vanished supercontinents.

76 Palaeomagnetic results can conveniently be expressed in terms of palaeopoles that are
77 calculated using the geocentric axial dipole field model. In turn, those palaeopoles can be
78 used to construct Apparent Polar Wander Paths (APWPs). This way, instead of plotting the
79 motion of a continent while holding the rotation axis fixed, the motion of the polar axis
80 relative to the continent is visualized (Fig. 1). The motion of continents relative to the Earth's
81 spin axis may be either due to the drift of individual continents or due to a rotation of the
82 entire Earth relative to its spin axis — the latter is called true polar wander (TPW). Creer,
83 Irving and Runcorn were the first to publish an APWP for 'Europe' as early as 1954, based on
84 late Precambrian to Eocene palaeomagnetic poles from Britain. Those poles all differed
85 markedly from the present-day pole and were interpreted at first as due to a slow change in
86 the axis of rotation of the Earth with respect to its surface, i.e. TPW. Two years later,
87 however, Runcorn (1956) published an APWP for North America and this allowed him to
88 compare the European and North American paths. He noted that they were broadly similar in
89 shape, but some 30° apart in longitude, which he interpreted as caused by the opening of the
90 modern Atlantic. This was the first independent geophysical evidence for 'continental drift'
91 (*sensu* Wegener, 1912).

92 If the relative positions of a number of continents are reasonably well known, all being
93 defined in the same plate circuit, then palaeomagnetic data from these continents can be
94 combined into a Global APWP (GAPWaP). Widely used GAPWaP's have been published by
95 Besse and Courtillot (2002) covering the last 200 M.y. and by Torsvik et al. (2008a) starting
96 at 320 Ma when the supercontinent Pangaea began to be assembled. Conventional
97 palaeomagnetic reconstructions constrain ancient latitudes and orientations (rotations) of

98 continents, but not their palaeolongitudes. This allows a degree of freedom in making
99 palaeogeographic models unless additional information is available that constrains
100 palaeolongitude. Such information can sometimes be provided by choosing a reference plate
101 that has remained stationary (or quasi-stationary) with respect to longitude. In other words, if
102 there is a reason to suppose that a specific continent has moved little in an east-west sense
103 since the time represented by the reconstruction, that continent can be used as the reference
104 plate. Other continents, partnering in the same plate circuit, will then be seen to occupy their
105 own palaeo-longitudinal positions relative to the deep mantle. Because Africa meets the
106 criteria required of a reference plate, at least since Pangaea breakup (Burke and Torsvik,
107 2004, Torsvik et al., 2008a, b), we can tie all other continental motions to a ‘fixed’ African
108 plate. This is important for estimating TPW (Section 7) and to develop semi-absolute
109 reference frames from palaeomagnetic data.

110 Building on the GAPWaP of Torsvik et al. (2008a) we present two different GAPWaP's for
111 the past 320 million years (M.y.): (1) One without TPW correction to be used in classical
112 palaeo-geographic/-climatic reconstructions and as reference frame for new palaeomagnetic
113 data, where the true relation to the spin-axis is imperative, and (2) one with TPW correction
114 that leads to a smoother plate model that only describes ‘continental drift’, and that *must* be
115 used, for example, to calculate net lithosphere rotation (Section 7) or to compare surface
116 processes with heterogeneities in the deepest mantle (Torsvik et al., 2010a).

117 In addition to the construction of a new and more robust GAPWaP, back to the time when
118 Pangaea assembled, we also construct new Palaeozoic APWPs for Gondwana, Laurentia,
119 Baltica and Siberia back to the dawn of the Phanerozoic. After the Silurian Caledonian
120 Orogeny we can combine palaeomagnetic data from Laurentia and Baltica to produce a joint
121 APWP for Laurussia.

122 Asian blocks such as North and South China, the Tibetan blocks, Tarim, Annamia
123 (Indochina), Kolyma-Omolon, Kazakhstan elements, Sunda blocks, and Tethyan
124 (Cimmerian) terranes are not represented and are left white in Fig. 2, because tectonic
125 activity, such as local rotation and intense deformation, introduces too much noise in the
126 construction of their APWPs.

127 Palaeomagnetic data (Figs. 2-3; Table 1) were compiled and graded according to Van der
128 Voo’s classification system (Van der Voo, 1990, 1993), and rotated with a given continent to
129 its reconstructed position; rotation parameters (e.g., Table 2) for most of the relative fits

130 follow Torsvik et al. (2008a) unless noted in the text. Only palaeomagnetic data with a
131 quality factor $Q \geq 3$ (Van der Voo, 1990) are used, but paleomagnetic poles that knowingly
132 fail the assumption that the magnetization age equals the actual rock age are not included in
133 our analysis. Our procedures to generate APWPs (either running mean or spherical spline
134 paths; Jupp and Kent, 1987) are detailed in Torsvik et al. (1992, 1996, 2008a). Running mean
135 paths are non-weighted whereas input poles in all spherical spline paths were weighted by
136 Van der Voo's (1990) quality factor Q (Table 1). Instead of weighting the data by 95%
137 confidence ovals (α_{95} , "criterion 2" in Van der Voo's classification system) we weighted the
138 data by $7/Q$. This causes the smooth path to pass close to the data which score "7" (full-
139 marks).

140

141 Van der Voo and Torsvik (2004) analysed the APWP of Baltica/Stable Europe for Permian
142 times, paying particular attention to aspects that could introduce a systematic bias. They
143 identified three problems: (1) palaeopoles from some (but not all) detrital sedimentary rocks
144 exhibited a paleolatitudinal offset when compared to latitudes calculated from coeval igneous
145 rocks (e.g., Estérel results, Zijderveld, 1975), (2) palaeopoles based on outmoded
146 demagnetization methodologies revealed a minor bias with respect to results obtained by
147 principal component analysis (e.g., Kirschvink 1980; Kent et al., 1983), and (3) palaeopoles
148 associated with dubious or no radiometric age dating revealed a bias of some 10° on average
149 with respect to results based on $^{40}\text{Ar}/^{39}\text{Ar}$ or U/Pb methods. Importantly, observation (3)
150 produced the most substantial bias. It is not (yet) feasible to remedy the bias of items (2) and
151 (3) by omission of potentially flawed data, because too many gaps would occur in the
152 temporal sequences of the APWPs. We can (and do here) remedy the situation of bias (1) by
153 correcting for (inferred) inclination errors in all results obtained from detrital sedimentary
154 rocks. Similar efforts have begun to be applied in other studies (e.g., Tauxe and Kent, 2004;
155 Kent and Tauxe, 2005; Yan et al., 2005; Kodama, 2009; Bilardello and Kodama, 2010a; Kent
156 and Irving, 2010; Domeier et al., 2011a), and are likely to become standard in the very near
157 future.

158 Inclination (I) error in sediments is latitude dependent and antisymmetric. This bias closely
159 mimics errors produced by octupole fields of the same sign as the dipole field (Rochette and
160 Vandamme, 2001; Torsvik and Van der Voo, 2002; Tauxe, 2005, Domeier et al., 2012). The
161 degree of inclination shallowing depends on rock type and remanence acquisition/shallowing
162 mode. Inclination shallowing is commonly predicted from:

163 $\tan(\text{INC}_{\text{Observed}}) = f \tan(\text{INC}_{\text{Field}})$,

164 where INC is the inclination and f is the degree of inclination error (King 1955) — *In this*
165 *paper all detrital sedimentary poles have been corrected for inclination shallowing using a*
166 *commonly observed f value of 0.6, unless inclination shallowing was corrected for by the*
167 *original authors using the Tauxe and Kent (2004) E/I method or the magnetic fabric method*
168 *of Kodama (2009)* — this is a little more conservative than f values derived from laboratory
169 experiments (0.4-0.55; King, 1955, Løvlie and Torsvik, 1984; Tauxe and Kent, 1984).
170 Correcting detrital sediments with a f value of 0.6 amounts to a maximum latitude correction
171 of 14.5° (1600 km) at around 50° N/S. This is comparable to the effects of octupole
172 contributions as high as 22%. All detrital sedimentary sequences used in the spline fits in our
173 paper are corrected for inclination shallowing.

174 In total, our Phanerozoic palaeomagnetic data compilation includes 626 poles (Table 1). For
175 analysis and visualization we primarily used the GMAP software (Torsvik and Smethurst,
176 1999) in addition to GMT (Wessel and Smith, 1991). A new and improved version of GMAP
177 will be made available in 2012 (work in progress) along with all our palaeomagnetic data in
178 digital GMAP and GPlates (www.gplates.org; Boyden et al., 2011) format.

179

180 2. From Laurentia to Laurussia and Laurasia: Overview

181 The Palaeozoic continent Laurentia is represented largely by cratonic North America, but also
182 includes Greenland, Ellesmere and parts of present-day Europe (e.g., Scotland, NW Ireland
183 and Svalbard). It was drifting independently until collision with Baltica and Avalonia
184 produced the Caledonian Orogeny at 430-420 Ma (Figs. 4-3). Laurentia then became the
185 western portion of Laurussia, which in turn became part of the Pangaea Supercontinent during
186 the Late Carboniferous (Cocks and Torsvik, 2011). By Late Permian times, Siberia had
187 essentially joined Baltica, and along with other European and Asian elements, the combined
188 continent is referred to as Laurasia.

189

190 2.1 Laurentia (North America and Greenland)

191 Due to a steadily growing palaeomagnetic database, many updated APWPs have been
192 published in the past 50 years for North America (e.g., Irving, 1964, 1979; Runcorn, 1965;
193 Hoppers and Van Andel, 1970; McElhinny, 1973; Van der Voo and French, 1974; Van der
194 Voo, 1981, 1990; Irving and Irving, 1982; Mac Niocaill and Smethurst, 1994). Compared to

earlier compilations for the Palaeozoic by Torsvik et al. (1996) and for late Palaeozoic (<320 M.y.) and younger times (Torsvik et al., 2008a), we have included 64 additional poles in the present compilation. Most are based on new studies but some are ‘old’ sedimentary poles corrected for I-error using the inclination-elongation method of Tauxe and Kent (2004) or the anisotropy of magnetic susceptibility information (Kodama, 2009).

Our pole collection from the Phanerozoic of Laurentia (North America and Greenland) includes 195 poles ranging in age from 0.5 to 532 Ma (Table 1). Poles from Greenland have been rotated to account for seafloor spreading in the Labrador Sea/Baffin Bay (67→33 Ma) as well as pre-drift extension back to Cretaceous (Barremian) times (Table 2). Most poles from North America are from the cratonic core (Figs. 2, 5) except for a few poles derived from young rocks that accreted to North America during the Mesozoic/Cenozoic (Table 1).

A moderately smoothed spherical spline path in 10 M.y. intervals, with results from detrital sedimentary rocks corrected for I-error along with their associated 95% confidence ovals (based on α_{95}) or A95 (rare; see Table 1) for the input poles is shown in Fig. 6a (Table 3). We also show a running mean path (Fig. 6b) with or without correction for I-error (thick blue line with A95 ovals, or thin red line in Fig. 6b, respectively). The different APW paths show gross similarities: keeping North America fixed, and using the present-day distribution of continents as a descriptive reference, the South Pole was located in NW Africa in the Cambrian, it had moved to South America (Brazil-Ecuador) by the Early Devonian, followed by southward movement and arrival to the east of Patagonia (southernmost South America) by Permian and early Mesozoic times. The South Pole has stayed close to Antarctica since the Late Triassic, but with a pronounced easterly trend during the Jurassic (~200-140 Ma), followed by the well-known Cretaceous still-stand (120-60 Ma, marked by yellow oval). The Jurassic trend is dominated by a TPW signal (Steinberger and Torsvik, 2008 and Section 7).

Data-coverage is notably poor for Laurentia between 340 and 400 Ma, implying that the running mean poles for 350-360 Ma and 380-390 Ma (red dots in Fig. 6b) are all interpolated; this is the so-called Siluro-Devonian cusp that has previously been interpreted as TPW (Van der Voo, 1994). The paucity of data in this section of the APWP results in markedly different ‘fits’ between the spline-fitted and running mean methods. The effect of correcting detrital sedimentary rock results for I-error can also be seen in Fig. 6b: On average the great-circle difference (GCD) between a pair of coeval poles from each of the two paths is small ($2.8 \pm 2.9^\circ$; mean and standard deviation), but the Late Jurassic-Early Cretaceous (140-160 Ma) and

227 Late Devonian (360-370 Ma) APWP segments show larger and more systematic differences
228 of as much as 8-11°. Although the GCD is always greater than or equal to zero, and hence its
229 distribution is not truly Gaussian, we nevertheless use the normal definition of standard
230 deviation as a simple means of describing the variance.

231 Statistically (in this case) there is no significant change in A95's but the inclination-corrected
232 path is considerably smoother than the non-corrected one. More importantly, the
233 systematically higher corrected-pole latitudes during the Jurassic become important when
234 comparing the Laurentia APWP with Europe/Baltica and Gondwana (Sections 2.3, 3). The
235 spline and running mean paths (both I-error corrected) differ on average by $1.9 \pm 1.4^\circ$ with a
236 peak difference of 6.2° during the Middle Cambrian ([Table 3](#)).

237 *2.2 Baltica and Stable or Extra-Alpine Europe*

238 Numerous APW paths have been published for Baltica and its younger incarnations (e.g.,
239 Stable or Extra-Alpine Europe) over the past decades. Our present compilation includes 167
240 palaeomagnetic poles (0.5-535 Ma), 44 more than in our previous 2005 compilation (Torsvik
241 et al., 2008a), but nine of these poles are from stable Siberia and one Early Cretaceous pole is
242 from peri-Siberia (Mongolia). Siberia was quasi-stable in its position relative to
243 Baltica/Laurussia between Late Triassic and Early Jurassic times, but the estimated correction
244 is so small (a few degrees around an Euler pole of 77°N and 144.6°E; Buiter and Torsvik,
245 2007) that we include the few Siberian poles (mostly Siberian Traps, ~251 Ma poles) from the
246 Permo-Triassic boundary and onwards in our compilation. Cambrian and Ordovician poles
247 are exclusively from Baltica but for Silurian (~430 Ma) and younger times we progressively
248 include more and more poles from areas that can be characterized as having become part of
249 Stable Europe. The oldest of these 'Stable' Europe poles are from Scotland and were derived
250 from undeformed Silurian granites ('Newer' Granites) and Lower Devonian volcanics that
251 postdate Iapetus closure across the British Caledonide sector. Poles from these rocks also
252 compare well with similar-aged poles from the core of Baltica (Torsvik et al., 1996).

253 The Baltica/Europe APWP ([Fig. 7](#), 355° in GCD length) is considerably longer than the
254 Laurentian APWP (269°), owing to widely separated Cambrian and Ordovician palaeopoles
255 from Baltica/Europe (the cumulate APW is measured here from the respective spline paths).
256 With respect to a fixed Baltica/Europe, the mean South Poles for the Cambrian ([Fig. 7b](#)) are
257 located in Arctic Siberia, followed by a drift of the pole over Arabia and Central Africa in the
258 Ordovician to the Atlantic off the NE corner of Brazil in the Siluro-Devonian cusp. We recall

259 that this cusp was also seen in Laurentia's APWP. Subsequent southward movement brought
260 the South Pole near Patagonia in the Triassic, after which the pole remained close to
261 Antarctica in the Jurassic.

262 Spline and running mean APWPs are grossly similar ($3.5 \pm 3.5^\circ$) but differences can be as
263 much as $\sim 19^\circ$ in the Early Ordovician (Table 4), given the rapid and significant shift of the
264 mean poles between 510 and 430 Ma. Running mean paths, corrected as well as uncorrected
265 for I-error differ on average by $1.4 \pm 2.8^\circ$ but this reaches values between $7\text{--}14^\circ$ in Cambrian-
266 Early Ordovician times. As was the case for Laurentia, there are very few poles between 400
267 and 310 Ma and the Mid-Devonian to Late Carboniferous APW segment is thus largely
268 interpolated.

269 *2.3 Laurussia/Laurasia*

270 Laurentia (including Scotland and Greenland) collided with Baltica and Avalonia at ~ 430 Ma
271 (Figs. 4-3) and from then on we can combine Laurentia and Baltica/Stable Europe poles into
272 one APWP with the correction for younger pre-drift extension and the opening of the North
273 Atlantic Ocean in early Palaeogene time. Avalonia's results from Lower and Middle
274 Palaeozoic rocks, possibly having suffered local or regional rotations (Torsvik et al., 1993),
275 are not included in our current analysis. From 251 Ma onwards we also include poles from
276 Siberia as part of the larger Laurasian continent.

277 A fit published by Bullard et al. (1965) is typically preferred for rotation of North American
278 poles into European coordinates (or vice versa); this fit (Euler pole latitude = 88.5°N ,
279 longitude = 27.7°E , angle = -38.0°) matches poles quite well, but leads to a rather loose fit
280 between the opposing continental edges in the NE Atlantic. Torsvik et al. (2001, 2008a) have
281 therefore proposed more geologically plausible (and tighter) fits that can account for the pre-
282 drift extension history along the opposing Norwegian and Greenland margins. In this paper
283 we use a tight mid-late Palaeozoic-early Mesozoic fit of Torsvik et al. (2006), elaborated in
284 Alvey (2009 and manuscript in preparation) and Domeier et al. (2012), and tested/confirmed
285 by estimates of lithosphere stretching based on gravity inversion and seismic refraction data
286 (Alvey, 2009). This 'tighter' fit (seen in Fig. 5) is broadly similar to that used by Torsvik et
287 al. (2008a), which was based on a 2005 plate-circuit compilation. Reconstruction parameters
288 for Europe vs. North America and Greenland are listed in 5 Myr intervals in Table 2. The
289 Cenozoic spreading history for both the NE Atlantic and the Labrador Sea follows that of
290 Gaina et al. (2002) and Gaina's unpublished data (listed in Torsvik et al., 2008a).

After adjusting for seafloor spreading and pre-drift extension in the North Atlantic realm, the APWPs for Laurentia and Baltica/Europe resemble each other quite well, except for (1) the Late Carboniferous-Early Permian (note discordant 310-290 mean poles in [Fig. 8a](#)) and (2) the Jurassic-Early Cretaceous. In the latter case, Laurentian poles systematically plot at lower latitudes, a problem noted in numerous papers (e.g., Van der Voo, 1992; Courtillot et al. 1994). We note that correcting clastics for I-error leads to smoother APWPs and better agreement between pairs of coeval poles from each of the two paths (GCD reduced from $8.2 \pm 5.0^\circ$ to $7.0 \pm 3.8^\circ$ after correction; [Fig. 8c](#)).

336 poles are included in our Laurussia (from 430 Ma) and Laurasia (from 251 Ma) APWP ([Table 5](#)) and are represented both in a spherical spline path ([Fig. 9a](#)) and in running mean path segments ([Fig. 9](#)). The running mean path is based on an average of 17 poles for each mean pole with A95 averaging to $4.7 \pm 2.8^\circ$ (corrected for I-error) and $4.9 \pm 3.0^\circ$ (uncorrected). The average difference between coeval points on the uncorrected and corrected running mean paths is $2.1 \pm 2.4^\circ$. A95 errors are slightly reduced when correcting for I-error and the path becomes notably smoother.

The difference between coeval poles from the spline and running mean paths is $2.0 \pm 1.7^\circ$ with peak values of $6-7^\circ$ in the Late Devonian (370 Ma) and Silurian (410, 430 Ma) segments. The 390 to 340 Ma segment; however, is based on a single pole from the Catskill Formation (370 Ma) and renders this segment less reliable and dominated by interpolation (see red dots in [Fig. 9b](#) and [Table 5](#)). Middle Devonian to Early Carboniferous palaeomagnetic poles are urgently needed for Laurussia. The combined running mean and spline paths are broadly similar ([Fig. 9](#)).

3. Gondwana: Overview

Published APWPs for the combined Gondwana continents (e.g., Morel and Irving, 1978; Hurley and Van der Voo, 1987; Bachtadse and Briden, 1990; Schmidt and Embleton, 1990; Chen et al., 1994) differ widely and depend critically on data selection/rejection criteria employed by the authors resulting in a large variety of shapes/loops (e.g., portrayed in Van der Voo, 1993, *fig. 5.15*; see also Kent and Van der Voo, 1990). Our syn- to post-Pangaea data selection (<320 Ma) follows Torsvik et al. (2008a), whilst pre-Pangaea data are updated from the compilation of Torsvik and Van der Voo (2002). Gondwana ([Fig. 10](#)) was mostly assembled at around 550 Ma (Meert and Van der Voo, 1997) although the fusion of some cratonic elements (Amazonia, West Africa) with the central Gondwanan elements may have

occurred during Mid to Late Cambrian times (Tohver et al., 2006, 2010, 2012; Trindade et al., 2006). Relative fits for Gondwana are listed in [Table 6](#) for the reconstructions with respect to Southern Africa of the following cratons: Western Australia, East Antarctica, the Indian subcontinent, Madagascar, South America (Amazonia, Parana, Colorado and Patagonia), NW and NE Africa, Somalia, and Arabia. Compared with the Torsvik et al. (2008a) plate circuit compilation, the relative fits within the Indian Ocean (e.g., for India; Cande et al., 2010) and internal fits for Africa (e.g., for Somalia; Horner-Johnson et al., 2007) and South America (e.g., Patagonia; Torsvik et al., 2009) have been updated. In our compilation we have not included results from transient peri-Gondwana elements ([Fig. 4](#)) such as Avalonia and the Armorian/Cadomian Terrane Assemblage (e.g., Spain, France), that rifted from Gondwana during the Early Ordovician (opening of the Rheic Ocean; [Fig. 10](#)) or the Early Devonian (opening of the Palaeotethys) respectively (Torsvik and Cocks, 2011).

335

Our selection ([Fig. 11](#)) from the former Gondwana continents contains 229 poles (including 49 ‘new’ poles and 59 sedimentary poles corrected for potential I-errors). Two poles are included from volcanic provinces in Kerguelen (27 Ma) and West Antarctica (5 Ma) ([Table 1](#)) that were part of East Antarctica at their time of eruption. For cratonic Australia we exclude all poles within the Tasman Fold-belt or east of the Tasman Line, following Torsvik and Van der Voo (2002). Here we also exclude three Cambrian poles from Pakistan (listed in Torsvik and Van der Voo, 2002) due to possible structural corrections owing to oroclinal bending in the Himalayas (Klootwijk, 1996). However, exclusion/inclusion of these poles produces only minor changes (<5°) in the Gondwana 540 and 530 Ma mean poles.

345

The new APWP for Gondwana ([Table 7](#)) shows gross similarities to that of Torsvik and Van der Voo (2002): Keeping Southern Africa fixed, the APW of the South Pole tracks from near Brazil’s coast in the latest Precambrian (550 Ma), thence to NW Africa during most of the Late Cambrian and Ordovician, followed by a rapid cusp during Silurian to Early Devonian times. During the Late Devonian, the South Pole was located in equatorial Africa and then migrated south-eastward during the Carboniferous. Since the Triassic (~230 Ma), the south-pole has remained close to East Antarctica ([Fig. 11](#)). Thus, this Palaeozoic APWP for Gondwana can be summarized by a simple SE-ward track from NW Africa to Antarctica (Path X of Morel and Irving, 1978), with superimposed a back-and-forth loop (path Y of Morel and Irving, 1978) between 430 and 380 Ma. The variety in Gondwana APWP shapes

356 published by different authors, and referred to above, is related to acceptance or rejection of
357 one or both of these superimposed loops.

358

359 The spline and the running mean path resulting from our selection of palaeopoles show gross
360 similarities except for the Early Devonian where a single pole causes the deviation. The
361 effect of correcting poles from detrital sediments for I-error is most notable in the
362 Carboniferous-Triassic section of the path ([Fig. 11b](#)), with implications for Pangaea fits (e.g.,
363 Rochette and Vandamme, 2001; Domeier et al., 2011b, 2012). The difference between the
364 spline ([Fig. 11a](#)) and running mean path ([Fig. 11b](#)) is $3.4 \pm 3.0^\circ$ with peak values of $11\text{--}14^\circ$ in
365 the Silurian and Early Devonian. The Silurian segments, however, are entirely interpolated
366 due to the scarcity of palaeomagnetic data for that interval.

367

368 **4. Siberia: Palaeozoic Update**

369 The Siberian palaeocontinent includes political Siberia and adjacent areas of Mongolia,
370 eastern Kazakhstan, and NW China (Cocks and Torsvik, 2007). Siberia was essentially an
371 independent continent during late Precambrian and Palaeozoic times and became part of
372 Pangaea during the early Mesozoic. Palaeozoic palaeomagnetic data were reviewed by Cocks
373 and Torsvik in 2007 but due to a newly published Silurian pole from Siberia (Shatsillo et al.,
374 2007) that supersedes two less reliable poles (435 and 439 Ma Lena River Sediments poles in
375 *Table 1a* of Cocks and Torsvik, 2007) we have here substantially modified the APWP for
376 Siberia for Silurian and Early Devonian times ([Fig. 12](#)). In essence, our revised APWP and
377 implied reconstructions place Siberia at lower and mostly tropical latitudes during Silurian
378 and Early Devonian times. There is only one reliable palaeomagnetic pole between Silurian
379 and Permo-Triassic times (360 Ma pole in [Fig. 12](#)) and thus the late Palaeozoic APWP is
380 essentially interpolated, albeit showing convergence with the Baltica/Stable Europe APWP in
381 Permian time (Bazhenov et al., 2008). Our revised Siberia APWP ([Table 8](#)) is a spline path
382 and is shown in South Siberian co-ordinates where Cambrian to Silurian palaeomagnetic
383 poles from the southern and northern parts of Siberia are fitted with an Euler pole of 60°N ,
384 120°E and a rotation angle of 13° (see Cocks and Torsvik, 2007).

385

386 **5. Global Polar Wander: Overview**

387 Gondwana and the intervening terranes collided with Laurussia during the Late Carboniferous
388 (~320 Ma), and from then on we combine all palaeomagnetic data into a Global Apparent

389 Polar Wander Path (GAPWaP). A Pangaea-A type fit is our preferred configuration
390 (Dominguez et al., 2011; Domeier et al., 2012) but other alternatives exist (e.g., Irving, 1977,
391 2004; Muttoni et al., 2003). Relative fits between Gondwana (NW Africa) and
392 Laurussia/Laurasia (North America) are given in [Table 9](#) and the closure fit follows that of
393 Labails et al. (2010), which slightly modifies the fit of Torsvik et al. (2008a).

394

395 [Fig. 13](#) shows a comparison of Laurussia/Laurasia and Gondwana running mean APWPs in a
396 Pangaea-A type fit. Poles from detrital sedimentary rocks are corrected for I-error and for the
397 bulk of the Phanerozoic, the two paths overlap at the 95% confidence interval. In particular,
398 we note the very good fit of Carboniferous to Triassic mean poles in the Pangaea-A type
399 configuration. On average the GCD between a pair of coeval poles from each of the two
400 paths is $5.0 \pm 3.3^\circ$ with the largest differences during Late Jurassic times ($\sim 16^\circ$). Correction
401 for I-error leads to a markedly improved correlation of the two APWPs ([Fig. 13a, inset
402 diagram](#)), most notably for the Permian section of the APWPs (see also Domeier et al., 2012).

403

404 Our new GAPWaP, combining *five hundred* Laurussia/Laurasia and Gondwana poles, is
405 shown in [Fig. 13b](#). This is a running mean path that is also compared with the same path
406 using uncorrected poles from detrital sediments (red line). We also compare our new running
407 mean GAPWaP with a moderately smoothed spline path ([Fig. 13c](#)). Owing to the now large
408 number of input poles (and no large age gaps), the running mean and spline paths are almost
409 identical ($GCD = 1.5 \pm 1.1^\circ$). We therefore use the running mean GAPWaP in our further
410 analysis because it can be easily reproduced by other workers. Conversely, when data-
411 coverage is poor we prefer to use spline-derived APWPs. Our new running mean GAPWaP is
412 also listed in North America, Europe, India, Australia and East Antarctica co-ordinates in
413 [Table 11](#).

414

415 In comparison to previously published GAPWaP's [Torsvik et al. (2008a) back to 320 Ma;
416 Besse and Courtillot (2002) back to 200 Ma] our new compilation differs on average from
417 those compilations by 3.9° (Torsvik et al., 2008a) and 2.6° (Besse and Courtillot, 2002). In
418 [Fig. 14](#) we compare our GAPWaP with a 230 to 50 Ma running mean path of Kent and Irving
419 (2010). The Kent and Irving (2010) path (hereafter K&I) is constructed from volcanic rocks,
420 and detrital sedimentary rocks, but the latter only when individual poles were corrected for I-
421 errors using the E/I method of Tauxe and Kent (2004). The Triassic section (230-200 Ma) of
422 the K&I GAPWaP compares well with our GAPWaP but the Jurassic 'spike' ([Fig. 14a](#); note

423 190-140 Ma poles) seen in the K&I path differs strongly from our and all other published
424 paths (e.g. Besse and Courtillot, 2002). The K&I GAPWaP differs on average $4.1 \pm 2.6^\circ$
425 from ours with a peak deviation of 10.4° at 160 Ma. In Fig. 14b we also compare these two
426 paths in North American co-ordinates and all mean poles between 230 and 140 Ma are also
427 plotted as North poles (as in fig. 6 in Kent and Irving, 2010). In the K&I path there is 12° of
428 APW between 200 and 190 Ma ($1.2^\circ/\text{M.y.}$) and 30° of APW between 160 and 145 Ma that
429 amounts to $2^\circ/\text{M.y.}$! The 190-160 Ma section of the K&I GAPWaP is also characterized by a
430 near still-stand in APW (Fig. 14b). In contrast, our GAPWaP's show a smooth path from 200
431 to 140 Ma. These differences arise mainly from the low number of input poles used by K&I.
432 As an example, their 160 Ma mean pole is based on only four poles, one from North America,
433 one from Australia and two Patagonian poles. Conversely, our mean pole is derived from 19
434 poles (including the four input poles used by K&I) from six different continents (Table 1).
435 We also use different reconstruction parameters (most notably for Patagonia).

436

437 **6. Palaeogeography and Plate Speeds**

438 In this section we calculate latitudinal drift-velocities and angular rotation rates (Figs. 15-16)
439 and present ten new reconstructions in 50 million year intervals from 500 to 50 Ma. We focus
440 on the location and evolution of Gondwana, Laurentia and Baltica and their joint fusions into
441 Laurussia, Laurasia and Pangaea. Palaeozoic reconstructions (Figs. 17-19) largely follow
442 Torsvik et al. (1992, 1996), Torsvik (1998), McKerrow et al. (2000a,b), Cocks and Torsvik
443 (2002, 2005, 2007, 2011), and Torsvik and Cocks (2004, 2009, 2011a, b), but are refined and
444 modified in accordance with our new APWPs. Pre-Pangaean maps and plate velocities are
445 based on I-error corrected spherical spline paths from the various continental blocks, whilst
446 maps for 300 Ma and younger are based on the running mean GAPWaP.

447

448 Our reconstructed maps are based on more than 300 time-dependent plate polygons (terrane
449 boundaries), e.g. Cocks and Torsvik (2005, 2007, 2011) and seen in our Figs. 2, 4, 5 and 9,
450 currently summarized in industry reports (e.g. Labails et al., 2009), but soon to be made
451 public in digital form. The maps were generated with the open-source GPlates software
452 (www.gplates.org; Boyden et al., 2011). They include some spreading centres and subduction
453 zones, but for the Palaeozoic the geometry and even the polarity of subduction can be
454 disputed. These tentative features should therefore be treated with caution.

455

456 6.1 Early Palaeozoic (*Cambrian to Silurian*)

457 The Palaeozoic was extraordinary in Earth history for several reasons, not only for the
458 blossoming of complex life forms (Cambrian), dispersion of major taxa (Ordovician) and the
459 catastrophic extinction at the end of the Palaeozoic, but also in terms of unique
460 palaeogeographic conditions. The continents covered the globe from the tropics to southern
461 polar latitudes. Greenhouse climates prevailed but were punctuated by Icehouse periods in
462 the Late Ordovician (short-lived) and in the Permo-Carboniferous (Figs. 4, 15, 16).
463 Latitudinal mean mass-centres (independent of absolute or relative palaeolongitude) were
464 calculated from our global maps (reconstructed polygons) at 10 M.y. intervals. The
465 latitudinal continental mean mass-centre was located in polar latitudes throughout the early
466 Palaeozoic (Fig. 4). Reconstructed polygons comprise the areal extent of continental
467 lithosphere and their stretched continental margins through time. For the Phanerozoic, our
468 global model of continents/extended margins amounts to $143\text{-}199 \times 10^6 \text{ km}^2$ or ~28-39% of
469 the Earth's total surface area.

470

471 Gondwana was the largest amalgamation, almost 100 million km^2 in size during the early
472 Palaeozoic covering ~20% of the Earth's surface (see also Torsvik and Cocks, 2009, 2011b).
473 In the Late Cambrian and Early Ordovician (Fig. 17), Gondwana stretched from the South
474 Pole (northern Africa) to the equator (Australia). The pole-facing margin was fringed with
475 peri-Gondwanan elements such as Avalonia, the Armorican Terrane Assemblage (ATA, e.g.
476 Iberia and France) and many others that rifted from Gondwana at various times, and in the
477 process generated vast Palaeozoic Oceans such as the Rheic (Fig. 17) and the Palaeotethys
478 (Fig. 18). Fig. 16 shows the palaeo-latitude development, latitudinal drift-rates and rotations
479 for a location in Central Africa. During the Cambrian, Central Africa drifted rapidly
480 southward at rates as high as 10 cm/yr or more, which was associated with counterclockwise
481 rotations as high as $2^\circ/\text{M.y.}$ These values are significantly higher than those seen in the same
482 time period for Baltica and Laurentia (Fig. 15). Central Africa remained at latitudes at around
483 40°S during most of Ordovician and Silurian times.

484

485 The Palaeozoic latitudinal drift and rotational history for Baltica (Stable Europe) and
486 Laurentia (North America) for the given geographic location are shown in Fig. 15. Baltica
487 was at intermediate to high southerly latitudes in the Late Cambrian, and almost
488 geographically inverted. Between the Early Ordovician and Mid-Silurian, Baltica drifted

489 towards the tropics, followed by southward drift after collision with Laurentia (Caledonian
490 Orogeny and formation of Laurussia; [Fig. 5](#)). Latitudinal drift-rates are within plate tectonic
491 'speed limits' and always lower than 10 cm/yr. Baltica rotated counterclockwise ($1\text{--}2^\circ/\text{M.y.}$)
492 from Cambrian to Early Devonian times ($\sim 160^\circ$ in total from 500 to 400 Ma); the destruction
493 of the Iapetus Ocean (Harland and Gayer, 1972) was dominated by N-S closure and the long-
494 lasting rotation of Baltica was probably accommodated by low-latitude Euler pole geometries
495 (Torsvik 1998, *fig. 8*) that brought Baltica from high Cambrian/Early Ordovician latitudes to
496 near equatorial latitudes by the Late Silurian (compare [Figs. 17](#) and [5](#)). After the Caledonian
497 Orogeny there is a distinct decrease in the rate of rotation and the Devonian to Permian
498 interval is characterized by minor, but systematic clockwise rotations, in the order of
499 $0.5^\circ/\text{M.y.}$ ([Fig. 15](#)).

500

501 Laurentia was located in equatorial to low southerly latitudes during most of the early
502 Palaeozoic, and was separated from Baltica by the Iapetus Ocean. The Iapetus Ocean
503 between Laurentia and Baltica (up to 3000 km wide) and the Avalonian sector of Gondwana
504 (up to 5000 km wide) was at its widest in the Early Ordovician. Avalonia rifted from
505 Gondwana in the Early Ordovician (Tremadocian), opening the Rheic Ocean in its wake
506 (Cocks and Fortey, 2009), which reached a maximum width of 5000–5500 km during Late
507 Ordovician to Mid-Silurian time. Avalonia and Baltica merged obliquely in a relatively soft
508 docking near the Ordovician–Silurian boundary (~ 443 Ma), and thus Avalonia was only an
509 independent terrane during Ordovician time (Torsvik and Rehnström, 2003). The end of the
510 Ordovician was also marked by the short, but nevertheless intense Hirnantian glaciation ([Fig.](#)
511 [17](#)).

512

513 During the closure of the Iapetus Ocean, the rotating and northward moving Baltica (together
514 with Avalonia) collided with a quasi-stationary Laurentia. Subsequently all these continents
515 (Laurussia) drifted southward until ~ 400 Ma followed by systematic northward drift.
516 Compared with our early to mid 1990's compilations (Torsvik et al., 1992, 1996; Gurnis and
517 Torsvik, 1994), a previously noted velocity burst in the Late Silurian (as high as 20 cm/yr. for
518 Laurentia), is no longer recognized in our improved data-sets (below 8 cm/yr in [Fig. 15](#)).
519 Laurussia, including the loosely connected high Arctic, Ellesmere, Svalbard and Kara
520 Terranes, covered a surface area of 37 million km².

521

522 *6.2 Late Palaeozoic (Devonian to Permian)*

523 The Rheic Ocean started to close during the Middle Silurian and by the Early Devonian (Fig.
524 17) the Amazonia-Laurussia segment of the Rheic was reduced to 750-1500 km (McKerrow
525 et al., 2001a). Laurussia drifted to more southerly latitudes (Fig. 15) with plate speeds and
526 rotations peaking at 10 cm/yr and 2°/M.y. respectively. By the Early Devonian, Laurussia
527 stretched from the equator to almost 60°S whilst Gondwana was nearly centred on the South
528 Pole. From Late Devonian times, Gondwana systematically drifted northward, accompanied
529 by large clockwise rotations that peaked at ~ 360 Ma (>4°/M.y.).
530

531 The exact timing of separation between the Armorican Terrane Assemblage (ATA) and
532 Gondwana during the opening of the Palaeotethys Ocean is poorly constrained. In our
533 reconstruction at 400 Ma, we show a developing Paleotethys Ocean and consider the initial
534 onset of spreading to be of earliest Devonian age (Fig. 18). If the ATA is to reach a proximal
535 Laurussian position by the Early Carboniferous, the opening of the Paleotethys must have
536 proceeded rapidly and was accompanied by sinistral displacement along the NW Gondwana
537 margin. In this context, the Variscan Orogeny (particularly in the Sudetes area of Perunica)
538 shows a tectono-metamorphic peak in the Early Carboniferous (~340 Ma; Lange et al., 2005).
539 The Rheic Ocean was about 5000 km wide between ATA and Laurussia in the Early
540 Devonian and reduced to near zero by the Early Carboniferous — this would require
541 convergence rates in the order of 10 cm/yr.

542
543 By the Early Carboniferous, the entire segment of the Rheic Ocean was narrow. Laurussia
544 rotated slowly clockwise and Siberia and Kazakh terranes were approaching each other (Fig.
545 18). The Variscan Orogeny waned in Late Carboniferous (end-Westphalian) times, when
546 crustal shortening ceased after the amalgamation of Laurussia and Gondwana. By then, the
547 bulk of Pangaea was already formed, centred on the equator and stretching from pole-to-pole
548 by the Late Permian (Fig. 20). Since the Late Devonian, Laurussia and Gondwana (Figs. 15-
549 16) and later their fusion into Pangaea (from 320 Ma; Fig 20) have drifted almost
550 systematically northward (Fig. 4). During the fairly long-lived and extensive Permo-
551 Carboniferous glaciations in Gondwana (Fig. 19), the South Pole was located in southern
552 Africa. We note that the Permo-Carboniferous glaciations are contemporaneous with Pangaea
553 formation and the destruction of intervening gateways for oceanic circulation (such as the
554 Rheic Ocean).

555

556 It should be emphasized that the paucity of Devonian and Early Carboniferous
557 palaeomagnetic data is a global phenomena (Fig. 3; Table 1) and thus the initial phases of
558 Pangaea formation are uncertain. The available data suggest an Early Carboniferous Pangaea
559 B-C type configuration (Gondwana located 'east' of Laurussia; see Fig. 18) evolving into a
560 Pangaea-A configuration during the Late Carboniferous (Domeier et al., 2012).

561

562 Siberia was already close to Laurussia by the Early Carboniferous (Fig. 18) along with many
563 of the Kazakh terranes. The latter had mostly fused with Baltica/Laurussia by the Late
564 Carboniferous (Uralides) but Siberia (Buiter and Torsvik, 2007; Cocks and Torsvik, 2007)
565 and many smaller terranes such as Tarim were still evolving in terms of their relative position
566 to Laurussia until the early Mesozoic (Van der Voo, 1993; Van der Voo et al., 2006;
567 Abrajevitch et al., 2008).

568

569 Pangaea ('All Land') did not truly include all continental crust. For example, the North and
570 South China Blocks were not part of Pangaea at any given time. Also during the Early
571 Permian phase of Pangaea assembly, the Neotethys opened (Fig. 19), and Cimmerian terranes
572 (Şengör et al., 1984) such as Lut, Helmand, Taurides, Qiangtang (N Tibet) and Sibumasu
573 drifted away from the northeast Gondwana margin. Pangaea achieved its maximum size
574 during late Palaeozoic and early Mesozoic times, but the most important growth phase
575 occurred during the Late Carboniferous when Gondwana, Laurussia and intervening terranes
576 collided, and in the process produced the Hercynian Orogenic Belt in Western Europe (Matte
577 2001; Torsvik and Cocks, 2004). We calculate a Pangaea size of 160 million km² at 250 Ma,
578 i.e. 93% of all continental material (Siberia included) and ~30% of the Earth's surface.

579 *6.3 Mesozoic and Early Cenozoic (Triassic to Palaeogene)*

580 The Mesozoic is a remarkable story about Pangaea dispersal, and in fact Pangaea is the only
581 supercontinent in Earth's history that can be modelled with some, if any, confidence. In this
582 section all of our analysis is based on the GAPWaP, southern Africa is the reference plate and
583 all other continents are modelled according to their position in the plate circuit hierarchy.
584 Pangaea and post-Pangaea (i.e. Africa) evolution (modelled for a Central African location in
585 Fig. 20) is mostly characterized by northward drift (typically around 2-4 cm/yr) and slow
586 angular rotations (typically less than 1°/M.y.). Pangaea's (~Africa's) northward drift,
587 however, appears to be almost 8 cm/yr between 210 and 220 Ma, some of which (~ 2 cm/yr.)
588 can be related to TPW (section 7). Throughout the Mesozoic, the latitudinal continental mean

589 mass-centre was located in tropical latitudes (Fig. 4). In Palaeogene times, however, at
590 around 50 Ma, there is a marked transition with the mean mass-centre migrating towards
591 northern latitudes; this pronounced global shift is associated with a global transition to
592 Icehouse climate conditions (Fig. 4).

593

594 Perhaps the most dynamic phase of Pangaea break-up occurred during (and shortly after) the
595 emplacement of the Central Atlantic Magmatic Province (CAMP) (200 Ma, e.g. Deenen et al.,
596 2010) and the subsequent opening of the Central Atlantic Ocean at ~ 195 Ma (Labails et al.,
597 2010). The emplacement of CAMP probably resulted in the break-up of Pangaea, manifested
598 as the separation of Laurasia and Gondwana and accompanied by the initial fragmentation of
599 long-lived Gondwana (Figs. 4 and 21).

600 The most important step after initial Pangaea rifting is the Jurassic separation of West (e.g.
601 Africa and South America) and East Gondwana (e.g. Madagascar, India, East Antarctica and
602 Australia). The exact timing of seafloor spreading initiation is uncertain, prolonged extension
603 took place in late Palaeozoic and early Mesozoic times, break-up may have occurred as early
604 as 180-177 Ma, with the first identifiable magnetic anomaly M25 (~155 Ma) in the oceanic
605 crust of the Somali (Eagles and König, 2008) and Mozambique Basins (König and Jokat,
606 2010) (Fig. 21). The Mesozoic evolution of the Neo- and Palaeotethys is not detailed here,
607 but the China Blocks probably fused with Asia (Laurasia) in Mid to Late Jurassic time and
608 thus *after* the initial rifting of Pangaea.

609

610 In West Gondwana, the South Atlantic opened at around 130 Ma, starting in the south and at
611 100 Ma (Fig. 22) there was a full oceanic connection with the Central Atlantic (Torsvik et al.,
612 2009). During the earliest opening of the South Atlantic, seafloor spreading between
613 Madagascar and Africa (Somalia) ceased (Eagles and König, 2008). At ~ 130 Ma, seafloor
614 spreading was initiated between East Antarctica and India (Gaina et al., 2007), and at the
615 same time, India broke off from Australia (Mihut and Müller, 1998; Heine et al., 2004;
616 Torsvik et al., 2008c). At around 85 Ma, India and the Seychelles drifted off Madagascar
617 following thermal upwelling associated with the Marion hotspot (e.g. Storey et al., 1995;
618 Torsvik et al., 2000; Meert and Tamrat, 2006).

619

620 Fifty million years ago (Fig. 22), the promontory of India (extended continental crust
621 separated from the Indian subcontinent by oceanic basins; van Hinsbergen et al., 2011a)

622 collided with Eurasia. India had separated from the Seychelles at ~ 62 Ma (Ganerød et al.,
623 shortly after the Deccan magmatic event (65 Ma). During break-up India attained
624 velocities of up to 18 cm/yr. This is the highest velocity recorded for any continental plate in
625 Mesozoic and Cenozoic times, and was propelled by thermal buoyancy of the Reunion hot
626 spot (van Hinsbergen et al., 2011b; Cande and Stegman, 2011).

627

628 In the North Atlantic, seafloor spreading was underway in the Labrador Sea (starting at ~ 67
629 Ma and stopping at ~ 33 Ma), the Norwegian-Greenland Sea (started at ~ 54 Ma;) and the
630 Eurasian Basin in the Arctic (started at ~ 55 Ma) (Chalmers and Laursen, 1995; Gaina et al.,
631 2002, 2009; Mosar et al., 2002). Seafloor spreading between Greenland and Europe was
632 associated with vast Large Igneous Province (LIP) activity, the North Atlantic Igneous
633 Province (e.g., Ganerød et al., 2010). Gateways from pole-to-pole across the central part of
634 the former Pangaean continent from ~50 Ma may have paved the way for the cold global
635 climate (Fig. 4) since then, and the first known bipolar glaciations in Earth history (e.g.,
636 Tripati et al., 2005).

637

638 **7. True Polar Wander (TPW)**

639 APWPs records a combined signal from the two sources of absolute motion: motion of
640 lithospheric plates relative to the Earth's mantle ("continental drift") and the rotation of the
641 entire solid Earth with respect to the spin axis. The latter component, commonly referred to
642 as TPW, arises from the gradual redistribution of density heterogeneities within the mantle
643 and corresponding changes in the planetary moment of inertia (Goldreich and Toomre, 1968;
644 Steinberger and Torsvik, 2010). To establish the magnitude of TPW with confidence, the
645 absolute velocity field and the plate geometry for both continental and oceanic lithosphere are
646 required as well as a robust set of palaeomagnetic data. This is difficult for pre-Cretaceous
647 time because no useful connection exists for reconstructing the motion of oceanic plates in the
648 Pacific domain prior to ~84 Ma (e.g., Doubrayne and Tarduno, 2008a,b). Furthermore,
649 APWPs for the Pacific plate are not considered reliable given the limited quality of Pacific
650 palaeomagnetic poles (see Torsvik et al., 2002; Cottrell and Tarduno, 2003; Tarduno, 2007 for
651 discussion). Estimates of the relative magnitude of TPW should therefore rely on continental
652 palaeomagnetic data.

653 In spite of these difficulties, we attempt to determine the magnitude of TPW by extracting the
654 coherent (mean) rotation of all the continents around their common centre of mass in the

655 palaeomagnetic reference frame, an approach taken and tested by Marcano et al. (1999) for
656 Pangaea in Permian and Triassic time. The rationale for this approach is that a common
657 rotation of all continents is more easily explained, if it occurs *jointly* with the underlying
658 mantle (TPW) rather than *relative to* it. A rotation of all continents corresponds to a large
659 toroidal component of plate motion, and it has been suggested that convection with surface
660 plates tends towards a state that minimizes the toroidal (strike-slip and plate spin)-poloidal
661 (convergence and divergence) ratio (O'Connell et al., 1991). Hence episodes of large toroidal
662 power are not expected to be associated with 'continental drift', and we therefore argue that
663 coherent rotations of very large plates are more likely due to TPW.

664 The motion of the center of mass of all continents could be either due to TPW or plate motion
665 relative to the mantle. Northward and southward motion can be determined in the
666 palaeomagnetic frame. In order to assign the eastward or westward component of motion an
667 additional assumption is made that the axis of finite rotation for the *African* plate in the
668 palaeomagnetic reference frame always remains on the equator. We can refer to this as the
669 quasi-stationary African assumption whereby Africa does not substantially move eastward or
670 westward. While this choice of the African plate as a "reference plate" is somewhat arbitrary,
671 we argue that this assumption is reasonable (Torsvik et al., 2008b). Based on the quasi-
672 stationary African assumption, it is found that the longitude of the centre of mass of all
673 continents, as well as its antipode, remained close to the longitudes of the centre of masses of
674 the African and Pacific Large Low Shear-wave Velocity Provinces (LLSVPs), respectively.
675 These LLSVPs are associated with large-scale geoid highs, dominated by degree two terms of
676 the spherical harmonic expansion of the Earth's gravity potential (Hager, 1984; Burke et al.,
677 2008). Both the LLSVP's and their inherently associated geoid highs are expected to have
678 remained stable for at least 300 M.y. (Burke and Torsvik, 2004; Torsvik et al., 2006, 2010a).
679 This is based on the observation that most reconstructed LIPs and kimberlites since Pangaea
680 assembly are sourced by plumes from the edges of the LLSVPs, and thus these must have
681 remained stationary since then. TPW is by definition a rotation about an equatorial axis.
682 Additionally, because the maximum of the degree two geoid corresponds to the axis of
683 minimum moment of inertia it should remain at the equator during TPW. Given that the
684 center of mass of continents and the African LLSVP (and corresponding geoid highs) are at
685 similar longitudes, we regard it as unlikely that northward or southward motions of the center
686 of mass of all continents are due to TPW and therefore interpret all such motion as continental
687 drift relative to the mantle. In contrast, a rotation of all continents around their common

688 center of mass (located on the equator) corresponds to a large toroidal component of plate
689 motion and most likely represents TPW.

690 *7.1 TPW since Pangaea assembly*

691 To define the magnitude of TPW, we follow the method developed by Steinberger and
692 Torsvik (2008) (see Appendix 1 for details). Based on the motion of continents in the
693 palaeomagnetic frame, evaluated on a 1° grid, both the coherent rotation of all continents
694 around an equatorial axis at the same longitude as their center of mass (interpreted as largely
695 due to TPW) and around an equatorial axis at 90° from the first one (interpreted as mostly
696 continental drift) are determined. Episodes of CW and CCW TPW thus determined (from the
697 red continuous line in Fig. 23) are similar to those presented by Steinberger and Torsvik
698 (2008). Differences are due to updates in (1) the African absolute plate motion in the
699 palaeomagnetic reference frame, i.e. the African APWP, (2) relative plate motions and (3)
700 plate geometry.

701 Interpretation of the cumulative rotation of all continents about their centre of mass (Fig. 23)
702 suggests four episodes of TPW: (1) a CCW rotation in the time interval 250-200 Ma followed
703 by (2) the same amount of CW rotation between 200 and 150 Ma, (3) a CW rotation during
704 the 150-140 Ma interval, and (4) a rotation with a similar magnitude but in opposite sense
705 (CCW) between 110 and 100 Ma. The latter rotation is consistent with the Early Cretaceous
706 episode of TPW suggested by a comparison of the motion of Africa in palaeomagnetic and
707 hotspot reference frames (e.g., Besse and Courtillot, 2002; Torsvik et al., 2008a; Steinberger
708 and Torsvik, 2010).

709 Fig. 24 shows that the continental motion in these time intervals is indeed largely a coherent
710 rotation around an equatorial axis: (1) 250-200 Ma at longitude 32.3°W, (2) 200-150 Ma at
711 longitude 5.1°E, (3) 150-140 Ma at longitude 11.3°E, and (4) 110-100 Ma at longitude
712 17.1°E. In the last three time intervals (after 200 Ma), the axis of this coherent rotation is at a
713 longitude similar to the center of mass of all continents, which is also at a similar longitude as
714 the center of mass of the African LLSVP and the antipode of the Pacific LLSVP. Longitudes
715 of the center of mass of continents and the axis of coherent rotation depend on the reference
716 frame used. In a hotspot reference frame (Steinberger et al., 2004; O'Neill et al., 2005) they
717 would be 5 to 9° further west, in a slab-fitting reference frame (van der Meer et al., 2010) they
718 would be placed 8 to 18° further west. Nonetheless, they would remain close to the LLSVP
719 (antipodal) centres of mass. The one exception is for the time interval from 250-200 Ma

720 where the axis of rotation is displaced substantially further west. This may indicate a distinct
721 TPW axis, but it may also represent a superposition of (1) a rotation around a similar axis as
722 for the later episodes, that we consider to be due to TPW, and (2) a northward motion of the
723 continents, at that time still assembled in Pangaea, relative to the mantle. This northward
724 motion would be at similar speeds as during the time interval 320-250 Ma, for which no TPW
725 was inferred. Here we prefer the second interpretation, and leave the axis of TPW rotation at
726 a constant equatorial location of 11°E ([Table 12](#)), close to the center of mass of the African
727 LLSVP (15.6°S, 13°E) as well as its antipode at the Pacific LLSVP (11°S, 197.1°E) (Burke et
728 al., 2008). This corresponds to the minimum moment of inertia axis for both LLSVPs at
729 2.7°S, 11.9°E (Steinberger and Torsvik, 2010) and the long-term geoid high and the
730 geotectonic bipolarity axis at 0°N, 10°E (Pavoni, 1985). This conceptually simple model
731 should be regarded as an approximation. The orientation of the minimum moment of inertia
732 axis of the Earth (and hence TPW) is mainly controlled by LLSVPs, but its position may
733 change through time due to mass variations from subducted slabs and rising plume heads. As
734 an example, the present-day minimum moment of inertia for the geoid is located at 15°W
735 (Steinberger and Torsvik, 2010).

736 As a consequence of the above, we modify our plate motion model by subtracting the inferred
737 TPW from the African plate motion relative to the spin axis (i.e. the motion in the
738 palaeomagnetic reference frame). In our simple model, we apply four subsequent stage
739 rotations about the equatorial axis at 11°E, with the magnitudes (rotation angles) listed in
740 [Table 12](#). If the assumption of the zero longitude motion for Africa is valid, the resulting
741 TPW-corrected rotations describe the motion of Africa in an absolute reference frame fixed
742 with respect to the entire solid Earth (i.e., relative to the Earth's mantle). We then re-calculate
743 the stage and finite rotations of all plates with the same relative plate motions and recompute
744 the mean continental coherent rotations in the TPW-corrected reference frame. The results
745 are shown by the dotted lines in [Fig. 23](#). As expected, coherent rotations around the center of
746 mass of the continents were substantially reduced. What remains is a strong northward
747 motion of all the continents prior to about 190 Ma. If we had adopted an axis of TPW
748 rotation further west in the initial time interval, the resulting northward motion would be
749 much less and the coherent rotation would remain small. It will require further study and
750 geodynamic modelling to determine whether such a rapid northward motion of Pangaea (~6
751 cm/yr) is geodynamically reasonable, or whether there are reasons to assume that the degree-
752 two geoid high and TPW axis of rotation was located further west.

753 7.2 TPW: Influence on APW Rates and Net Lithosphere Rotation

754 TPW rates are on the order of $0.45\text{--}0.8^\circ/\text{M.y.}$ but cumulative TPW since the Late
755 Carboniferous is close to zero. [Fig. 25a](#) ([Table 13](#)) shows the TPW-corrected GAPWaP by
756 simply adding the Euler rotations listed in [Table 12](#) (but with opposite sign of rotation).
757 Cumulative APW before correction amounts to 139° for the past 320 M.y. with a mean APW
758 rate of $0.44 \pm 0.23^\circ/\text{M.y.}$ ([Fig. 25b](#)). This is reduced to 110° and $0.34 \pm 0.18^\circ/\text{M.y.}$ after TPW
759 correction ([Fig. 25c](#)), i.e. ~20% reduction for the past 320 million years but 37% over the time
760 range (250–100 Ma) actually adjusted for TPW. TPW correction reduces APW rates (green
761 shading in [Fig. 25b](#)), and most notably between 110 and 100 Ma where the APW rate is
762 reduced from 1.2 to $0.39^\circ/\text{M.y.}$ This is also readily observed in angular rotations for a Central
763 African location ([Fig. 20c](#)), which for the past 310 M.y. never exceeded $0.5^\circ/\text{M.y.}$ after TPW
764 correction (see reduction in peaks between 100–110 Ma and 140–150 Ma). Similarly,
765 latitudinal velocities for Africa are reduced to ~6 cm/yr or less since the Late Carboniferous
766 ([Fig. 20b](#)).

767

768 The magnitude of TPW not only affects APWPs, but also the magnitude of net lithospheric
769 rotation (NR) derived from a palaeomagnetic reference frame. If mantle convection is the
770 principal driving-force for plate motions, NR should approximate zero, and small deviations,
771 typically less than $0.2^\circ/\text{M.y.}$ for the past 50 Ma (thick light brown line in [Fig. 23b](#)), are
772 commonly explained by lateral viscosity variations (Ricard et al., 1991; O'Connell et al.,
773 1991). In an ideal world, NR calculations require absolute plate motion models (mantle
774 models) and plate polygons for both continental and oceanic lithosphere (Torsvik et al.,
775 2010b). Unfortunately, global absolute plate models are increasingly unreliable prior to the
776 Late Cretaceous (~83 Ma) due to (1) models of hotspot motion becoming poorer, (2) lack of
777 hotspot tracks, and (3) lack of relative plate circuits between the Pacific and Indo-Atlantic
778 realm (Doubrovine and Tarduno, 2008a,b).

779

780 We have previously estimated NR back to the Late Jurassic ([Fig. 25c](#)) based on mantle
781 models (0–100 Ma) and a TPW-corrected global palaeomagnetic model back to 150 Ma
782 (Torsvik et al., 2010b). We observed that NR fluctuated and gradually increased back in time,
783 but by removing a linear time-trend we estimated an average of $0.12^\circ/\text{Myr}$ for the past 150
784 Myr. A pronounced peak between 60 and 50 Ma ($0.33^\circ/\text{M.y.}$) was attributed to the
785 unprecedented acceleration and deceleration of the Indian plate. As a comparison and as a

TPW sensitivity test we here calculate NR purely based on reconstructions of the continental lithosphere (28-39% of the Earth's surface) through time, but extended back to the Late Carboniferous. Mean NR is higher, as expected, averaging to $0.45 \pm 0.25^\circ/\text{M.y.}$ for the past 300 Myr with conspicuous peaks at 110-105 Ma and 150-145 Ma, which reaches almost $1^\circ/\text{M.y.}$ Because TPW is associated with toroidal components of plate motion, these and many other highs are reduced after TPW correction resulting in the lowering of the NR mean to $0.35 \pm 0.21^\circ$ for the past 300 Ma and $0.28 \pm 0.14^\circ$ for the past 150 M.y. NR calculated from only continental lithosphere should generally be considered as maximum values, but except for a notable spike between 40 and 50 Ma, such simplified NR estimates for the past 150 M.y. (corrected for TPW) show gross similarities with 'properly' determined NR. Interestingly, NR estimates purely based on continental lithosphere are considerable lower than the HS3 model of Gripp and Gordon (2002). The latter model (NR=0.43°/M.y.) is widely used in the geodynamic community but not recommended (Torsvik et al., 2010b).

799

800 8. Conclusions and Future Outlook

In this extensive review of Phanerozoic palaeomagnetic poles, mostly derived from the cratonic elements of Gondwana, Laurentia, Baltica/Europe and Siberia, we have constructed new APWPs for Laurentia and Baltica, their Caledonian (Silurian) merger into Laurussia, and subsequent Late Permian merger of Laurussia and Siberia into Laurasia. After the main Pangaea assembly phase (~320 Ma), palaeomagnetic poles from Gondwana and Laurussia/Laurasia were combined to a Global APWP (GAPWaP). We have generated APWPs without/with correction for potential inclination error and conclude that all detrital sedimentary poles should be corrected for inclination shallowing, unless previously corrected using either the inclination-elongation method or anisotropy of magnetic susceptibility information (Tauxe and Kent 2004; Kodama, 2009). We use a benchmark flattening (f) value of 0.6, which leads to much smoother APWPs and elimination of Pangaea reconstruction artefacts (see also Domeier et al., 2011a, 2012).

Our new I-error corrected GAPWaP is based on five hundred Laurussia/Laurasia and Gondwana poles, and owing to the large number of poles and absence (mostly) of large age gaps, running mean and spline paths are almost identical. We employ the running mean GAPWaP for palaeogeographic reconstructions and dynamic calculations because it is more easily reproduced. On the other hand, when data-coverage is poorer (i.e. before 320 Ma) we

use spline-derived APWPs for all our reconstructions. With the exception of a few intervals where data are truly scarce (e.g., Mid-Devonian to Early Carboniferous) or where palaeomagnetic misfits still exist (e.g., between Jurassic Europe and North America), the palaeomagnetic data are robust. As examples, we have constructed ten palaeogeographic reconstructions from the Late Cambrian to the Palaeogene in 50 M.y. intervals. The Palaeozoic maps mainly address the location of Gondwana and peri-Gondwana terranes (e.g. Avalonia), Baltica and Laurentia, and they portray the complex evolution of large oceans such as Iapetus, Rheic Ocean, and the Palaeotethys. Maps for the times after Pangaea assembly are more global in nature and demonstrate that Pangaea was drifting systematically northward until break-up occurred in the Central Atlantic (shortly after 200 Ma and eruption of the CAMP), causing Laurasia to separate from Gondwana.

We devise two new GAPWaP's, (1) one without correction of TPW to be used in classic palaeogeographic reconstructions (Figs. 17-19, 21-22) where the relations to the spin axis or climate zones are of importance, and (2) one with TPW correction in order to link plate reconstructions to mantle geodynamic models. The latter should always be employed when attempting to correlate surface volcanism (e.g., LIPs) with heterogeneities in the deepest mantle (e.g. LLSVPs) because the latter are kept fixed in these exercises. Net-rotation calculations must also be carried out in a TPW-corrected reference frame to avoid toroidal spikes in the analysis. We have identified four important episodes of TPW since Pangaea assembly. These episodes are recognized between 250 and 100 Ma and comprise 37% of the GAPWaP in this time interval. TPW rates vary between 0.45 and 0.8°/M.y. but cumulative TPW is nearly zero since the Late Carboniferous due to both clockwise and counterclockwise episodes of TPW centered on 0°N and 11°E. The latter observations are 'good' news because errors in linking plate reconstructions with (for instance) the eruption location of LIPs and with LLSVPs in the deep mantle are 'minimized' with low cumulative TPW. This is why palaeomagnetic reference frames corrected or not corrected for TPW both show a striking correlation between surface LIPs and the LLSVPs (e.g., compare Torsvik et al., 2006 and 2010a).

Quantifying TPW back to the dawn of the Phanerozoic is much more difficult because relative (and absolute!) longitudes are unknown, except between the major Gondwana continents. After Pangaea times we used Africa as a plate that was quasi-stable in longitude, in order to derive semi-absolute longitudes but this approach cannot be used for the Palaeozoic. We are therefore limited to identify periods of rapid APW rates and/or major

851 cusps in the APWPs for the major continental players. APW rates for the past 320 M.y. (Figs.
852 25b, 26) average to $\sim 0.4^\circ/\text{M.y.}$ with a maximum value of $1.12^\circ/\text{M.y.}$ (Fig. 20b) for the
853 GAPWaP. These values are considerably lower than Palaeozoic rates for only Gondwana,
854 Laurussia or Laurentia, which can be as high as $2^\circ/\text{M.y.}$ (Fig. 26). Thus at face value there
855 could be considerable TPW in the available data-sets. Of course, it can also be a factor that
856 the quality of the APWPs may be degraded with increasing age.

857

858 A Siluro-Devonian cusp in the APWPs is an obvious candidate for TPW (Van der Voo, 1993;
859 see also Evans, 2003), and is prominent in the Laurussian path (Fig. 9), and to a lesser extent
860 in the Gondwanan path (Fig. 11); however, note the unfortunate over-reliance on only a single
861 410 Ma pole in the Gondwana path, whereas in the Siberian APWP (Fig. 12) the Devonian
862 segment is heavily interpolated. We note, however, that the Rheic ocean, once separating
863 Laurussia and Gondwana, was narrowing dramatically during Silurian and Early Devonian
864 times (see Figs. 17, 18) and thus there must also have been a *significant* component of
865 ‘continental drift’ in the APWPs between 430 and 400 Ma. Van der Voo (1993) estimated a
866 cumulative TPW of 75° from the Late Ordovician to Late Devonian times (~ 75 M.y.) which
867 on average amounts to $1^\circ/\text{M.y.}$ For Laurussia we now consider that TPW may have occurred
868 between 430 and 410 Ma. Total APW is $\sim 40^\circ$ (Figs. 9a, 26; $2^\circ/\text{M.y.}$) but a substantial part
869 must include ‘continental drift’ as ~ 2500 km of the Rheic Ocean was subducted at an average
870 rate of 12 cm/yr in this important Mid Silurian-Early Devonian interval. After 410 Ma there
871 is no need to appeal for TPW as APW rates are as low as $0.5^\circ/\text{M.y.}$ on average (Fig. 26).
872 Conversely, Piper (2006) argues for 90° Inertial Interchange TPW between 410 and 390 Ma
873 ($4.5^\circ/\text{M.y.}$); this captivating claim is not justified by palaeomagnetic data.

874

875 To explore TPW in detail for times before Pangaea, we need to establish a semi-absolute
876 longitude model. The plume generation zone (PGZ) method (Torsvik et al., 2008b, 2010b)
877 may provide the much needed longitude information. However, this approach assumes that
878 the Earth has remained in degree-two mode for the entire Phanerozoic, and that the African
879 and Pacific LLSVPs have remained the same throughout the Phanerozoic (see Zhong et al.,
880 2007; Torsvik et al., 2008b). The stability of the LLSVPs before Pangaea (Torsvik et al.,
881 2010b) is currently being tested and refined by restoring continents longitudinally based on
882 their contained LIPs and kimberlites. Satisfying the PGZ method, LIP and kimberlite
883 occurrences should coincide with the edges of the African and/or Pacific LLSVPs. If the
884 resulting reconstructed continents and plate motion histories are consistent with geological

records, the stability of LLSVPs for the entire Phanerozoic and perhaps longer may become a viable model — This will have profound implications for determining ancient longitude and to better quantify Palaeozoic TPW.

888

889 Acknowledgements

This paper stems from a palaeomagnetic workshop in Luleå (2009), locally organized by Sten-Åke Elming, and building upon numerous Scandinavian workshops that first started in Helsinki (1986) under the excellent leadership of Lauri Pesonen. Compilations and analysis were further developed at the Center for Advanced Study of the Norwegian Academy of Science and Letters (2010-2011). RVdV and MD were supported by a grant from the U.S. National Science Foundation, Division of Earth Sciences (Tectonics Program), and NSF's Office of International Science and Engineering (Americas Program), grant EAR-0634807. We also acknowledge funding from Statoil (Akademiavtalen), the Norwegian Research Council (Mantle Forcing: Grant Number 195911), Estonian Science Foundation (Grant Number 8701), and the European Research Council under the European Union's Seventh Framework Programme (FP7/2007-2013) / ERC Advanced Grant Agreement Number 267631 (Beyond Plate Tectonics).

902

903 Appendix 1: Computing TPW in the absence of hotspot tracks.

Finite and stage rotations for all plates, which are required to determine the motion of continents, are computed in 1 M.y. intervals. These plates are South Africa, Northwest Africa, North America, Eurasia, Greenland, South America, Antarctica, Australia, Central Indian Basin, Madagascar, India, Somalia, Northeast Africa, and Arabia. We determine for each point on a 1° latitude-longitude grid that is located on a continent (here using the -200 m contour line as a proxy for the continent-ocean boundary) whether it is located on one of these plates (except for the "Central Indian Basin"). Points that are inside polygons for Northwest Africa, Greenland, Madagascar, Somalia and Northeast Africa are assigned to these plates. Any remaining points that are inside the present-day plate boundaries for South Africa, North America, Eurasia, South America, Antarctica, Australia, India and Arabia are assigned to those plates.

915 All continental points are then reconstructed back in time in 1-M.y. intervals. To each point,
916 an area $1 \text{ deg}^2 \cos(\text{latitude})$ is assigned as its "mass". From these, the center of mass and the
917 moment of inertia tensor \mathbf{I} are determined in 1-M.y. intervals. For each 1-M.y. step, we also
918 calculate the angular momentum \mathbf{L} , using differences between consecutive locations of
919 reconstructed points. A mean rotation $\boldsymbol{\omega}$ of all continents can thus be found by solving the
920 equation $\mathbf{L} = \mathbf{I}\boldsymbol{\omega}$. This mean rotation is decomposed into three components in a coordinate
921 system with one axis along the Earth's spin axis, one in the equatorial plane and passing
922 through the longitude of the center of mass of all continents, and one in the equatorial plane
923 90° away. These components are "integrated" (i.e. added up) back in time, which gives the
924 red and blue contiguous lines in the top panel of Fig. 23a. Although these "cumulative"
925 rotations are not finite rotations in the true sense, even in a rotating coordinate system in
926 which the zero meridian is fixed to the longitude of the center of mass, they nevertheless
927 provide a simple qualitative way for examining the changes in the mean continental motion
928 through time and defining episodes of TPW.

929

930 References

- 931 Abdul Aziz, H., Hilgen, F.J., Krijgsman, W., Sanz, E., Calvo, M., 2000. Astronomical forcing
932 of sedimentary cycles in the middle to late Miocene continental Calatayud Basin (NE
933 Spain). *Earth and Planetary Science Letters*, 177, 9-22.
- 934 Abdul Aziz, H., van Dam, J., Hilgen, F.J., Krijgsman, W., 2004. Astronomical forcing in
935 Upper Miocene continental sequences: Implications for the Geomagnetic Polarity Time
936 Scale. *Earth and Planetary Science Letters*, 222, 243-258.
- 937 Abels, H.A., Abdul Aziz, H., Ventra, D., Hilgen, F.J., 2009. Orbital climate forcing in
938 mudflat to marginal lacustrine deposits in the Miocene Teruel Basin (northeast Spain).
939 *Journal of Sedimentary Research*, 79, 831-847.
- 940 Abels, H.A., Hilgen, F.J., Krijgsman, W., Kruk, R., Raffi, I., Turco, E., Zachariasse, W.J.,
941 2005. Long-period orbital control on middle Miocene global cooling: Integrated stratigraphy
942 and astronomical tuning of the Blue Clay Formation on Malta. *Paleoceanography*, 20, doi:
943 10.1029/2004PA001129.
- 944 Abou Deeb, J.M., Tarling, D.H., 2005. A palaeomagnetic study of the volcanic rocks of El-
945 Mane mountain, south of Damascus, Syria. *Geofisica Internacional*, 44, 187-195.

- 946 Abou Deeb, J.M., Otaki, M.M., Tarling, D.H., Abdeldayem, A.L., 1999. A palaeomagnetic
947 study of Syrian volcanic rocks of Miocene to Holocene age. *Geofisica Internacional*, 38, 17-
948 26.
- 949 Abrajevitch, A., R. Van der Voo, M.L. Bazhenov, N.M. Levashova, P.J.A. McCausland, 2008.
950 The role of the Kazakhstan orocline in the late Paleozoic amalgamation of Eurasia.
951 *Tectonophysics*, 455, 61-76.
- 952 Alvey, A. 2009. Using crustal thickness and continental lithosphere thinning factors from
953 gravity inversion to refine plate reconstruction models for the Arctic & North Atlantic. Ph.D
954 thesis, University of Liverpool, 189 pp.
- 955 Audin, L., Quidelleur, X., Coulié, E., Courtillot, V., Gilder, S., Manighetti, I., Gillot, P.Y.,
956 Tapponnier, P., Kidane, T., 2004. Palaeomagnetism and K-Ar and 40 Ar/39 Ar ages in the
957 Ali Sabieh area (Republic of Djibouti and Ethiopia): Constraints on the mechanism of Aden
958 ridge propagation into southeastern Afar during the last 10 Myr. *Geophysical Journal
959 International*, 158, 327-345.
- 960 Bachtadse, V., Briden, J. C., 1990. Palaeomagnetic constraints on the position of Gondwana
961 during Ordovician to Devonian Times, in *Palaeozoic Palaeogeography and Biogeography*,
962 eds McKerrow, W. S. & Scotese, C. R., Geological Society, London, 43-48.
- 963 Bazhenov, M. L., Grishanov, A. N., Van der Voo, R., Levashova, N. M., 2008. Late Permian
964 paleomagnetic data east and west of the Urals. Geophysical and geological implications,
965 *Geophysical Journal International*, 173, 395-408.
- 966 Becker, T.W., Boschi, L., 2002. A comparison of tomographic and geodynamic mantle
967 models. *Geochem. Geophys. Geosyst.* 3, 1003, doi:10.1029/2001GC000168
- 968 Besse, J., Courtillot, V., 2002. Apparent and true polar wander and the geometry of the
969 geomagnetic field over the last 200 Myr. *Journal of Geophysical Research*, 107,
970 doi:10.1029/200JB000050.
- 971 Bilardello, D., Kodama, K.P., 2010a. Paleomagnetism and magnetic anisotropy of
972 Carboniferous red beds from the Maritime Provinces of Canada: Evidence for shallow
973 paleomagnetic inclinations and implications for North American apparent polar wander.
974 *Geophysical Journal International*, 180, 1013-1029.
- 975 Bilardello, D., Kodama, K.P., 2010b. Rock magnetic evidence for inclination shallowing in
976 the early Carboniferous Deer Lake Group red beds of western Newfoundland. *Geophys. J.
977 Int.*, 181, 275-289.
- 978 Boyden, J.A., R.D. Müller, M. Gurnis, T.H. Torsvik, J.A. Clark, M. Turner, H. Ivey-Law, R.
979 J. Watson, J.S. Cannon, 2011. Next-generation plate-tectonic reconstructions using GPlates,

- 980 in G. R. Keller and C. Baru, eds., *Geoinformatics: Cyberinfrastructure for the Solid Earth Sciences*, Cambridge University Press, 95-113.
- 981
- 982 Brandt, D., Ernesto, M., Rocha-Campos, A. C., Dos Santos, R., 2009. Paleomagnetism of the
983 Santa Fé Group, central Brazil: Implications for the late Paleozoic apparent polar wander
984 path for South America. *Journal of Geophysical Research*, 114 (B02101), doi:
985 10.1029/2008JB005735.
- 986 Brown, L.L., Singer, B.S., Gorring, M.L., 2004. Paleomagnetism and $^{40}\text{Ar}/^{39}\text{Ar}$ chronology of
987 lavas from Meseta del Lago Buenos Aires, Patagonia. *Geochemistry, Geophysics, Geosystems*,
988 5, Q01H04, doi:10.1029/2003GC000526.
- 989 Buiter, S.J.H., Torsvik, T.H., 2007. Horizontal movements in the eastern Barents Sea
990 constrained by numerical models and plate reconstructions. *Geophysical Journal
991 International*, 171, 1376-1389.
- 992 Bullard, E., Everett, J.E., Smith, A.G., 1965. The fit of continents around the Atlantic.
993 *Philosophical Transactions of the Royal Society of London, Series A: Mathematical and
994 Physical Sciences*, 258 (1088), 41-51.
- 995 Burke, K., Torsvik, T.H., 2004. Derivation of large igneous provinces of the past 200 million
996 years from long-term heterogeneities in the deep mantle. *Earth and Planetary Science
997 Letters*, 227, 531-538.
- 998 Burke, K., Steinberger, B., Torsvik, T.H., Smethurst, M.A., 2008. Plume Generation Zones at
999 the margins of Large Low Shear Velocity Provinces on the Core-Mantle Boundary. *Earth
1000 and Planetary Sciences*, 265, 49-60.
- 1001 Bryan, P., Gordon, R.G., 1990. Rotation of the Colorado Plateau: An updated analysis of
1002 paleomagnetic data. *Geophys. Res. Lett.* 17, 1501–1504, doi:10.1029/GL017i010p01501.
- 1003 Camps, P., Henry, B., Nicolaysen, K., Plenier, G., 2007. Statistical properties of
1004 paleomagnetic directions in Kerguelen lava flows: Implications for the late Oligocene
1005 paleomagnetic field. *Journal of Geophysical Research - Solid Earth*, 112, B06102,
1006 doi:10.1029/2006JB004648.
- 1007 Cande, S.C., Stegman, D.R., 2011. Indian and African Plate motions driven by the push force
1008 of the Reunion plume head. *Nature*, 475, 47-52.
- 1009 Cande, S. C., Patriat, P., Dymond, J. 2010. Motion between the Indian, Antarctica and African
1010 plates in the early Cenozoic. *Geophysical Journal International*, 183, 127–149.
- 1011 Ceja, M.R., Goguitchaichvili, A., Calvo-Rathert, M., Morales-Contreras, J., Alva-Valdivia,
1012 L., Elguera, J.R., Urrutia-Fucugauchi, J., Granados, H.D., 2006, Paleomagnetism of the

- 1013 Pleistocene Tequila volcanic field (Western Mexico). *Earth, Planets and Space*, 58, 1349-
1014 1358.
- 1015 Chalmers, J.A., K.H. Laursen, 1995. Labrador Sea: the extent of continental and oceanic crust
1016 and the timing of the onset of seafloor spreading. *Mar. Petrol. Geol.*, 12, 205–217,
1017 doi:10.1016/0264-8172(95)92840-S.
- 1018 Chen, Z., Li, Z.-X., Powell, C.M., Balme, B.E., 1994. An early Carboniferous pole for
1019 Gondwanaland: new results from the Mount Eclipse Sandstone in the Ngalia Basin, central
1020 Australia. *Journal of Geophysical Research*, 99, 2909-2924.
- 1021 Clyde, W.C., Hamzi, W., Finarelli, J.A., Wing, S.L., Schankler, D., Chew, A., 2007, Basin-
1022 wide magnetostratigraphic framework for the Bighorn Basin, Wyoming. *Geological Society
1023 of America Bulletin*, 119, 848-859.
- 1024 Cocks, L.R.M., Torsvik, T.H., 2002. Earth Geography from 500 to 400 million years ago: a
1025 faunal and palaeomagnetic review. *J. Geol. Soc. Lond.*, 159, 631-644.
- 1026 Cocks, L.R.M., Torsvik, T.H., 2005. Baltica from the late Precambrian to mid Palaeozoic: the
1027 gain and loss of a terranes's identity. *Earth Science Reviews*, 72, 39-66
- 1028 Cocks, L.R.M., Torsvik, T.H., 2007. Siberia, the wandering northern terrane and its changing
1029 geography through the Palaeozoic. *Earth Science Reviews*, 82, 29-74.
- 1030 Cocks, L.R.M., Torsvik, T.H., 2011. The Palaeozoic geography of Laurentia and western
1031 Laurussia: A stable craton with mobile margins. *Earth Science Reviews*, 106, 1-51.
1032 doi:10.1016/j.earscirev.2011.01.007
- 1033 Cojan, I., Moreau, M.G., 2006. Correlation of terrestrial climatic fluctuations with global
1034 signals during the Upper Cretaceous-Danian in a compressive setting (Provence, France).
1035 *Journal of Sedimentary Research*, 76, 589-604.
- 1036 Cottrell R.D., Tarduno, J.A., 2003. A late Cretaceous pole for the Pacific plate: implications
1037 for apparent and true polar wander and the drift of hotspots. *Tectonophysics*, 362, 321-333
- 1038 Courtillot, V., Davaille, A., Besse, J., Stock, J., 2003. Three distinct types of hotspots in the
1039 Earth's mantle. *Earth Planet. Sci. Lett.* 205, 295-308.
- 1040 Courtillot, C., J. Besse, and H. Théveniaut, 1994. North American Jurassic apparent polar
1041 wander: The answer from other continents? *Phys. Earth Planet. Inter.*, 82, 87–104.
- 1042 Creer, K.M., Irving, E. Runcorn, S.K., 1954. The direction of the geomagnetic field in remote
1043 epochs in Great Britain. *Journal of Geomagnetism and Geoelectricity*, 250, 164-168.
- 1044 Dawes, P.R., 2009. Precambrian-Palaeozoic geology of Smith Sound, Canada and Greenland:
1045 key constraint to palaeogeographical reconstructions of northern Laurentia and the North
1046 Atlantic region. *Terra Nova*, 21, 1–13.

- 1047 Deenen, M.H.L., Ruhl, M., Bonis, N.R., Krijgsman, W., Kuerschner, W., Reitsma, M., van
1048 Bergen, M.J., 2010. A new chronology for the end-Triassic mass extinction. *Earth and*
1049 *Planetary Science Letters*, 291, 113-125.
- 1050 De Kock, M. O., Kirschvink, J.L., 2004. Paleomagnetic Constraints on the Permian-Triassic
1051 Boundary in Terrestrial Strata of the Karoo Supergroup, South Africa: Implications for
1052 Causes of the End-Permian Extinction Event. *Gondwana Research*, 7, 175-183.
- 1053 Derder, M. E. M., Henry, B., Amenna, M., Bayou, B., Djellit, H., Guemache, M.A., Hemmi,
1054 A., 2009. New structural implications for the central Sahara (Algeria), from the revisited
1055 Upper Carboniferous “Hassi Bachir” formation: Paleomagnetic constraints. *Tectonophysics*,
1056 463, 69-76.
- 1057 Derder, M.E.M., Henry, B., Bayou, B., Ouabadi, A., Bellon, H., Djellit, H., Khaldi, A.,
1058 Amenna, M., Baziz, K., Hemmi, A., Guemache, M. A., 2006. New African Lower
1059 Carboniferous paleomagnetic pole from intrusive rocks of the Tin Serririne basin (southern
1060 border of the Hoggar, Algeria). *Tectonophysics*, 418, 189-203.
- 1061 Domeier, M., Van der Voo, R., Denny, F.B. 2011a. Widespread inclination shallowing in
1062 Permian and Triassic paleomagnetic data from Laurentia: Support from new paleomagnetic
1063 data from Middle Permian shallow intrusions in southern Illinois (USA) and virtual
1064 geomagnetic pole distributions. *Tectonophysics*, 511, 38-52.
- 1065 Domeier, M., Van der Voo, R., Tohver, E., Tomezzoli, R.N., Vizan, H., Torsvik, T.H.,
1066 Kirshner, J., 2011b. New Late Permian paleomagnetic data from Argentina: Refinement of
1067 the apparent polar wander path of Gondwana. *Geochem., Geophysics, Geosystems*, 12,
1068 Q07002, doi:10.1029/2011GC003616.
- 1069 Domeier, M., Van der Voo, R., Tomezzoli, R.N., Tohver, E., Hendriks, B.W.H., Torsvik,
1070 T.H., Vizan, H., Dominguez, A.R., 2011c. Support for an “A-type” Pangea reconstruction
1071 from high-fidelity Late Permian and Early-Middle Triassic paleomagnetic results from
1072 Argentina. *Journal of Geophysical Research*, 116, B12114, doi:10.1029/2011JB008495.
- 1073 Domeier, M., Van der Voo, R., Torsvik, T.H., 2012. Paleomagnetism and Pangea: the Road to
1074 Reconciliation. *Tectonophysics*, 514-517, 14-43 doi: 10.1016/j.tecto.2011.10.021.
- 1075 Dominguez, A. R., Van der Voo, R., Torsvik, T.H., Hendriks, B.W.H., Abrajevitch, A.,
1076 Domeier, M., Larsen, B.T., Rousse, S., 2011. The ~270 Ma paleolatitude of Baltica and its
1077 significance for Pangea models. *Geophysical Journal International* 186, 529-550.
- 1078 Donohoo-Hurley, L.L., Geissman, J.W., Lucas, S.G., 2010. Magnetostratigraphy of the
1079 uppermost Triassic and lowermost Jurassic Moenave Formation, western United States:

- 1080 Correlation with strata in the United Kingdom, Morocco, Turkey, Italy and the eastern
1081 United States. Geological Society of America Bulletin, 122, 1936-1950.
- 1082 Dupont-Nivet, G., Sier, M., Campisano, C.J., Arrowsmith, J.R., DiMaggio, E., Reed, K.,
1083 Lockwood, C., Franke, C., Hüsing, S., 2008. Magnetostratigraphy of the eastern Hadar
1084 Basin (Ledi-Geraru research area, Ethiopia) and implications for hominin
1085 paleoenvironments, *in* Quade, J., Wynn, J.G., eds., The Geology of Early Humans in the
1086 Horn of Africa. Geological Society of America Special Paper, 446, 67-85.
- 1087 Doubrovine, P.V., Tarduno, J.A., 2008a. A revised kinematic model for the relative motion
1088 between Pacific oceanic plates and North America since the Late Cretaceous. Journal of
1089 Geophysical Research 113, B121011, doi:10.1029/2008JB005585.
- 1090 Doubrovine, P.V., Tarduno, J.A., 2008b. Linking the Late Cretaceous to Palaeogene Pacific
1091 plate and the Atlantic bordering continents using plate circuits and paleomagnetic data,
1092 Journal of Geophysical Research 113, B07104, doi:10.1029/2008JB005584.
- 1093 Eagles, G., König, M., 2008. A model of plate kinematics in Gondwana breakup. Geophysical
1094 Journal International, 173, 703-717.
- 1095 Evans, D.A.D., 2003. True polar wander and supercontinents. Tectonophysics 362, 303-320.
- 1096 Font, E., Ernesto, M., Silva, F., Correia, B., Nascimento, M. A. L., 2009. Paleomagnetism,
1097 rock magnetism and AMS of the Cabo Magmatic Province, NE Brazil, and the opening of
1098 the South Atlantic. Geophysical Journal International, 179, 905-922.
- 1099 Gaina, C., Roest, W., Mueller, R.D., 2002. Late Cretaceous-Cenozoic deformation of
1100 Northeast Asia. Earth and Planetary Science Letters, 197, 273-286.
- 1101 Gaina, C., R.D. Müller, B. Brown, T. Ishihara, and K.S. Ivanov, 2007. Breakup and early
1102 seafloor spreading between India and Antarctica. Geophysical Journal International,
1103 doi:10.1111/j.1365-246X.2007.03450.x.
- 1104 Gaina, C., Gernigon, L., Ball, P., 2009. Palaeocene–Recent plate boundaries in the NE
1105 Atlantic and the formation of the Jan Mayen microcontinent. Journal Geological Society,
1106 166, 601-616.
- 1107 Gallet, Y., Pavlov, V., 1996. Magnetostratigraphy of the Moyero River Section (North-
1108 Western Siberia): Constraints on geomagnetic reversal frequency during the early
1109 Palaeozoic. Geophysical Journal International, 125, 95–105.
- 1110 Ganerød, M., Smethurst, M.A., Rousse, S., Torsvik, T.H., Prestvik, T., 2008. Reassembling
1111 the Paleogene-Eocene North Atlantic igneous province: New paleomagnetic constraints
1112 from the Isle of Mull, Scotland. Earth and Planetary Science Letters, 272, 464-475.

- 1113 Ganerød, M., Smethurst, M.A., Torsvik, T.H., Prestvik, T., Rousse, S., McKenna, C., van
1114 Hinsbergen, D.J.J., Hendriks, B.W.H., 2010. The North Atlantic Igneous Province
1115 reconstructed and its relation to the Plume Generation Zone: The Antrim Lava Group
1116 revisited. *Geophysical Journal International*, 182, 183-202.
- 1117 Ganerød, M., Torsvik, T.H., van Hinsbergen, D., Gaina, C., Corfu, F., Werner, S., Owen-
1118 Smith, T.M., Ashwal, L.D., Webb, S.J., Hendriks, B.W.H., 2011. Palaeoposition of the
1119 Seychelles microcontinent in relation to the Deccan Traps and the Plume Generation Zone
1120 in Late Cretaceous-Early Palaeogene time. In: Van Hinsbergen, D.J.J., Buiter, S.J.H.,
1121 Torsvik, T.H., Gaina, C. & Webb, S.J. (eds) *The Formation and Evolution of Africa: A*
1122 *Synopsis of 3.8 Ga of Earth History*. Geological Society, London, Special Publications, 357,
1123 229–252. DOI: 10.1144/SP357.12
- 1124 Geuna, S. E., Escosteguy, L. D., 2004. Paleomagnetism of the Upper Carboniferous – Lower
1125 Permian transition from Paganzo basin, Argentina. *Geophysical Journal International*, 157,
1126 1071-1089.
- 1127 Geuna, S. E., Somoza, R., Vizán, H., Figari, E. G., Rinaldi, C. A., 2000. Paleomagnetism of
1128 Jurassic and Cretaceous rocks in central Patagonia: a key to constrain the timing of rotations
1129 during the breakup of southwestern Gondwana? *Earth and Planetary Science Letters*, 181,
1130 145-160.
- 1131 Goguitchaichvili, A., Petronille, M., Henry, B., Valdivia, L.A., Morales, J., Urrutia-
1132 Fucugauchi, J., 2007. Paleomagnetism of the Eastern Alkaline Province (Mexico):
1133 Contribution to the time-averaged field global database and geomagnetic instability time
1134 scale. *Earth, Planets and Space*, 59, 775-783.
- 1135 Goldreich, P., Toomre, A., 1969. Some remarks on polar wandering. *Journal of Geophysical*
1136 *Research* 74, 2555-2569.
- 1137 Gradstein, F.M., Ogg, J.G., Smith, A.G. (Eds.), 2004. *A Geologic Time Scale 2004*.
1138 Cambridge University Press, Cambridge, 589 pp.
- 1139 Gripp, A., Gordon, R.G., 2002. Young tracks of hotspots and current plate velocities.
1140 *Geophys. J. Int.* 150, 321–361.
- 1141 Gurevitch, E.L., Heunemann, C., Radko, V., Westphal, M., Bachtadse, V., Pozzi, J. P.,
1142 Feinberg, H., 2004. Palaeomagnetism and magnetostratigraphy of the Permian-Triassic
1143 northwest central Siberian Trap Basalts. *Tectonophysics*, 379, 211-226.
- 1144 Gurnis, M., Torsvik, T.H., 1994. Rapid drift of large continents during the late Precambrian
1145 and Palaeozoic: Palaeomagnetic constraints and dynamic models. *Geology*, 22, 1023-1026.

- 1146 Hager, B. H. 1984. Subducted slabs and the geoid: Constraints on mantle rheology and flow.
1147 J. Geophys. Res., 89, 6003–6015.
- 1148 Harlan, S.S., Morgan, L.A., 2010. Paleomagnetic results from Tertiary volcanic strata and
1149 intrusions, Absaroka Volcanic Supergroup, Yellowstone National Park and vicinity:
1150 Contributions to the North American apparent polar wander path. Tectonophysics, 485, 245-
1151 259.
- 1152 Harlan, S. S., Geissman, J. W., Whisner, S. C., Schmidt, C. J., 2008. Paleomagnetism and
1153 geochronology of sills of the Doherty Mountain area, southwestern Montana; implications
1154 for the timing of fold-and-thrust belt deformation and vertical-axis rotations along the
1155 southern margin of the Helena Salient. Geological Society of America Bulletin, 120, 1091-
1156 1104.
- 1157 Harland, W.B., Gayer, R.A., 1972. The Arctic Caledonides and earlier oceans, Geological
1158 Magazine 109, 289–314.
- 1159 Heine, C., R.D. Müller, C. Gaina, 2004. Reconstructing the Lost Eastern Tethys Ocean Basin:
1160 Convergence history of the SE Asian margin and marine gateways. In *Continent-Ocean*
1161 *Interactions in Southeast Asia*, eds. P. Clift, D. Hayes, W. Kuhnt, and P. Wang. American
1162 Geophysical Union Geophysical Monograph 149:37-54.
- 1163 Horner-Johnson, B.C., Gordon, R.G., Argus, D.F., 2007. Plate kinematic evidence for the
1164 existence of a distinct plate between the Nubian and Somalian plates along the Southwest
1165 Indian Ridge. Journal Geophysical Research, 112, BO5418, doi:10.1029/2006JB004519.
- 1166 Hospers, J., Van Andel, S.I., 1968. Palaeomagnetic data from Europe and North America and
1167 their bearing on the origin of the North Atlantic Ocean. Tectonophysics, 6, 475-490.
- 1168 Hurley, N., Van der Voo, R., 1987. Paleomagnetism of Upper Devonian reefal limestones,
1169 Canning basin, western Australia. Geological Society of America Bulletin, 98, 138146.
- 1170 Iglesia-Llanos, M.P., Riccardi, A.C., Singer, S.E., 2006. Paleomagnetic study of Lower
1171 Jurassic marine strata from the Neuquén Basin, Argentina: A new Jurassic apparent polar
1172 wander path for South America. Earth and Planetary Science Letters, 252, 379-397.
- 1173 Iosifidi, A.G., Mac Niocaill, C., Khramov, A.N., Dekkers, M.J., Popov, V., 2010. Palaeogeographic implications of differential inclination shallowing in Permo-Carboniferous sediments from the Donets Basin, Ukraine. Tectonophysics, 490, 229-240.
- 1176 Irving, E., 1964. Paleomagnetism and its application to geological and geophysical problems.
1177 Wiley and Sons, New York, 399 pp.
- 1178 Irving, E., 1977. Drift of the major continental blocks since the Devonian: Nature, 270, 304-
1179 674

- 1180 Irving, E., Irving, G.A., 1982. Apparent polar wander paths Carboniferous through Cenozoic
1181 and the assembly of Gondwana. *Geophysical Surveys*, 5, 141-188.
- 1182 Irving, E., 1979. Paleopoles and paleolatitudes of North America and speculations about
1183 displaced terrains. *Canadian Journal of Earth Sciences*, 16, 669-694.
- 1184 Irving, E., Baker, J., Wynne, P. J., Hamilton, T. S., Wingate, M. T. D., 2000. Evolution of the
1185 Queen Charlotte Basin; further paleomagnetic evidence of Tertiary extension and tilting.
1186 *Tectonophysics*, 326, 1-22.
- 1187 Irving, E., 2004. The Case for Pangea B, and the Intra-Pangean Megashear. In: *Timescales of*
1188 *the paleomagnetic field*, J.E.T. Channell, D.V. Kent, W. Lowrie and J. G. Meert, Editors,
1189 AGU Geophys. Monogr. 145, 13-27.
- 1190 Jay, A. E., Mac Niocaill, C., Widdowson, M., Self, S., Turner, W., 2009. New
1191 palaeomagnetic data from the Mahabaleshwar Plateau, Deccan flood basalt province, India.,
1192 implications for the volcanostratigraphic architecture of continental flood basalt provinces.
1193 *Journal of the Geological Society London*, 166, 13-24.
- 1194 Jelenska, M., Bakhmutov, V., Konstantinienko, L., 2005. Paleomagnetic and rock magnetic
1195 data from the Silurian succession of the Dniester basin, Ukraine. *Physics of Earth and*
1196 *Planetary Interiors*, 149, 307-320.
- 1197 Johnson, A. H., Nairn, A. E. M., 1972. Jurassic paleomagnetism. *Nature*, 240, 551-552.
- 1198 Jones, D L., Duncan, R A., Briden, J C., Randall, D E., MacNiocaill, C., 2001. Age of the
1199 Batoka basalts, northern Zimbabwe, and the duration of Karoo large igneous province
1200 magmatism. *Geochemistry, Geophysics, Geosystems*, 2, paper no. 2000GC000110.
- 1201 Jupp, P.E. and J.T. Kent 1987. Fitting smooth paths to spherical data. *Applied Statistics*, 36,
1202 34–36.
- 1203 Kent, D.V., Irving, E., 2010. Influence of inclination error in sedimentary rocks on the
1204 Triassic and Jurassic apparent pole wander path for North America and implications for
1205 Cordilleran tectonics. *Journal of Geophysical Research*, 115, B10103,
1206 doi:10.1029/2009JB007205.
- 1207 Kent, D.V., Olsen, E., 2008. Early Jurassic magnetostratigraphy and paleolatitudes from the
1208 Hartford continental rift basin (eastern North America); testing for polarity bias and abrupt
1209 polar wander in association with the Central Atlantic magmatic province. *Journal of*
1210 *Geophysical Research*, 113, no. B6, Citation B06105, doi:10.1029/2007JB005407.
- 1211 Kent, D.V., Tauxe, L., 2005. Corrected Late Triassic latitudes for continents adjacent to the
1212 North Atlantic. *Science*, 307, 240-244.

- 1213 Kent, D.V., Van der Voo, R., 1990. Paleozoic paleogeography from paleomagnetism of the
1214 Atlantic-bordering continents, in: Paleozoic Biogeography, S. McKerrow and C.R. Scotese
1215 (eds.). Geological Society of London Memoir, 12, 4956.
- 1216 Kent, J.T., Briden, J.C. & Mardia, K.V., 1983. Linear and planar structure in ordered
1217 multivariate data as applied to progressive demagnetisation of palaeomagnetic remanence.
1218 Geophysical Journal of the Royal Astronomical Society, 81, 75–87.
- 1219 Khramov, A. N., Iosifidi, A. G., 2009. Paleomagnetism of the Lower Ordovician and
1220 Cambrian sedimentary rocks in the section of the Narva River right bank, for the
1221 construction of the Baltica kinematic model in the early Paleozoic. Izvestiya, Physics Solid
1222 Earth, 45, 465-481.
- 1223 Kidane, T., Platzman, E., Ebinger, C.J., Abebe, B., Rochette, P., 2006. Palaeomagnetic
1224 constraints on continental break-up processes: Observations from the Main Ethiopian Rift,
1225 in Yirgu, G., Ebinger, C.J., Maguire, P.K.H., eds., The Afar Volcanic Province within the
1226 East African Rift System. Geological Society London, Special Publication, 259, 165-183.
- 1227 King, R.F., 1955. The remanent magnetism of artificially deposited sediments. Monthly
1228 Notices Royal Astronomical Society Geophysics Supplement 7, 115-134.
- 1229 Kirschvink, J. L. 1980. The least-squares line and plane and the analysis of paleomagnetic
1230 data. Geophysical Journal of the Royal Astrological Society, 62, 699-718.
- 1231 Klootwijk, C.T., 1996. Phanerozoic configurations of greater Australia: evolution of the north
1232 west shelf. Part two: Palaeomagnetic and geological constraints on reconstructions,
1233 Australian Geol. Surv. Org. Rec. 52, 85 pp.
- 1234 Kluger-Cohen, K., Anderson, T. H., Schmidt, A., 1986. A paleomagnetic test of the proposed
1235 Mojave-Sonora megashear in northwestern Mexico. Tectonophysics, 131, 23-51.
- 1236 Knight, K. .B., Nomade, S., Renne, R., Marzoli, A., Bertrand, H., Youbi, N., 2004. The
1237 Central Atlantic magmatic province at the Triassic-Jurassic boundary; paleomagnetic and
1238 (⁴⁰Ar/ ³⁹Ar evidence from Morocco for brief, episodic volcanism. Earth
1239 and Planetary Science Letters, 228, p.143-160.
- 1240 Kodama, K.P., 2009. Simplification of the anisotropy-based inclination correction technique
1241 for magnetite- and hematite bearing rocks: A case study for the Carboniferous Glenshaw
1242 and Mauch Chunk formations, North America. Geophysical Journal International, 176,
1243 467-477.
- 1244 König, M. & Jokat, W., 2010. Advanced insights into magmatism and volcanism of the
1245 Mozambique Ridge and Mozambique Basin in the view of new potential field data.
1246 Geophysical Journal International, 180, 158–180.

- 1247 Kravchinsky, A., Konstantinov, K.M., Courtillot, V., Savrasov, J.I., Valet, J.P., Cherniy, S.
1248 D., Mishenin, S.G., Parasotka, B.S., 2002. Palaeomagnetism of East Siberian traps and
1249 kimberlites: two new poles and palaeogeographic reconstructions at about 360 and 250 Ma.
1250 Geophysical Journal International, 148, 1–33.
- 1251 Kristjánsson, L., M. T. Gudmundsson, J. L. Smellie, W. C. McIntosh, R. Esser, 2005.
1252 Palaeomagnetic, $^{40}\text{Ar}/^{39}\text{Ar}$, and stratigraphical correlation of Miocene-Pliocene basalts in
1253 the Brandy Bay area, James Ross Island, Antarctica, Antarctic Science, 17, 409-417.
- 1254 Labails C., Torsvik T.H., Gaina C., Cocks, L.R.M., 2009. Global Plate Polygons 2009.
1255 SPlates Model (version 2.0). *NGU Report* 2009.047, 270 pp. (confidential).
- 1256 Labails, C., Olivet, J.L., Aslanian, D., Roest, W.R., 2010, An alternative early opening
1257 scenario for the Central Atlantic Ocean. Earth and Planetary Science Letters 297, 355-368.
- 1258 Larochelle, A., 1971. Note on the paleomagnetism of two diabase dikes, Anticosti Island,
1259 Québec. Geological Association of Canada Proceedings, 23, 73-76.
- 1260 Lange, U., Bröcker, M., Armstrong, R. Żelaźniewicz, A., Trapp, E., Mezger, K. 2005.
1261 Orthogneisses of the Orlica-Śnieżnik complex (West Sudetes, Poland): geochemical
1262 characteristics, the importance of pre-Variscan migmatization and constraints on the cooling
1263 history. Journal of the Geological Society, London, 162, 973-984.
- 1264 Liss, D., Owens, W.H. Hutton, D.H.W., 2004. New palaeomagnetic results from the Whin
1265 Sill Complex: evidence for a multiple intrusion event and revised virtual geomagnetic poles
1266 for the Late Carboniferous for the British Isles. Journal of the Geological Society, London,
1267 161, 927-938.
- 1268 Lotfy, H., Van der Voo, R., 2007. Tropical northeast Africa in the middle–late Eocene:
1269 Paleomagnetism of the marine-mammals sites and basalts in the Fayum province, Egypt.
1270 Journal of African Earth Science, 47, 135-152.
- 1271 Mac Niocaill, C., Smethurst, M.A., 1994. Palaeozoic palaeogeography of Laurentia and its
1272 margins: a reassessment of Palaeomagnetic data. Geophysical Journal International. 116,
1273 715-725.
- 1274 Maciel Peña, R., Goguitchaichvili, A., Garduño Monroy, V.H., Ruiz Martinez, V.C., Aguilar
1275 Reyes, B., Morales, J., Alva-Valdivia, L., Caballero Miranda, C., Urrutia-Fucugauchi, J.,
1276 2009. Paleomagnetic and rock-magnetic survey of Brunhes lava flows from Tancitaro
1277 volcano, Mexico. Geofisica Internacional, 48, 375-384.
- 1278 Mankinen, E.A., 2008. Paleomagnetic study of late Miocene through Pleistocene igneous
1279 rocks from the southwestern USA: Results from the historic collections of the U.S.
1280 Geological Survey Menlo Park laboratory. Geochemistry, Geophysics, Geosystems, 9(5),

- 1281 Q05017, doi:10.1029/2008GC001957.
- 1282 Marcano, M.C., Van der Voo, R., Mac Niocaill, C., 1999. True polar wander during the
1283 Permo-Triassic. *Journal of Geodynamics*, 28, 75-95.
- 1284 Matte, P., 2001. The Variscan collage and orogeny (480-290 Ma) and the tectonic definition
1285 of the Armorica Microplate; a review. *Terra Nova*, 13, 122-128.
- 1286 McCausland, J.A., Van der Voo, R., Hall, C.M., 2007. Circum-Iapetus paleogeography of the
1287 Precambrian-Cambrian transition with a new paleomagnetic constraint from Laurentia.
1288 *Precambrian Research*, 156, 125-152.
- 1289 McElhinny, M. W., 1973. Paleomagnetism and Plate Tectonics. Cambridge University Press,
1290 Cambridge, 358 pp.
- 1291 McKerrow, W.S., Mac Niocaill, C., Alberg, P., Clayton, G., Cleal, C., Eagar, M., 2000a. The
1292 Late Palaeozoic Relations Between Gondwana and Laurussia. In: Franke, W., Haak, V.,
1293 Oncken, O., Tanner, D. (eds), *Orogenic Processes: Quantification and Modelling in the*
1294 *Variscan Belt of Central Europe*, Geological Society of London Special Publication, 179, 9-
1295 20.
- 1296 McKerrow, W.S., Mac Niocaill, C., Dewey, J.F., 2000b. The Caledonian Orogeny redefined.
1297 *Journal of the Geological Society London*, 157, 1149-1154.
- 1298 Meert, J.G., Van der Voo, R., 1997. The assembly of Gondwana 800–550 Ma. *J. Geodynamics*, 23, 223–235.
- 1300 Meert, J.G., Nédélec, A., Hall, C. M., 2003. The stratoid granites of central Madagascar:
1301 Paleomagnetism and further age constraints on Neoproterozoic deformation. *Precambrian*
1302 *Research*, 120, 101-129.
- 1303 Meert, J.G., Tamrat, E., 2006. Paleomagnetic evidence for a stationary Marion hotspot:
1304 Additional paleomagnetic data from Madagascar. *Gondwana Research*, 10, 340-348.
- 1305 Meijers, M.J.M., Hamers, M.F., van Hinsbergen, D.J.J., van der Meer, D.G., Kitchka, A.,
1306 Langereis, C.G., Stephenson, R. A., 2010. New late Paleozoic paleopoles from the Donbas
1307 Foldbelt (Ukraine): implications for the Pangea A vs. B Controversy. *Earth and Planetary*
1308 *Science Letters*, 297, 18-33.
- 1309 Mejia, V., Böhnel, H., Opdyke, N. D., Ortega-Rivera, M. A., Lee, J. K. W., Aranda-Gomez,
1310 J. J., 2005. Paleosecular variation and time-averaged field recorded in late Pliocene-
1311 Holocene lava flows from Mexico. *Geochemistry, Geophysics, Geosystems*, 6, Q07H19,
1312 doi:10.1029/2004GC000871.

- 1313 Mihut, D., R.D. Müller, 1998. Volcanic margin formation and Mesozoic rift propagators in
1314 the Cuvier abyssal plain off Western Australia. *Journal of Geophysical Research*, 103,
1315 27135-27150.
- 1316 Mitchell, R.N., Evans, D.A.D., Kilian, T.M, 2010. Rapid Early Cambrian rotation of
1317 Gondwana. *Geology*. 38, 755-758.
- 1318 Molina-Garza, R. S., Ortega-Rivera, A., 2006. Chronostratigraphy and paleomagnetism of the
1319 Balsas Group in the Tuzantlán-Copalillo basin, northern Guerrero state, Mexico. *Revista*
1320 *Mexicana de Ciencias Geologicas*, 23(2), 215-232.
- 1321 Montelli, R., Nolet, G., Dahlen, F., Masters, G., Engdahl, E., Hung, S., 2004. Finite-frequency
1322 tomography reveals a variety of mantle plumes. *Science* 303, 338-343.
- 1323 Morel, P., Irving, E., 1978. Tentative paleocontinental maps for the early Phanerozoic and
1324 Proterozoic. *Journal of Geology*, 86, 535-561.
- 1325 Mosar, J., Lewis, G., Torsvik, T.H., 2002. North Atlantic sea-floor spreading rates:
1326 implications for the Tertiary development of inversion structures of the Norwegian-
1327 Greenland Sea. *J. Geol. Soc. Lond.* 159, 503-515.
- 1328 Muttoni, G., Kent, D.V., Garzanti, E., Bracke, P., Abrahamsen, N., Gaetani, M., 2003. Early
1329 Permian Pangea B' to Late Permian Pangea A'. *Earth Planetary Science Letters*, 215, 379-
1330 394.
- 1331 Nawrocki, J., Fanning, M., Lewandowska, A., Polechonska, O., Werner, T., 2008.
1332 Palaeomagnetism and the age of the Cracow volcanic rocks (S Poland). *Geophysical Journal*
1333 International, 174, 475–488.
- 1334 Oakey, G.N. & Damaske, D., 2006. Continuity of basement structures and dyke swarms in the
1335 Kane Basin region of central Nares Strait constrained by aeromagnetic data. *Polarforschung*,
1336 74, 51–62.
- 1337 O'Connell, R.J., Gable, C.W., Hager, B.H., 1991. Toroidal-poloidal partitioning of
1338 lithospheric plate motions, in *Glacial Isostasy, Sea-Level and Mantle Rheology*, edited by
1339 R. Sabadini, pp. 535–551, Kluwer Acad., Dordrecht, Netherlands.
- 1340 O'Neill, C., Müller, R. D., Steinberger, B., 2005. On the uncertainties in hot spot
1341 reconstructions and the significance of moving hot spot reference frames. *Geochem.*
1342 *Geophys. Geosyst.*, 6, Q04003, doi:10.1029/2004GC000784.
- 1343 Palencia-Ortas, A., Ruiz-Martínez, V.C., Villalaín, J.J., Osete, M.L., Vegas, R., Touil, A.,
1344 Hafid, A., McIntosh, G., van Hinsbergen, D.J.J., Torsvik, T.H., 2011. A new 200 Ma
1345 paleomagnetic pole for Africa, and paleo-secular variation scatter from Central Atlantic

- 1346 Magmatic Province (CAMP) intrusives in Morocco (Ighrem and Foum Zguid dykes).
1347 Geophysical Journal International, 185, 1220–1234.
- 1348 Pavlov, E., Courtillot, V., Bazhenov, M. L., Veselovsky, R. V., 2007. Paleomagnetism of the
1349 Siberian Traps; new data and a new overall 250 Ma pole for Siberia. Tectonophysics, 443,
1350 72-92.
- 1351 Pavlov, V., Bachtadse, V., Mikhailov, V., 2008. New Middle Cambrian and Middle
1352 Ordovician palaeomagnetic data from Siberia; Llandelian magnetostratigraphy and relative
1353 rotation between the Aldan and Anabar-Angara blocks. Earth and Planetary Science Letters,
1354 276, 229-242.
- 1355 Pavoni, N. 1985. Pacific/anti-Pacific bipolarity in the structure of the Earth's mantle. Eos
1356 Trans. AGU, 66, 497.
- 1357 Petronis, M.S., Hacker, D.B., Holm, D.K., Geissman, J.W., Harlan, S., 2004. Magmatic flow
1358 paths and palaeomagnetism of the Miocene Stoddard Mountain laccolith, Iron Axis region,
1359 Southwestern Utah, USA, in Martin-Hernandez, F., Luneberg, C.M., Aubourg, C., Jackson,
1360 M., eds., Magnetic Fabric: Methods and Applications. Geological Society London, Special
1361 Publications, 238, 251-283.
- 1362 Plado, J., Preeden, U., Pesonen, L.J., Mertanen, S., Puura, V., 2010. Magnetic history of Early
1363 and Middle Ordovician sedimentary sequence, northern Estonia. Geophysical Journal
1364 International, 180, 147-157.
- 1365 Piper, J.D.A., 2006. A ~90° Late Silurian-Early Devonian apparent polar wander loop: The
1366 Latest inertial interchange of planet earth? Earth and Planetary Science Letters, 250, 345-
1367 357.
- 1368 Rakotosolofo, N. A., Tait, J. A., Carlotto, V., Cárdenas, J., 2006. Palaeomagnetic results from
1369 the Early Permian Copacabana Group, southern Peru: Implication for Pangea
1370 palaeogeography. Tectonophysics, 413, 287-299.
- 1371 Rapalini, A. E, Fazzito, S., Orue, D., 2006. A new Late Permian paleomagnetic pole for stable
1372 South America; the Independencia Group, eastern Paraguay. Earth, Planets and Space, 58,
1373 1247-1253.
- 1374 Rehnström, E.F., Torsvik, T.H., 2003. Cambrian sediments and Proterozoic granites in the
1375 Dividalen-Torneträsk area, northern Scandinavia; palaeomagnetism and U-Pb
1376 geochronology. Geol. Foren. Stockholm Forh., 125, 131-138.
- 1377 Reynolds, R.L., Goldhaber, M.B., Snee, L.W., 1997. Paleomagnetic and $^{40}\text{Ar}/^{39}\text{Ar}$ results
1378 from the Grant intrusive breccia and comparison to the Permian Downeys Bluff sill –

- 1379 evidence for Permian igneous activity at Hicks Dome, southern Illinois Basin, U.S.
1380 Geological Survey Bulletin, 2094-G, 16 pp.
- 1381 Ricard, Y., Doglioni, C., Sabbadini, R., 1991. Differential rotation between lithosphere and
1382 mantle; a consequence of lateral mantle viscosity. *Journal of Geophysical Research*, 96
1383 (B5), 8407-8415.
- 1384 Riisager, J., Riisager, P., Pedersen, A.K., 2003a. The C27n-C26r geomagnetic polarity
1385 reversal recorded in the West Greenland flood basalt province: How complex is the
1386 transitional field? *Journal of Geophysical Research*, 108, 2155, doi:10.1029/2002JB002124.
- 1387 Riisager, J., Riisager, P., Pedersen, A.K., 2003b. Paleomagnetism of large igneous provinces:
1388 Case-study from West Greenland, North Atlantic igneous province. *Earth and Planetary
1389 Science Letters*, 214, 409-425.
- 1390 Riisager, P., Knight, K.B., Baker, J.A., Ukstins Peate, I., Al-Kadasi, M., Al-Subbary, A.,
1391 Renne, P.R., 2005. Paleomagnetism and $^{40}\text{Ar}/^{39}\text{Ar}$ Geochronology of Yemeni Oligocene
1392 volcanics: Implications for timing and duration of Afro-Arabian traps and geometry of the
1393 Oligocene paleomagnetic field. *Earth and Planetary Science Letters*, 237, 647-672.
- 1394 Ritsema, H.J., van Heijst, J.H., Woodhouse, J.H., 1999. Complex shear velocity structure
1395 beneath Africa and Iceland. *Science* 286, 1925-1928.
- 1396 Rochette, P., Vandamme, D., 2001. Pangea B: an artifact of incorrect paleomagnetic
1397 assumptions? *Annali Geofisicae*, 44, 649-58.
- 1398 Ruiz-Martínez, V.C., Urrutia-Fucugauchi, J., Osete, M L., 2010. Palaeomagnetism of the
1399 western and central sectors of the Trans-Mexican volcanic belt; implications for tectonic
1400 rotations and palaeosecular variation in the past 11 Ma. *Geophysical Journal International*,
1401 180, 577-595.
- 1402 Runcorn, S.K., 1956. Palaeomagnetic comparisons between Europe and North America.
1403 *Proceedings of the Geological Association of Canada*, 8, 77-85.
- 1404 Runcorn, S.K., 1965. Palaeomagnetic comparisons between Europe and North America.
1405 *Philosophical Transactions of the Royal Society of London, Series A, Mathematical and
1406 Physical Sciences*, 258 (1088) 1-11.
- 1407 Schmidt, P.W., Embleton, B.J.J., 1990. The palaeomagnetism of the Tumblagooda Sandstone,
1408 Western Australia; Gondwana Palaeozoic apparent polar wandering. *Physics of the Earth
1409 and Planetary Interiors*, 64, 303-313.
- 1410 Schmidt, A.G., Riisager, P., Abrahamsen, N., Riisager, J., Pedersen, A.K., Van der Voo, R.,
1411 2005. Palaeomagnetism of Eocene Talerua Member lavas on Hareøen, West Greenland.
1412 *Bulletin of the Geological Society of Denmark*, 52, 27-38.

- 1413 Seguin, M-K., Singh, A., Fyffe, L., 1985. New paleomagnetic data from Carboniferous
1414 volcanics and red beds from central New Brunswick. *Geophysical Research Letters*, 12, 81-
1415 84.
- 1416 Şengör, A.M.C., Yilmaz, Y., Sungurlu, O., 1984. Tectonics of the Mediterranean
1417 Cimmerides: Nature and evolution of the western termination of Paleo-Tethys. *Geological
1418 Society London Special Publication*, 17, 77-112.
- 1419 Shatsillo, A.V., Paverman, V.I., Pavlov, V.E. 2007. Middle Paleozoic segment of the apparent
1420 polar wander path from the Siberian platform: New palaeomagnetic evidence for the
1421 Silurian of the Nyuya-Berezovskii facial province. *Izvestiya, Physics of the Solid Earth*, 43,
1422 880-889.
- 1423 Shive, N., Frerichs, W.E., 1974. Paleomagnetism of the Niobrara Formation in Wyoming,
1424 Colorado, and Kansas. *Journal of Geophysical Research*, 79, 3001-3007.
- 1425 Somoza, R., 2007. Eocene paleomagnetic pole for South America: Northward continental
1426 motion in the Cenozoic, opening of Drake Passage and Caribbean convergence. *Journal of
1427 Geophysical Research B Solid Earth*, 112, B03104, doi:10.1029/2006JB004610.
- 1428 Somoza, R., Zaffarana, C.B., 2008. Mid-Cretaceous polar standstill of South America, motion
1429 of the Atlantic hotspots and the birth of the Andean Cordillera. *Earth and Planetary Science
1430 Letters*, 271, 267-277.
- 1431 Steinberger, B., Torsvik, T.H., 2008. Absolute plate motions and true polar wander in the
1432 absence of hotspot tracks. *Nature*, 452, 620-623.
- 1433 Steinberger, B., Torsvik, T.H., 2010. Toward an explanation for the present and past locations
1434 of the poles. *Geochem. Geophys. Geosyst.*, 11, doi:10.1029/2009GC002889.
- 1435 Steiner, M.B., Helsley, C.E., 1974. Magnetic polarity sequence of the Upper Triassic Kayenta
1436 Formation. *Geology*, 2, 191-194.
- 1437 Steiner, M.B., 2003. A cratonic Middle Jurassic paleopole; Callovian-Oxfordian stillstand (J-2
1438 cusp), rotation of the Colorado Plateau, and Jurassic North American apparent polar wander.
1439 *Tectonics*, 22, 1020, doi:10.1029/2001TC001284.
- 1440 Storey, M., Mahoney, J.J., Saunders, A.D., Duncan, R.A., Kelley, S.P., Coffin, M.F., 1995.
1441 Timing of hot spot-related volcanism and the break-up of Madagascar and India, *Science*
1442 267, 852-855.
- 1443 Symons, D.T.A., Bormann, R.E., Jans, R.P., 1989. Paleomagnetism of the Triassic red beds of
1444 the lower Fundy Group and Mesozoic tectonism of the Nova Scotia Platform, Canada.
1445 *Tectonophysics*, 164, 13-24.

- 1446 Symons, D.T.A., Erdmer, P., McCausland, P.J.A., 2003. A new cratonic North American
1447 paleomagnetic pole from the Yukon shows post-Eocene mobility of the Canadian
1448 Cordilleran terranes. *Canadian Journal of Earth Science*, 40, 1321-1334.
- 1449 Symons, D.T.A., Kawasaki, K., McCausland, J.A., 2009. The Yukon-Tanana terrane: Part of
1450 North America at ~215 Ma from paleomagnetism of the Taylor Mountain batholith, Alaska.
1451 *Tectonophysics*, 465, 60-74.
- 1452 Szuradies, M., Bachmann, G.H., Menning, M., Nowaczyk, N.R. Kaeding, K.C., 2003.
1453 Magnetostratigraphy and high-resolution lithostratigraphy of the Permian-Triassic boundary
1454 interval in central Germany. *Earth and Planetary Science Letters*, 212, 263-278.
- Szuradies, M., 2004. Magnetostratigraphy; the key to a global correlation of the classic
Germanic Trias; case study Volpriehausen Formation (middle Buntsandstein), central
Germany. *Earth and Planetary Science Letters*, 227, 395-410.
- Tan, X.D., Kodama, K.P., Gilder, S., Courtillot, V., 2007. Rock magnetic evidence for
inclination shallowing in the Passaic Formation red beds from the Newark basin and a
systematic bias of the Late Triassic apparent polar wander path for North America. *Earth*
and Planetary Science Letters, 254, 345-357.
- Tarduno, J. A., 2007. On the motion of Hawaii and other mantle plumes. *Chemical Geology*,
241, 234-247.
- 1455 Tarduno, J.A., Cottrell, R.D., Smirnov, A.V., 2001. High geomagnetic intensity during the
1456 Mid-Cretaceous from Thellier analysis of single plagioclase crystals. *Science*, 291, 1779-
1457 1783.
- 1458 Tauxe, L., 2005. Inclination flattening and the geocentric axial dipole hypothesis. *Earth and*
1459 *Planetary Science Letters*, 233, 247-261.
- 1460 Tauxe, L., 2009. Essentials of Paleomagnetism: Web Edition 1.0 (<http://magician.ucsd.edu/Essentials/>)
- 1462 Tauxe, L., Kent, D.V., 1984. Properties of a detrital remanence carried by haematite from
1463 study of modern river deposits and laboratory redepositiomm sediments. *Geophysical*
1464 *Journal of the Royal Astronomical Society*, 76, 543-561.
- 1465 Tauxe, L., Kent, D.V., 2004. A simplified statistical model for the geomagnetic field and the
1466 detection of shallow bias in paleomagnetic inclinations: was the ancient magnetic field
1467 dipolar? in: *Timescales of the paleomagnetic field*, J. E.T. Channell, D. Kent, W. Lowrie J.
1468 G. Meert, (Eds), *Geophysical Monograph* 145, AGU, Washington, DC, 101 - 117.

- 1469 Tauxe, L., Gans, P., Mankinen, E. A., 2004. Paleomagnetism and $^{40}\text{Ar}/^{39}\text{Ar}$ ages from
1470 volcanics extruded during the Matuyama and Brunhes Chrons near McMurdo Sound,
1471 Antarctica. *Geochemistry, Geophysics, Geosystems*, 5, Q06H12, doi:10.1029/2003
1472 GC000656.
- 1473 Tohver, E., D'Agrella Filho, M., Trindade, R.I.F., 2006, Paleomagnetic record of Africa and
1474 South America for the 1200-500 Ma interval, and evaluation of Rodinia and Gondwana
1475 assemblies. *Precambrian Research*, 147, 193-222.
- 1476 Tohver, E., Trindade, R.I.F., Solum, J.G., Hall, C.M., Riccomini, C., Nogueira, A.C., 2010,
1477 Closing the Clymene Ocean and Bending a Brasiliano belt, Evidence for the Cambrian
1478 formation of Gondwana from SE Amazon craton. *Geology*, 38, 267-270.
- 1479 Tohver, E., Cawood, P.A., Rossello, E.A., F. Jourdan, 2012. Closure of the Clymene Ocean
1480 and formation of West Gondwana in the Cambrian: evidence from the Sierras Australes of
1481 the southernmost Rio de la Plata craton, Argentina". *Gondwana Research*,
1482 doi:10.1016/j.gr.2011.04.001 (in press).
- 1483 Torsvik, T.H., 1998. Palaeozoic Palaeogeography: A North Atlantic viewpoint. *Geol. For.*
1484 *Fohr.*, 120, 109-118.
- 1485 Torsvik, T.H., Smethurst, M.A. 1999. Plate Tectonic modeling: Virtual Reality with GMAP.
1486 *Computer & Geosciences*, 25, 395-402.
- 1487 Torsvik, T.H., Rehnström, E.F, 2001. Cambrian palaeomagnetic data from Baltica:
1488 Implications for true polar wander and Cambrian palaeogeography. *Journal of the*
1489 *Geological Society London*, 158, 321-329.
- 1490 Torsvik, T.H., Van der Voo, R., 2002. Refining the paleogeography of Gondwana and
1491 Pangea: Estimates of Phanerozoic non-dipole (octupole) fields. *Geophysical Journal*
1492 *International*, 151, 771-794.
- 1493 Torsvik, T.H., Rehnström, E.F, 2003. The Tornquist Sea and Baltica-Avalonia docking.
1494 *Tectonophysics*, 362, 67-82.
- 1495 Torsvik, T.H., Cocks, L.R.M., 2004. Earth geography from 400 to 250 million years: a
1496 palaeomagnetic, faunal and facies review. *Journal Geological Society London* 161, 555-572.
- 1497 Torsvik, T.H., Cocks, L.R.M., 2005. Norway in space and time: A Centennial cavalcade.
1498 *Norwegian Journal of Geology*, 85, 73-86.
- 1499 Torsvik, T.H., Cocks, L.R.M., 2009. The Lower Palaeozoic palaeogeographical evolution of
1500 the northeastern and eastern peri-Gondwanan margin from Turkey to New Zealand. In
1501 Bassett, M. G. (ed.) *Early Palaeozoic Peri-Gondwana Terranes: New Insights from*
1502 *Tectonics and Biogeography*. *Geological Society, London, Special Publications*, 325, 3-21.

- 1503 Torsvik, T.H., Cocks, L.R.M., 2011a. New global palaeogeographical reconstructions for the
1504 Lower Palaeozoic and their generation. Memoirs of the Geological Society London (in
1505 press).
- 1506 Torsvik, T.H., Cocks L.R.M., 2011b. The Palaeozoic palaeogeography of central Gondwana.
1507 In Van Hinsbergen, D.J J., Buiter, S.J.H., Torsvik, T.H., Gaina, C., Webb, S.J. (eds) The
1508 Formation and Evolution of Africa: A Synopsis of 3.8 Ga of Earth History. Geological
1509 Society, London, Special Publications, 357, 137–166. DOI: 10.1144/SP357.8
- 1510 Torsvik, T.H., Van der Voo, R., Redfield, T.F., 2002. Frontier - Relative hotspot motions
1511 versus True Polar Wander. Earth and Planetary Science Letters, 202, 185-200.
- 1512 Torsvik, T.H., Smethurst, M.A., Van der Voo, R., Trench, A., Abrahamsen, N., Halvorsen, E.,
1513 1992. Baltica - A synopsis of Vendian-Permian palaeomagnetic data and their
1514 palaeotectonic implications. Earth Science Reviews, 33, 133-152.
- 1515 Torsvik, T.H., Trench, A., Svensson, I., Walderhaug, H.J., 1993. Silurian palaeomagnetic
1516 results from Southern Britain:Palaeogeographic significance and major revision of the
1517 Apparent Polar Wander Path for Eastern Avalonia. Geophysical Journal International, 113,
1518 651-668.
- 1519 Torsvik, T.H., Gaina, C., Steinberg, M., Van der Voo, R., 2006. North Atlantic fits with
1520 implications for the Barents Sea. Norwegian Geol. Survey Industry Report (confidential).
- 1521 Torsvik, T.H., Tucker, R.D., Ashwal, L.D., Carter, L.M., Jamtveit, B., Vidyadharan, K.T.,
1522 Venkataramana, P., 2000. Late Cretaceous India-Madagascar fit and timing of break-up
1523 related magmatism. Terra Nova, 12, 220-224.
- 1524 Torsvik, T.H., Van der Voo, R., Meert, J.G., Mosar, J., Walderhaug, H.J., 2001.
1525 Reconstructions of the continents around the North Atlantic at about the 60th parallell. Earth
1526 Planet. Sci. Lett. 187, 55-69.
- 1527 Torsvik, T.H., Müller, R.D., Van der Voo, R., Steinberger, B., Gaina, C., 2008a. Global plate
1528 motion frames: Toward a unified model. Reviews of Geophysics, 46, RG3004, doi:
1529 10.1029/2007RG000227.
- 1530 Torsvik, T.H., Steinberger, B., Cocks, L.R.M., Burke, K., 2008b. Longitude: Linking Earth's
1531 ancient surface to its deep interior. Earth Planet Science Letters, 276, 273-283.
- 1532 Torsvik, T.H., Gaina, C., Redfield, T.F., 2008c. Antarctica and Global Paleogeography: From
1533 Rodinia, through Gondwanaland and Pangea, to the birth of the Southern Ocean and the
1534 opening of gateways. In Cooper, A. K., P. J. Barrett, H. Stagg, B. Storey, E. Stump, W.
1535 Wise, and the 10th ISAES editorial team (eds.) *Antarctica: A Keystone in a Changing*

- 1536 *World.* Proceedings of the 10th International Symposium on Antarctic Earth Sciences.
1537 Washington, DC: The National Academies Press, 125-140
- 1538 Torsvik, T.H., Smethurst, M.A., Meert, J.G., Van der Voo, R., McKerrow, W.S., Sturt, B.A.,
1539 Brasier, M.D., Walderhaug, H.J., 1996. Continental break-up and collision in the
1540 Neoproterozoic and Palaeozoic - a tale of Baltica and Laurentia. *Earth Science Reviews*,
1541 40, 229-258.
- 1542 Torsvik, T.H., Rousse, S., Labails, C., Smethurst, M.A., 2009. A new scheme for the opening
1543 of the South Atlantic Ocean and dissection of an Aptian Salt Basin. *Geophysical Journal
1544 International*, 177, 1315-1333.
- 1545 Torsvik, T.H. Burke, K., Steinberger, B., Webb, S.C., Ashwal, L.D., 2010a. Diamonds
1546 sourced by plumes from the core mantle boundary. *Nature* 466:doi:10.1038/nature09216352
- 1547 Torsvik, T.H., Steinberger, B., Gurnis, M., Gaina, C., 2010b. Plate tectonics and net
1548 lithosphere rotation over the past 150 My. *Earth and Planetary Science Letters*, 291, 106–
1549 112.
- 1550 Trindade, R. I. F.; D'Agrella Filho, M.S.; Epof, I.; Neves, B.B.B., 2006. Paleomagnetism of
1551 Early Cambrian Itabaiana mafic dikes (NE Brazil) and the final assembly of Gondwana.
1552 *Earth and Planetary Science Letters*, 244, 361-377.
- 1553 Tripati, A., Backman, J., Elderfield, H., Ferretti, P., 2005. Eocene bipolar glaciation
1554 associated with global carbon cycle changes. *Nature*, 436, 341-346.
- 1555 Turner, G.M., Michalk, D.M., Morgans, H.E.G., Walbrecker, J.O., 2007. Early Miocene
1556 magnetostratigraphy and a new palaeomagnetic pole position from New Zealand. *Earth,
1557 Planets and Space*, 59, 841-851.
- 1558 van der Meer, D., Spakman, W., van Hinsbergen, D.J.J., Amaru, M.L., Torsvik, T.H., 2010.
1559 Absolute plate motions since the Permian interred from lower mantle slab remnants. *Nature
1560 Geoscience*, doi:10.1038/NGEO708.
- 1561 Van der Voo, R., 1981. Paleomagnetism of North America: a brief review. In:
1562 Paleoreconstruction of the Continents, M.W. McElhinny D.A. Valencio, eds., Vol. 2
1563 Geodynamics Series, AGU, Washington, D.C., 159-176.
- 1564 Van der Voo, R., 1990. Phanerozoic paleomagnetic poles from Europe and North America
1565 and comparisons with continental reconstructions. *Reviews of Geophysics*, 28, 167-206.
- 1566 Van der Voo, R., 1992. Jurassic paleopole controversy: Contributions from the Atlantic-
1567 bordering continents. *Geology*, 20, 975–978.
- 1568 Van der Voo, R., 1993. Paleomagnetism of the Atlantic, Tethys and Iapetus Oceans,
1569 Cambridge University Press, 411 pp.

- 1570 Van der Voo, R., 1994. True polar wander during the middle Paleozoic? *Earth and Planetary*
1571 *Science Letters*, 122, 239-243.
- 1572 Van der Voo, R. French, R.B., 1974. Apparent polar wander for the Atlantic-bordering
1573 continents: Late Carboniferous to Eocene. *Earth Science Reviews*, 10, 99119.
- 1574 Van der Voo, R., Torsvik, T.H., 2004. The quality of the European Permo-Triassic paleopoles
1575 and its impact on Pangea reconstructions, AGU Monograph on Timescales of the
1576 paleomagnetic field, J. E. T. Channell, D. Kent, W. Lowrie J. G. Meert (Eds.), 29-42.
- 1577 Van der Voo, R., Levashova, N.M., Skrinnik, L.I., Kara, T.V., Bazhenov, M.L., 2006. Late
1578 orogenic, large-scale rotations in the Tien Shan and adjacent mobile belts in Kyrgyzstan and
1579 Kazakhstan, *Tectonophysics*, 426, 335-360.
- 1580 Van Fossen, M.C., Kent, D.V, 1990. High-latitude paleomagnetic poles from Middle Jurassic
1581 plutons and Moat Volcanics in New England and the controversy regarding Jurassic
1582 apparent polar wander for North America. *Journal of Geophysical Research*, 95, p.17,503-
1583 17,516.
- 1584 van Hinsbergen, D.J.J., Straathof, G.B., Kuiper, K.F., Cunningham, W.D., Wijbrans, J.,
1585 2008. No vertical axis rotations during Neogene transpressional orogeny in the NE Gobi
1586 Altai: Coinciding Mongolian and Eurasian early Cretaceous apparent polar wander paths.
1587 *Geophysical Journal International*, 173, 105-126.
- 1588 van Hinsbergen, D.J.J., Lippert, P.C., Dupont-Nivet, G., McQuarrie, N., Doubrovine, P.V.,
1589 Spakman, W. and Torsvik, T.H., 2011a. The Greater India enigma and two-stage collision
1590 during Cenozoic India-Asia convergence. *PNAS* (submitted).
- 1591 van Hinsbergen, D.J.J., Steinberger, B., Doubrovine, P.V., Gassmöller, R., 2011b.
1592 Acceleration and deceleration of India-Asia convergence since the Cretaceous: Roles of
1593 mantle plumes and continental collision. *Journal of Geophysical Research*, 116, B06101,
1594 doi:10.1029/2010JB008051.
- 1595 Vizán, H., Ixer, R., Turner, P., Cortes, J. M., Cladera, G., 2004. Paleomagnetism of Upper
1596 Triassic rocks in the Los Colorados Hill section, Mendoza Province, Argentina. *Journal of*
1597 *South American Earth Science*, 18, 41-59.
- 1598 Walderhaug, H., 1993. Rock magnetic and magnetic fabric variations across three thin
1599 alkaline dykes from Sunnhordland, western Norway; influence of initial mineralogy and
1600 secondary chemical alterations. *Geophysical Journal International*, 115, 97-108.
- 1601 Walderhaug, H.J, Eide, E.A., Scott, R.A., Inger, S. Golionko, E.G., 2005. Paleomagnetism
1602 and $^{40}\text{Ar}/^{39}\text{Ar}$ geochronology from the South Taimyr igneous complex, Arctic Russia; a

- 1603 Middle-Late Triassic magmatic pulse after Siberian flood-basalt volcanism. Geophysical
1604 Journal International, 163, 501-517.
- 1605 Wegener, A., 1912. Die Entstehung der Kontinente. Petermanns Geographische Mitteilungen,
1606 58 (I), 1-309.
- 1607 Weil, A.B., Yonkee, A., Sussman, A., 2010. Reconstructing the kinematic evolution of curved
1608 mountain belts: A paleomagnetic study of Triassic red beds from the Wyoming salient,
1609 Sevier thrust belt, U.S.A. Geological Society of America Bulletin, 122, 3-23.
- 1610 Wessel, P., Smith, W.H.F. 1991. Free software helps map and display data. Eos 72, 441.
- 1611 Yan, M.D., Van der Voo, R., Tauxe, L., Fang, X.M., Parés, J.M., 2005. Shallow bias in
1612 Neogene paleomagnetic directions from the Guide Basin, NE Tibet, caused by inclination
1613 error. Geophysical Journal International, 163, 944-948.
- 1614 Yuan, K., Van der Voo, R., Bazhenov, M.L., Bakhmutov, V., Alekhin, V., Hendriks, B.W.H.,
1615 2011. Permian and Triassic Paleolatitudes of the Ukrainian Shield with Implications for
1616 Pangea Reconstructions. Geophysical Journal International, 184, 595-610.
- 1617 Zhong, S., Zhang, N., Li, Z.-X., Roberts, J.H., 2007. Supercontinent cycles, true polar
1618 wander, and very long-wavelength mantle convection. Earth Planetary Science Letters 261,
1619 551–564.
- 1620 Zijderveld, J.D.A., 1975. Paleomagnetism of the Estérel rocks. PhD Thesis, University of
1621 Utrecht, 199 pp.

1622

1623

1624 FIGURE CAPTIONS

1625 **FIGURE 1** In (a) the situation depicted is that of a moving continent and a fixed polar axis;
1626 this used to be called "continental drift" before the term "plate tectonics" took over. As the
1627 continent drifts steadily northward during the last 60 million years, the magnetic field
1628 direction at a site in the continent gets recorded by rocks, which then retain a memory of these
1629 changing directions (declination and inclination) as a function of time. In (b) the situation is
1630 that the continent stays fixed, but that the polar axis is left to wander while following a path
1631 called Apparent Polar Wander Path. The word "apparent" denotes the caution that this
1632 wandering may or may not be real and that in reality the situation could be as in (a). The
1633 sequential locations of the poles are calculated from the declinations and inclinations in the
1634 Indian rocks. If all continents show the same apparent polar wander path, then they shared
1635 the same coherent motion with respect to the pole. In that case, it is warranted to call the path
1636 a True Polar Wander Path. Figure is based on Tauxe (2009) but here we show palaeomagnetic
1637 poles (60, 40 and 20 Ma) and reconstructions of India based on the global APWP developed
1638 in this paper. Stereographic (Wulff) projection.

1639 **FIGURE 2** World map with palaeomagnetic sampling sites for palaeomagnetic poles used
1640 in the present data compilation ([Table 1](#)). Their symbols and colours are differentiated by
1641 geological eras. Thin black lines are old terrane boundaries. Palaeomagnetic data are
1642 excluded from white areas. The oceanic areas show present day plate boundaries draped on
1643 satellite bathymetry (Smith and Sandwell, 1997). MAD=Madagascar, DML=Dronning Maud
1644 Land, NZ>New Zealand, TS=Tasmania, K=Kerguelen.

1645
1646 **FIGURE 3** Age frequency histogram (10 Myr bins) of palaeomagnetic poles ([Table 1](#))
1647 compiled in this study. Poles are subdivided into those obtained from detrital sedimentary
1648 rocks (labelled "clastics") and those of volcanic rocks/limestone. Note the near-total absence
1649 of reliable palaeomagnetic poles for Early Carboniferous (350-360 Ma) and Mid-Devonian
1650 (380-390 Ma) times.

1651 **FIGURE 4** (a) Phanerozoic time scale and icehouse (cold) vs. greenhouse (hot) conditions.
1652 (b) Schematic evolution for the formation and break-up of Pangaea (main continental
1653 players): The bulk of Pangaea formed by collision of Gondwana and Laurussia (Laurentia and
1654 Baltica/Avalonia that fused in the Mid Silurian) in the Late Carboniferous followed by Siberia

1655 in Late Permian-Triassic times. First major break-up was witnessed by the Early Jurassic
1656 opening of the Central Atlantic and separation of Gondwana and Laurasia. The Pangaea 250
1657 Ma reconstruction is an ‘absolute’ reconstruction with land, shelf and a modelled oceanic age
1658 grid (red is young, blue is old oceanic crust). Distribution of Siberian Trap rocks shown in
1659 yellow. The top reconstruction is for 150 Ma (relative to SAFR, southern Africa, held fixed)
1660 and is also shown with an oceanic age grid. SAFR serves as the reference continent relative to
1661 which the motion of all other plates is determined since Pangaea formation (ca. 320 Ma).
1662 Laurasia, West- and East-Gondwana continental elements shown with light brown, grey and
1663 dark grey shading. Abbreviations: EUR, stable Europe; GRE, Greenland; NAM, North
1664 America; NWAFR, northwest Africa; NEAFR, northeast Africa; ARAB, Arabia; SOM,
1665 Somalia; AMA, Amazonia (South America); PAR, Parana; COL, Colorado; PAT, Patagonia;
1666 IND, India; MAD, Madagascar; EANT, East Antarctica; AUS, Australia. (c) Continental
1667 (latitude) mass centre calculated from our plate polygon model. Mass centre calculation also
1668 includes the areas of submerged continental crust between coastlines and the continent-ocean
1669 boundary [e.g., light grey areas in 150 Ma reconstruction in (b)].

1670

1671 **FIGURE 5** The outline of Laurussia, plotted on a ca. 420 Ma reconstruction. Area of
1672 Caledonide orogenic deformation is tinted light brown, and the white lines from east
1673 Greenland to Scotland and in Norway represent the Caledonide Nappe Front. FJL, Franz Josef
1674 Land; IS, Iapetus Suture; NZ, Novaya Zemlya; SVB, Svalbard; WI, Wrangel Island.
1675 Simplified from Cocks and Torsvik (2011).

1676

1677 **FIGURE 6** (a) 95% confidence ovals for Laurentian input poles (white shading) and a fitted
1678 spherical spline path. The spline path is moderately smoothed (smoothing factor = 300) and
1679 input poles have been weighted by their Q-factor (see Torsvik et al., 1992, 1996 for
1680 procedure). Detrital sedimentary input poles and spline path are shown after correction for
1681 potential I-errors (flattening factor f of 0.6). (b) Running Mean path (20 M.y. window) shown
1682 with A95 ovals (grey shading) after I-error correction (black thick lines with ages in million
1683 years) and a running mean path without correction for inclination shallowing (black stippled
1684 line with no A95’s). A95 or dp/dm ovals are blue about a given palaeomagnetic pole if it is
1685 the only entry for its bin. Dark grey dots (black curve) are purely interpolated mean poles.
1686 *The recommended APWP is the spline path in (a). Orthogonal projection.*

1687 **FIGURE 7 (a)** 95% confidence ovals for Baltica/Stable Europe input poles (white shading)
1688 and a fitted spherical spline path. The spline path is moderately smoothed (smoothing
1689 factor=300) and input poles have been weighted by their Q-factor. Detrital sedimentary input
1690 poles and spline path shown after correction for potential inclination shallowing. Inset map
1691 shows Cambrian and Early Ordovician path segments based on spline fitting. **(b)** Running
1692 Mean path shown with A95 ovals (grey shading) after sedimentary inclination correction
1693 (black thick lines with ages in million years) and a running mean path without correction for
1694 inclination shallowing (black stippled line with no A95's). A95 or dp/dm ovals are white
1695 about a given palaeomagnetic pole if it is the only entry for its bin. Dark grey dots (black
1696 thick curve) are purely interpolated mean poles. *The recommended APWP is the spline path in*
1697 *(a).* Orthogonal projection

1698 **FIGURE 8 (a)** Running Mean paths for Baltica/Stable Europe and Laurentia (rotated to
1699 European co-ordinates), shown with A95 ovals. Dark grey dots are purely interpolated mean
1700 poles. Both paths are corrected for inclination shallowing in detrital sedimentary rocks **(b)**
1701 Same as (a) but not corrected for inclination shallowing and shown without A95's. **(c)** Great-
1702 circle distance (GCD) between poles of the same age from Baltica/Stable Europe and
1703 Laurentia with (black line) and without (grey thick line) correction for potential inclination
1704 shallowing.

1705

1706 **FIGURE 9 (a)** Combined spline path (smoothing 300, Q-factor weighted) for Laurussia and
1707 Laurasia (after 250 Ma). **(b)** Running Mean paths for Laurussia/Laurasia shown with (black
1708 line with grey A95's) and without (black stippled line) correction for inclination shallowing.
1709 Dark grey dots are purely interpolated mean poles. White oval represent a single dp/dm oval
1710 (Catskill Formation South pole, [Table1](#)). *The recommended APWP is the spline path in (a).*

1711 **FIGURE 10** Outline of Gondwana and peri-Gondwana, plotted on a 480 Ma
1712 reconstruction. Black lines are old terrane boundaries. Our palaeomagnetic compilation is
1713 only derived from areas shaded in dark green and does not include Ordovician data from peri-
1714 Gondwana terranes (e.g. Avalonia and ATA). ATA=Amorican Terrane Assemblage;
1715 MBL=Marie Bird Land; FI=Falkland Islands; DML=Dronning Maud Land;
1716 MAD=Madagascar. After Torsvik and Cocks (2011).

1717 **FIGURE 11** (a) 95% confidence ovals for Gondwana input poles in Southern Africa co-
1718 ordinates (white shading) and a fitted spherical spline path. The spline path uses a smoothing
1719 factor of 500 and input poles are weighted by their Q-factor. Spline path shown after
1720 correction for potential inclination shallowing. (b) Running Mean path (20 Myr window)
1721 shown with A95 ovals (grey shading) after sedimentary inclination correction (black thick
1722 lines with ages in million years) and a running mean path without correction for inclination
1723 shallowing (black stippled line with no A95's). White A95 ovals are dp/dm ovals from a
1724 single palaeomagnetic pole. Dark grey dots (black curve) are purely interpolated mean poles.
1725 *The recommended APWP is the spline path in (a).* Orthogonal projection.

1726 **FIGURE 12** (a) Revised APWP for Siberia (after Cocks and Torsvik 2007). Spline path
1727 with smoothing parameter of 300 and Q-factor weighted input poles. This path is based on
1728 one new Silurian pole (433 Ma; Shatsillo et al., 2007) and elimination of two similar-aged and
1729 less reliable poles from Siberia (see text). The Siberian spline path (black thick line) is
1730 compared with the spline path for Baltica (Fig. 7a).

1731 **FIGURE 13** (a) Bottom: Running Mean paths for Gondwana (thick black curve) and
1732 Laurussia/Laurasia (rotated to Southern Africa co-ordinates) shown with A95 ovals. Both
1733 paths are corrected for inclination shallowing. Top: Great-circle distance (GCD) between
1734 poles of the same age from Gondwana and Laurentia with (black thin line) and without (grey
1735 thick line) correction for inclination shallowing. (b) Global running mean APWP (GAPWaP),
1736 corrected (black line with A95's) and uncorrected (stippled line) for inclination shallowing.
1737 (c) Global spline path (smoothing parameter of 300 and Q-factor weighted input poles)
1738 compared with the running mean path in (b). Both are corrected for potential I-error. *The*
1739 *recommended APWP is the running mean path in (c).*

1740 **FIGURE 14** (a) Comparison of our new running mean GAPWaP (Fig. 13c) with that of
1741 Kent and Irving (2010) for the 50-230 Ma range. Mean South Poles are shown in Southern
1742 African co-ordinates as previous diagrams. (b) Same as (a) but shown as north poles in North
1743 American co-ordinates in the 320-140 Ma range (compare with fig. 4 in Kent and Irving
1744 2010).

1745

1746 **FIGURE 15** (a) Palaeozoic latitudinal drift for a location in Europe (black curve, 60°N,
1747 10°E) and North America (red curve, 60°N, 308°E) based on Baltica/Stable Europe and

1748 Laurentia spline paths. **(b)** Latitudinal velocities for Europe (light grey shaded histograms)
1749 and North America (black stippled curve) separated into northward and southward (minimum
1750 velocities, because palaeo-longitude is 'unknown'). After 430 Ma, Baltica/Laurentia have
1751 been combined into Laurussia and calculations were based on 60°N, 10°E (in European
1752 reference frame), and histograms are shaded dark grey for northward motion and white for
1753 southward motion. **(c)** Angle of rotation of Europe, North America and Laurussia; colours in
1754 analogy to (b). Laurentia curves are rotated to European frame before calculations.

1755

1756 **FIGURE 16** (a) Gondwana Palaeozoic latitudinal drift for a location in Africa (0°, 30°E)
1757 based on the Gondwana spherical spline path in Fig. 11a (b) Latitudinal velocities separated
1758 into northward and southward. (c) Angle of rotation separated into clockwise and counter-
1759 clockwise rotations.

1760

1761 **FIGURE 17** Late Cambrian and Late Ordovician reconstructions in orthogonal projection.
1762 The major continents are described in the main text but on our Palaeozoic maps we also
1763 tentatively show Arctic Alaska. Our present tectonic model takes into account results of new
1764 studies (e.g., Oakey and Damaske, 2006; Dawes, 2009) that postulate minor to moderate
1765 strike-slip motion along the Nares Strait (between Greenland and the southernmost Ellesmere
1766 Island) during the opening of the Labrador Sea and Baffin Bay. SW Ellesmere, including
1767 Devon Island, are semi-locked to the Greenland plate, and the other Ellesmerian Terranes
1768 (four in total in our model) are kept semi-locked to North America, until the Early Tertiary
1769 Eurekan Orogenesis (that continued until 33 Ma) caused compression within the combined
1770 'Greenland-SW Ellesmere-Arctic Canada' plate. Svalbard was composed of three or possible
1771 four different terranes, here portrayed as two principal terranes, both of Laurentia affinity,
1772 which were later juxtaposed by sinistral strike-slip faulting and subsequently transferred to the
1773 European plate (Cocks and Torsvik 2011).

1774

1775 **FIGURE 18** Early Devonian and Early Carboniferous (poor data coverage, see Fig. 3)
1776 reconstructions. Orthogonal Projection.

1777 **FIGURE 19** Late Carboniferous/Early Permian and Late Permian/Early Triassic
1778 reconstructions. Orthogonal Projection. Permo-Carboniferous ice-sheet after Torsvik and
1779 Cocks (2004).

1780 **FIGURE 20** (a) Latitudinal drift for a location in Africa (0° , 30°E) based on the GAPWaP
1781 (running mean path with I-error correction, Fig. 14a. (b) Latitudinal velocities separated into
1782 northward and southward drift. (c) Angle of rotation separated into clockwise (CW) and
1783 counterclockwise (CCW) rotations. Stippled lines in (b, c) between 250 and 100 Ma after
1784 correction for TPW with two black arrows demonstrating the large reduction in angular
1785 rotation after TPW correction.

1786 **FIGURE 21** Late Triassic/Early Jurassic and Late Jurassic reconstructions in orthogonal
1787 projection.

1788 **FIGURE 22** Cretaceous and Palaeogene reconstructions in orthogonal projection.

1789 **FIGURE 23** Cumulative rotation and north–south motion averaged for ‘all’ continents
1790 based on the GAPWaP. Solid black line shows rotation around an equatorial axis at the same
1791 longitude as the centre of mass of ‘all’ continents (green dots in Fig. 24), and positive values
1792 for a given time correspond to clockwise (CW) rotation since that time. Solid brown line
1793 shows rotation around an equatorial axis orthogonal to the first axis; negative values for a
1794 given time correspond to northward motion of continents since that time. Stippled lines are in
1795 a new reference frame, similar to the palaeomagnetic one, except that rotations (listed in the
1796 inset box) around an equatorial axis (0° , 11°E) at constant rate have been subtracted from the
1797 African plate motion.

1798

1799 **FIGURE 24** Motions of continents reconstructed in the palaeomagnetic reference frame
1800 during four time intervals. Total motions are shown as black lines, connected to blue dots
1801 (locations at the beginning of the time intervals). Large green dots with thick black lines
1802 indicate location and motion of the centre of mass of ‘all’ continents. Eurasia is here shown
1803 for reasons of simplicity as a coherent plate, but at the time of the lowermost diagram, for
1804 example, north and south China were in reality not part of Eurasia/Pangaea. Yellow dots
1805 marked A and P are the centres of mass for the African and the near antipodal Pacific
1806 LLSVPs (outlines above core-mantle boundary shown in red, based on the SMEAN
1807 tomography model of Becker and Boschi (2002)) (see text). Open white circle is the preferred
1808 centre for TPW. Blue and pink shading represent reconstruction at the start and at the end of
1809 the TPW episode.

1810

1811 **FIGURE 25** (a) Southern Africa GAPWaP (Fig. 14a) corrected for TPW 250-100 Ma
1812 (black line). (b) APW (10 Myr bins) before (black double line) and after TPW correction
1813 (black thick line). The most dramatic change occurs between 110 and 100 Ma although this
1814 segment is not seen as a cusp/bend in the APWP in (a). (c) Net lithosphere rotation (NR) for
1815 continents before (dark grey bars) and after TPW correction (thick black line). A more
1816 appropriate treatment of NR, calculated from both continental and oceanic lithosphere for the
1817 past 150 Myr (Torsvik et al., 2010), is shown as thick brown line. Episodes of clockwise
1818 (CW) and counter-clockwise (CCW) TPW are shaded.

1819

1820 **FIGURE 26** APW rates for Gondwana and Laurussia from 330 Ma and older. Laurussia
1821 from 330 to 530 Ma and before that is only based on Laurentia. Typical rates since Pangaea
1822 assembly are shown as grey shading (mean and standard deviation) and a black stippled
1823 double line (maximum). St.Dev, Standard deviation.

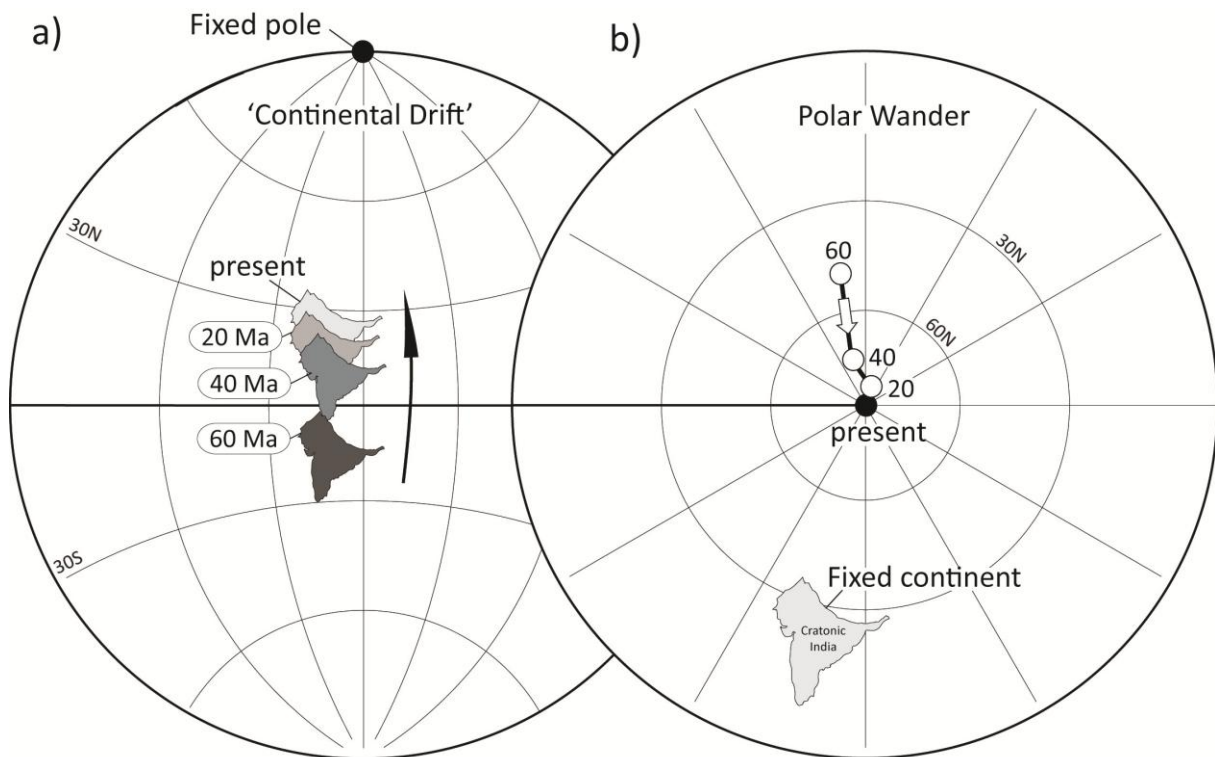


Figure 1 (Torsvik et al. ESR)

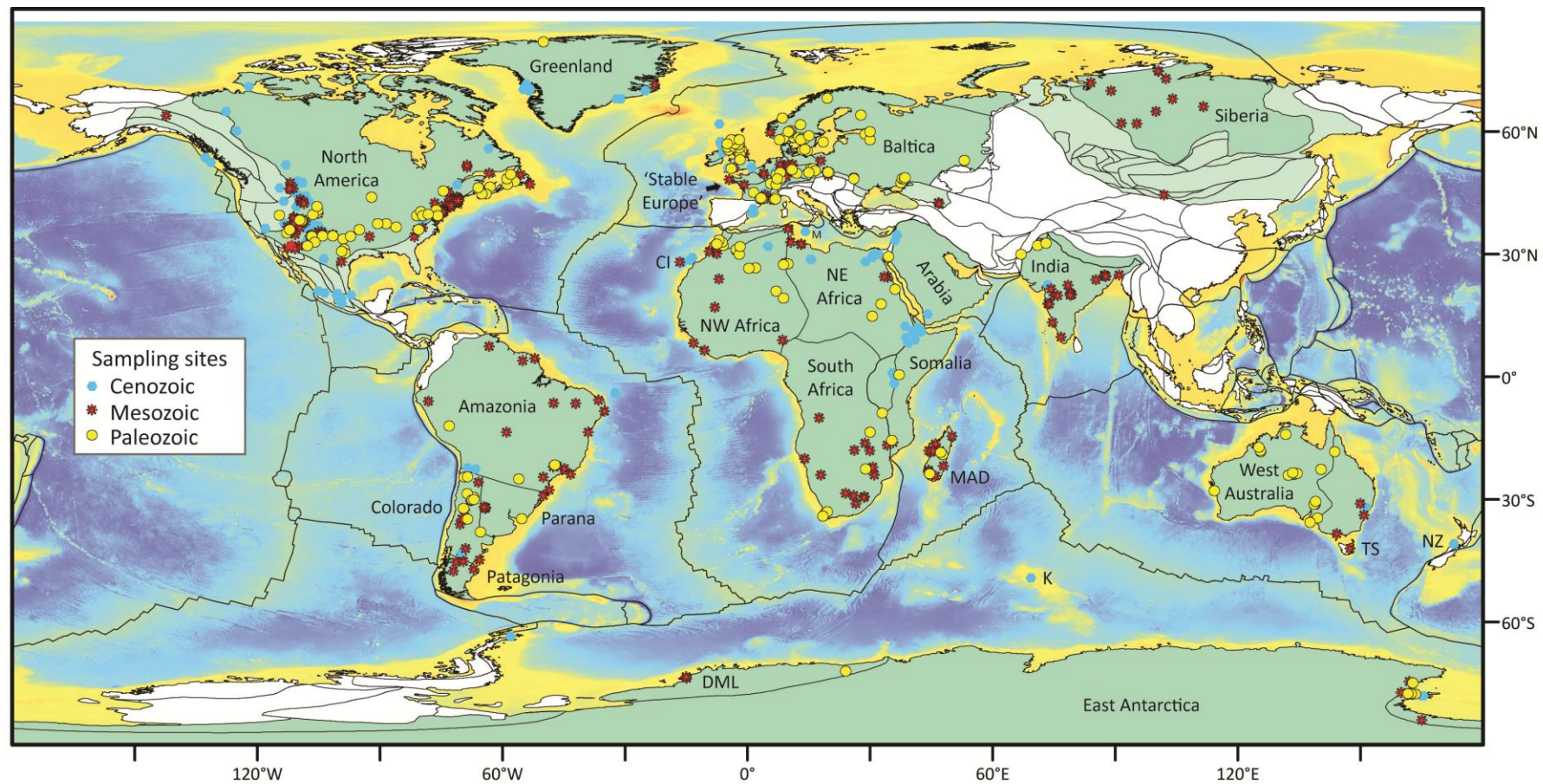


Figure 2 (Torsvik et al. ESR)

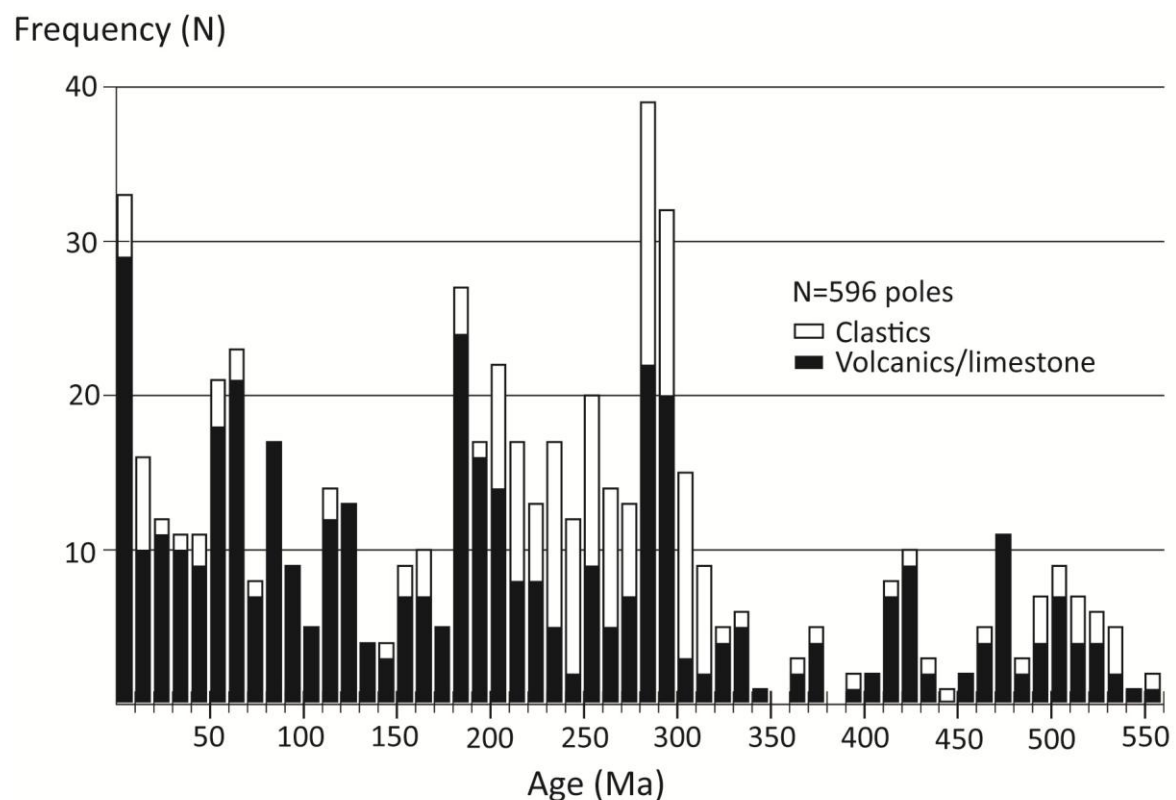


Figure 3 (Torsvik et al. ESR)

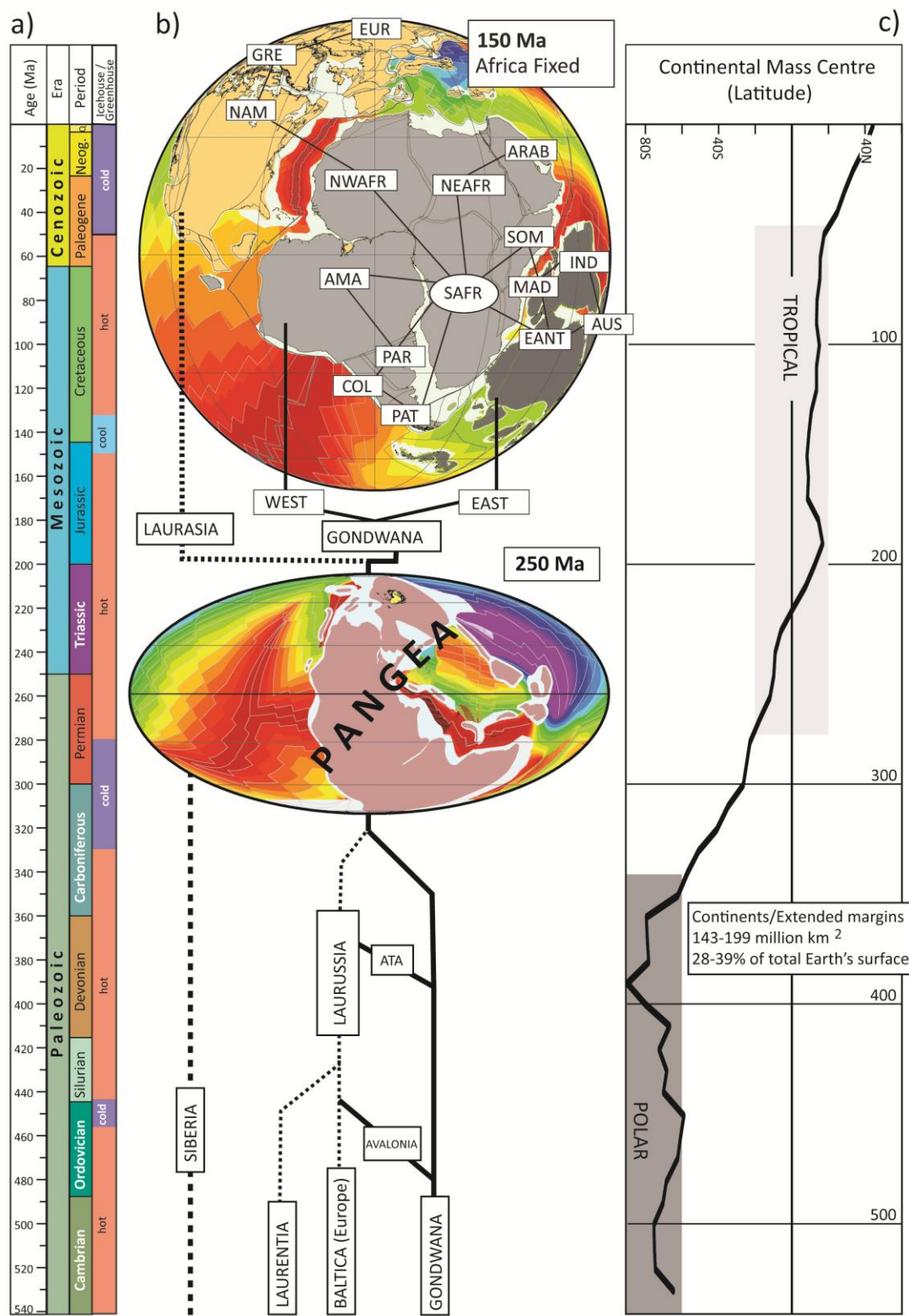


Figure 4 (Torsvik et al. ESR)



Figure 5 (Torsvik et al. ESR)

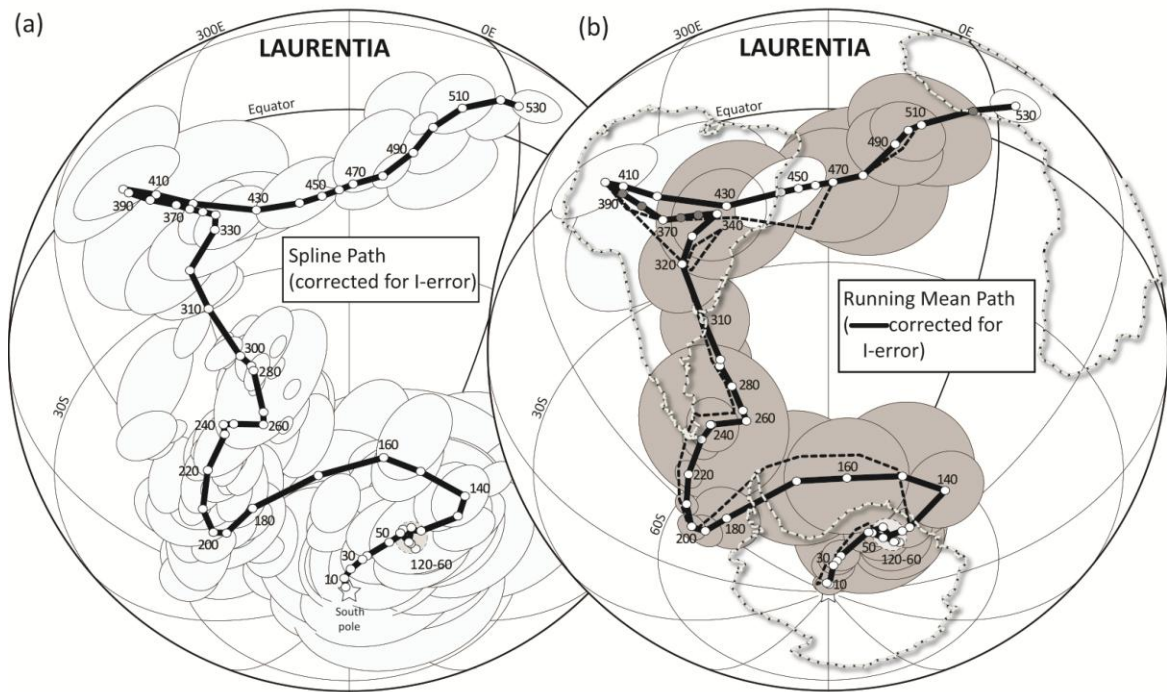


Figure 6 (Torsvik et al. ESR)

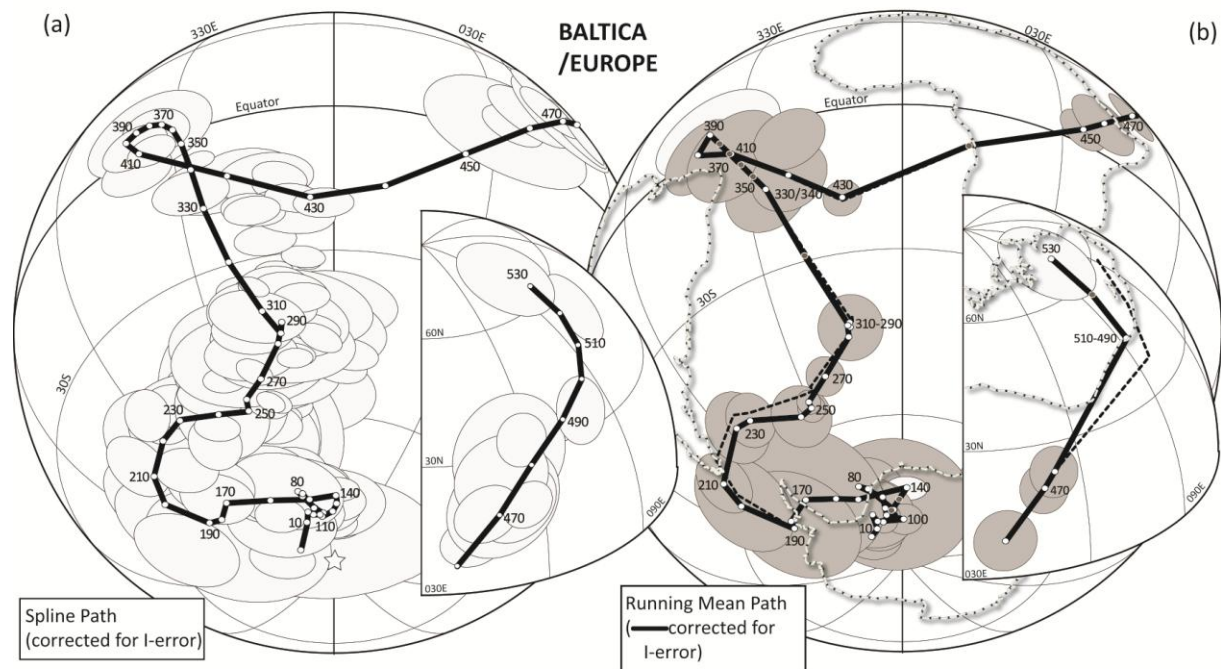


Figure 7 (Torsvik et al. ESR)

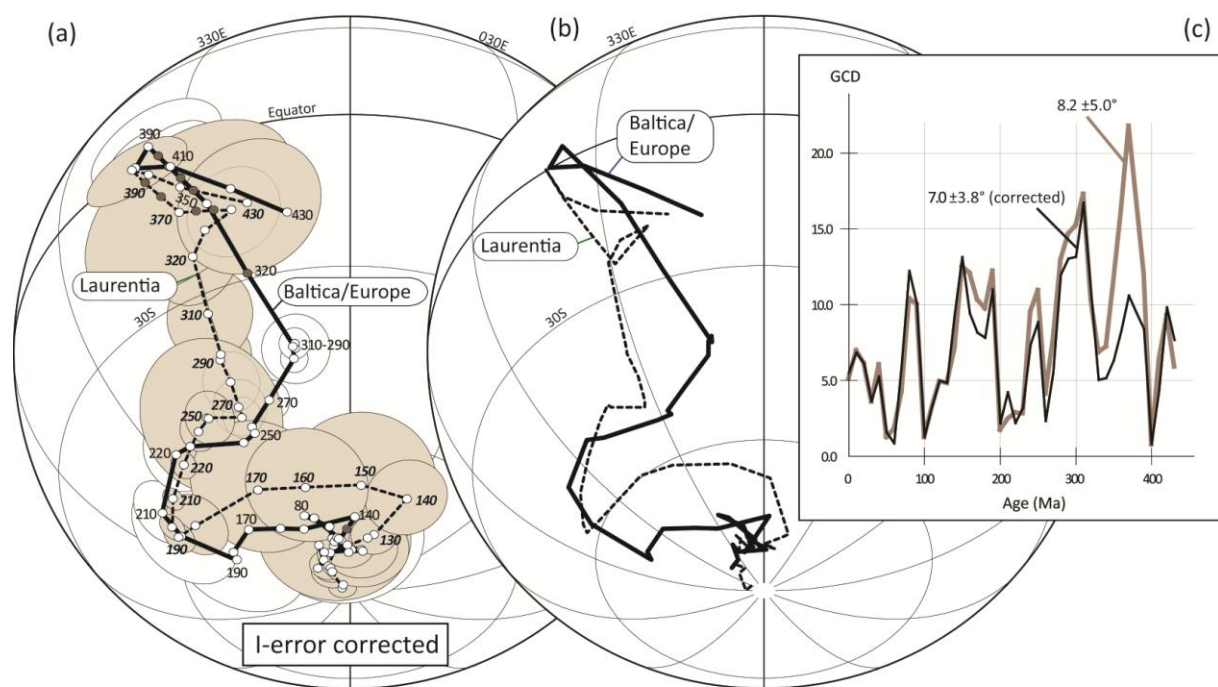


Figure 8 (Torsvik et al. ESR)

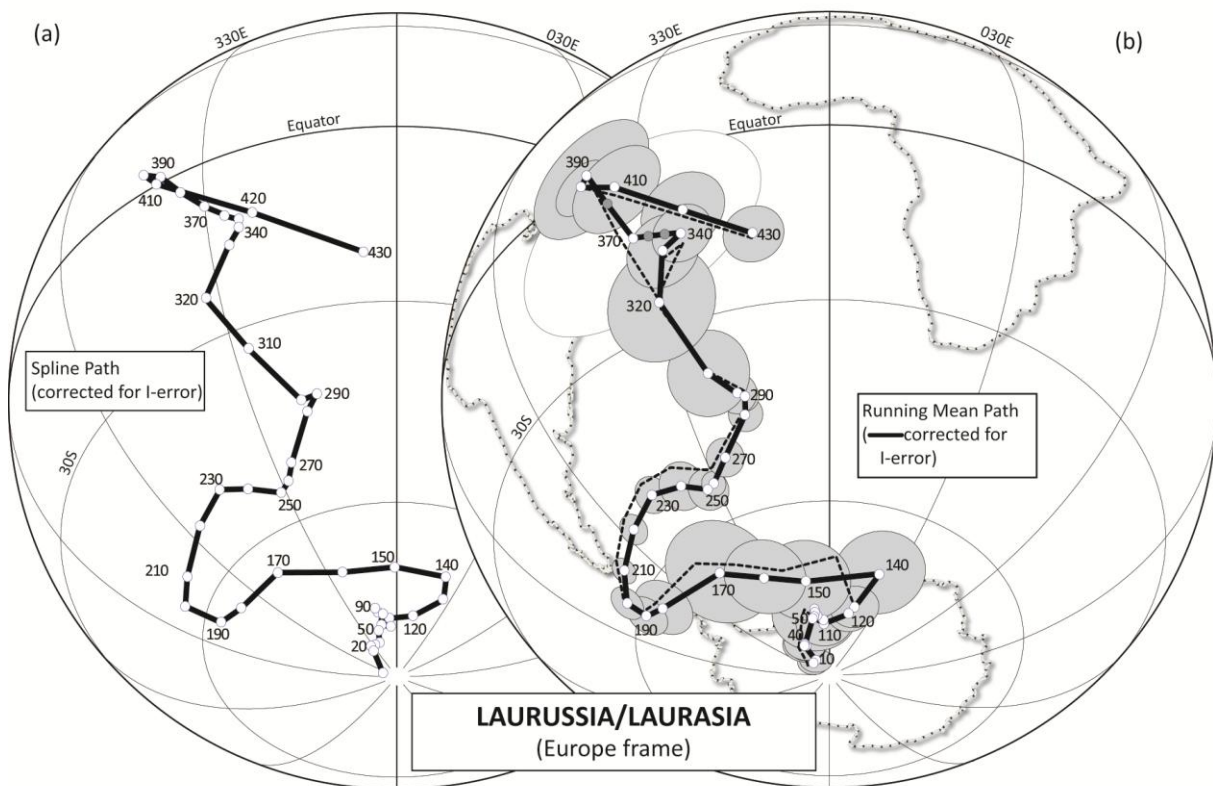


Figure 9 (Torsvik et al. ESR)



Figure 10 (Torsvik et al. ESR)

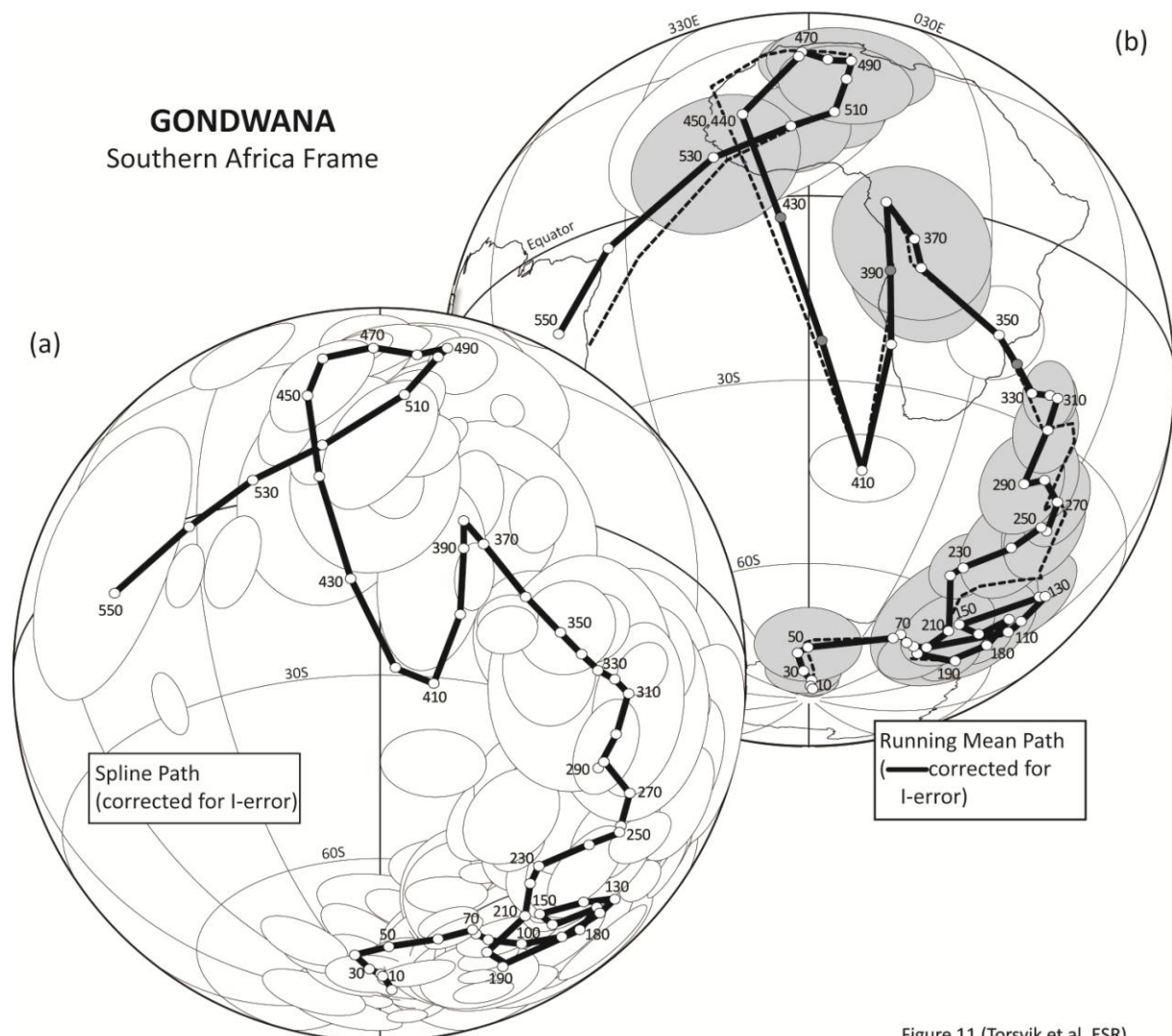


Figure 11 (Torsvik et al. ESR)

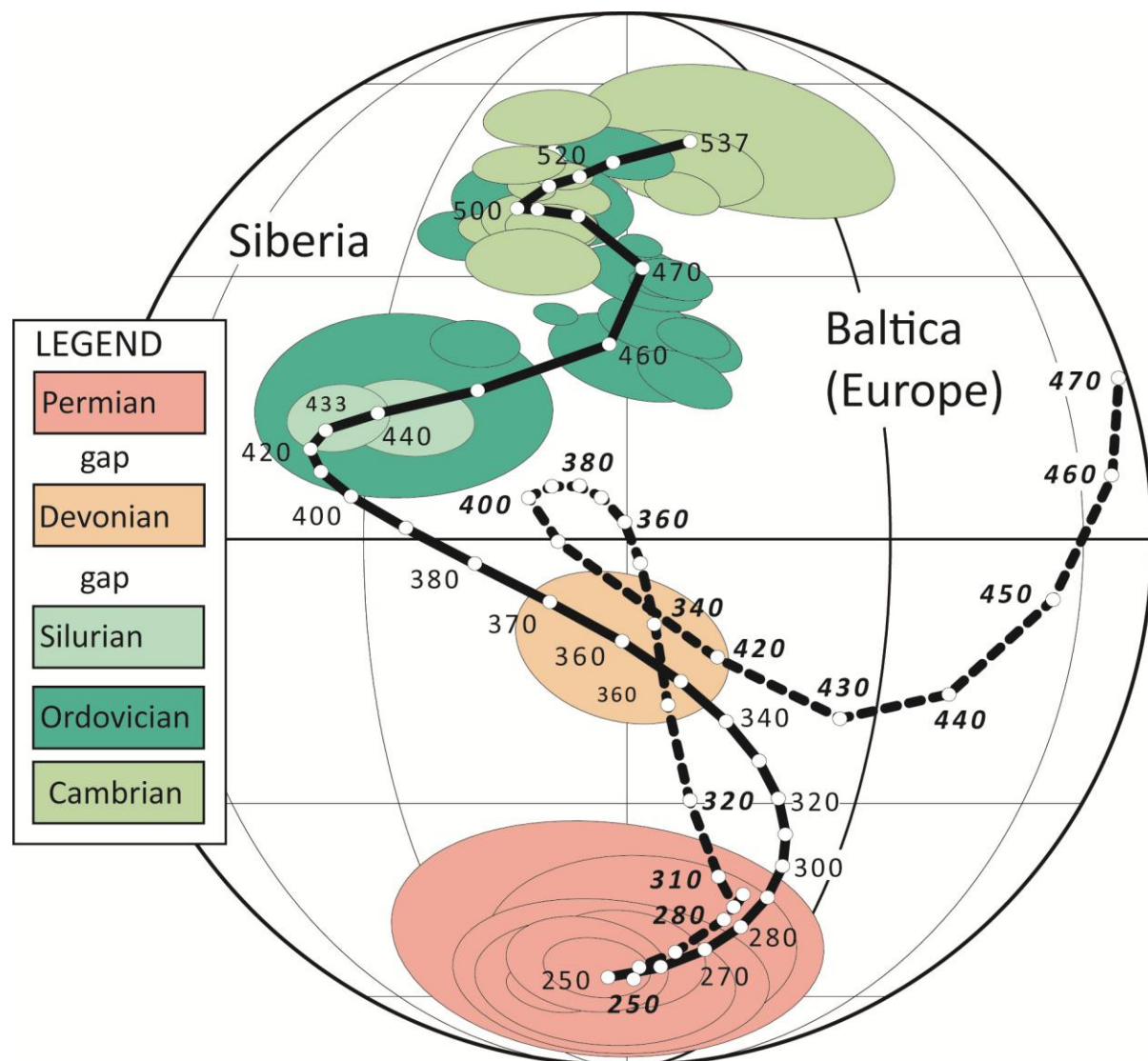


Figure 12 (Torsvik et al. ESR)

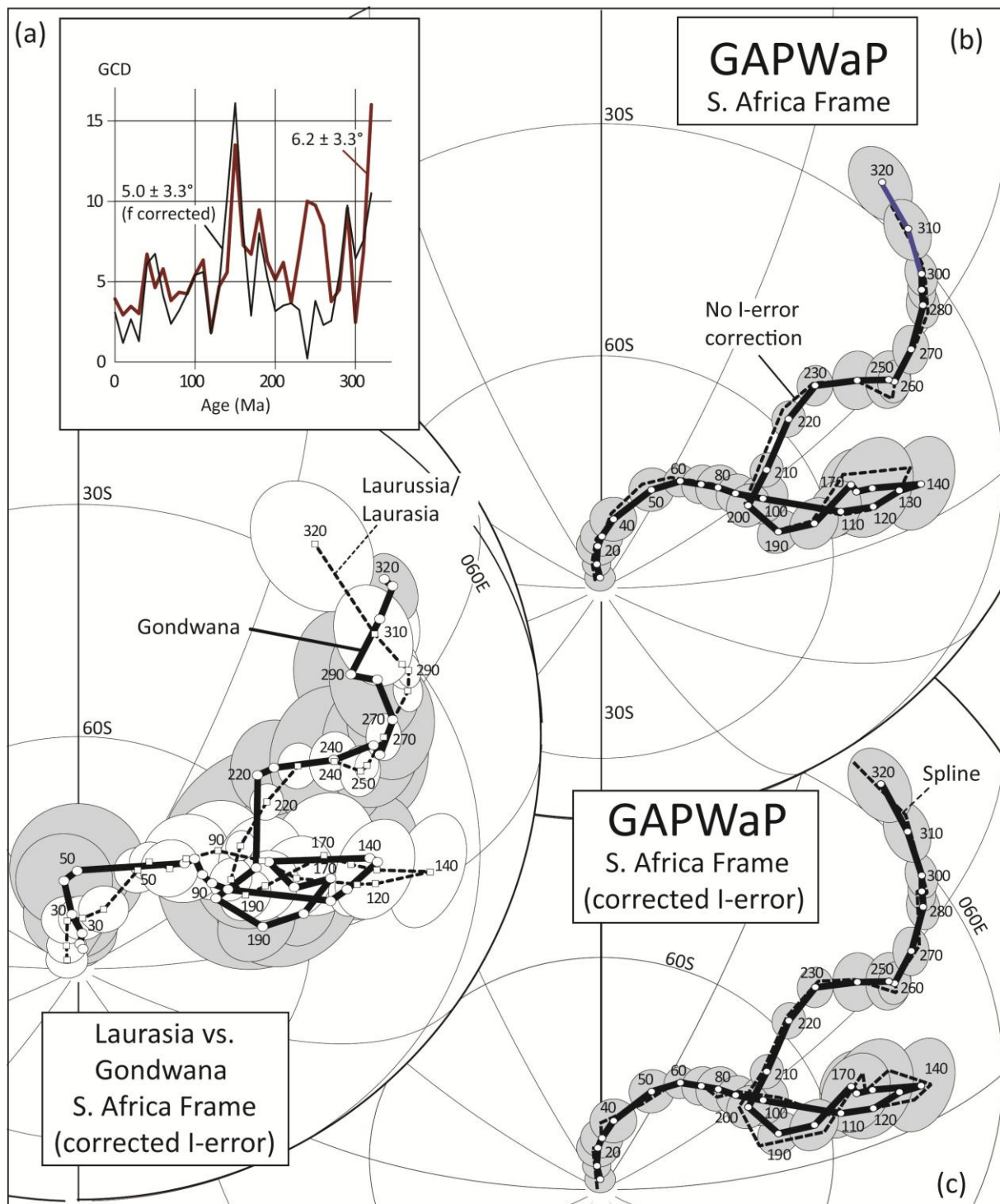


Figure 13 (Torsvik et al. ESR)

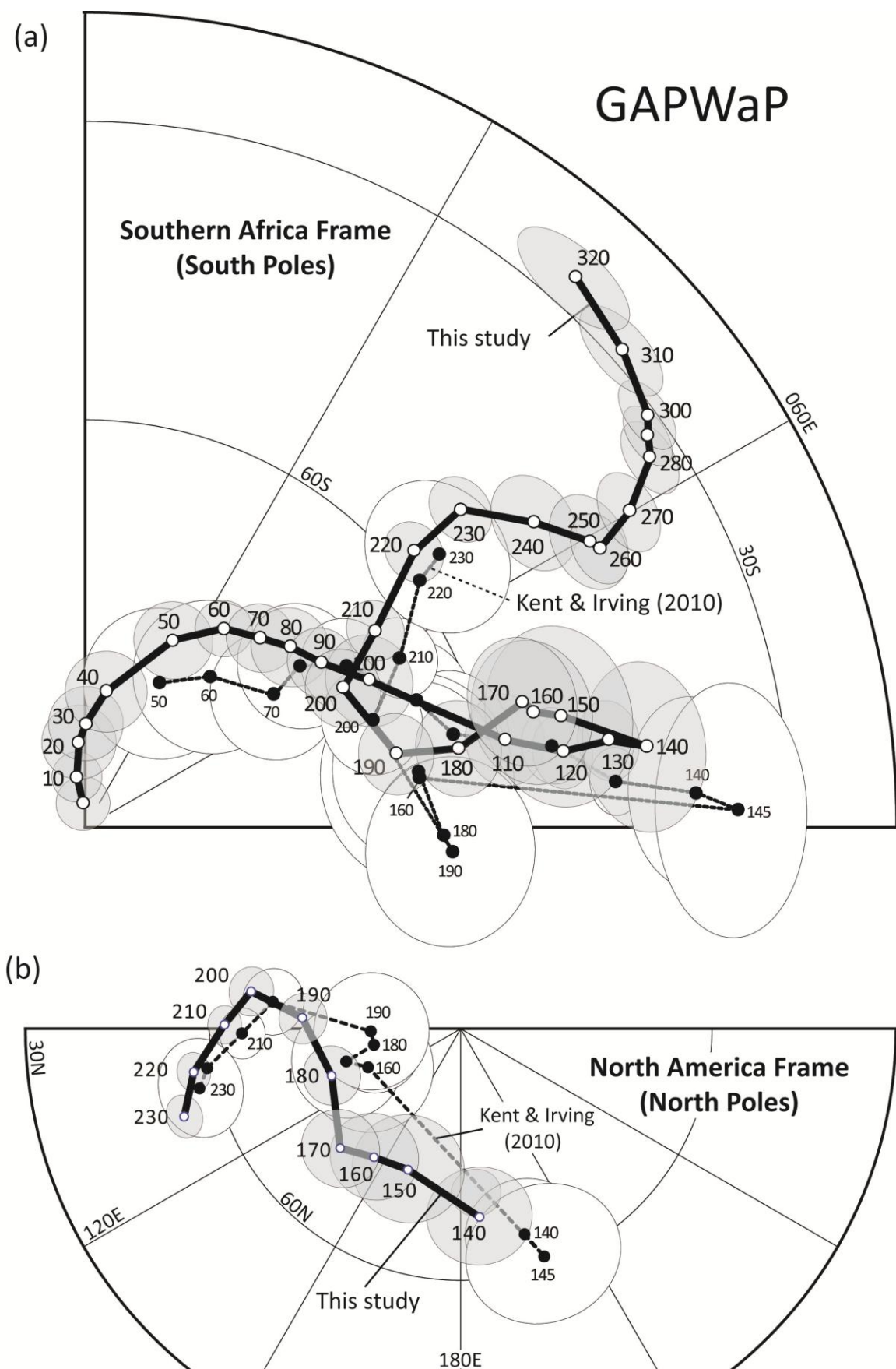


Figure 14 (Torsvik et al. ESR)

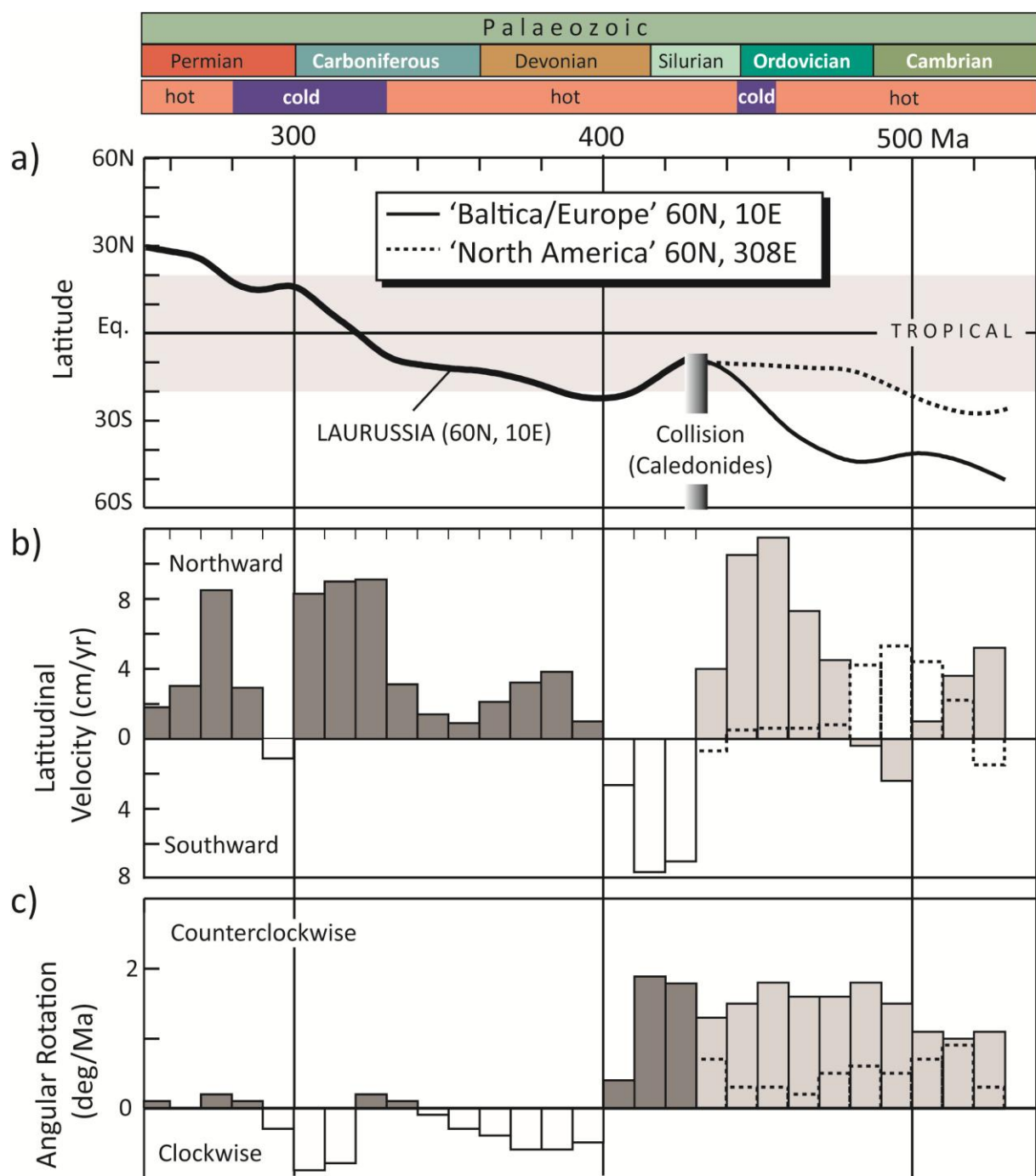


Figure 15 (Torsvik et al. ESR)

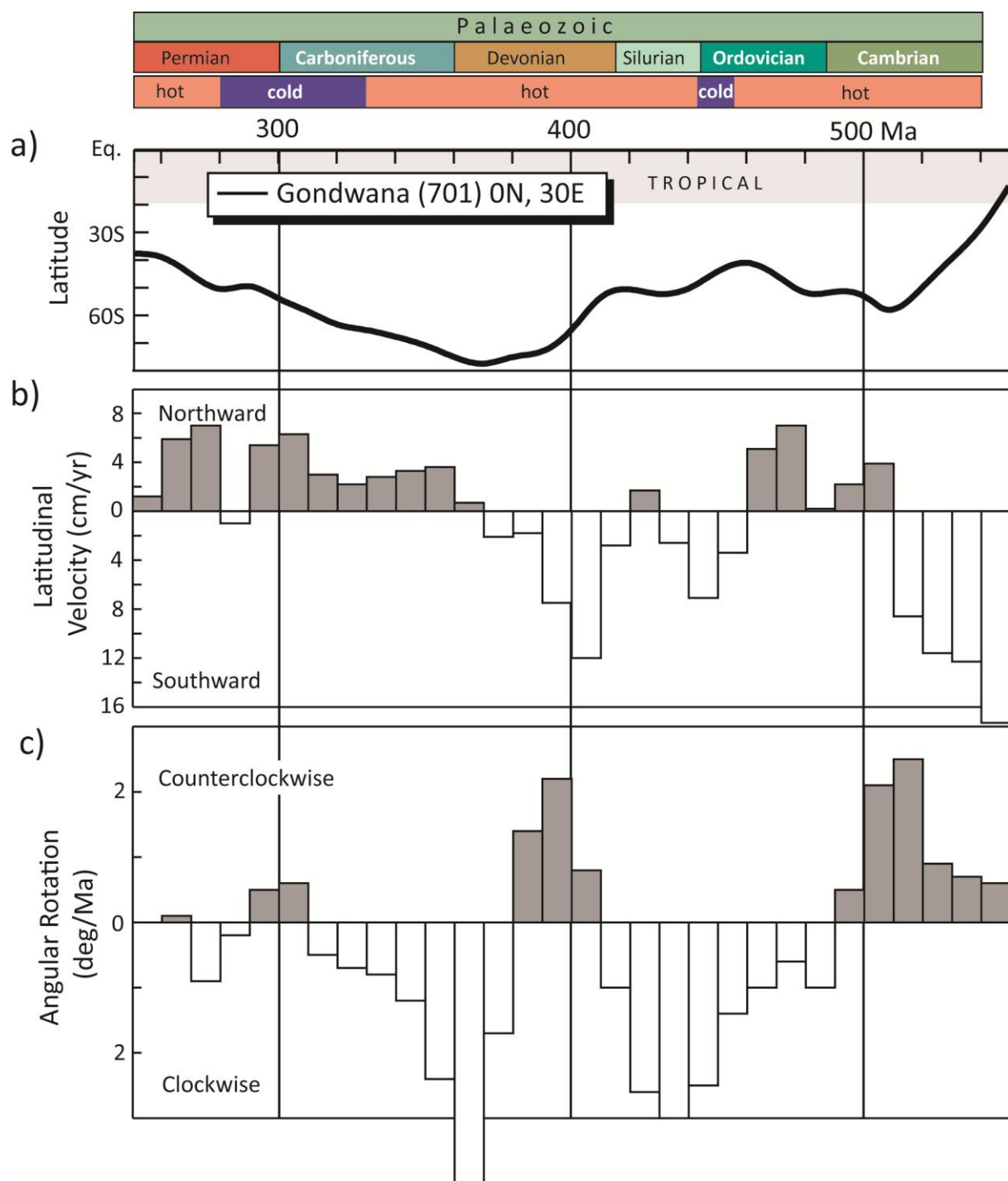


Figure 16 (Torsvik et al. ESR)

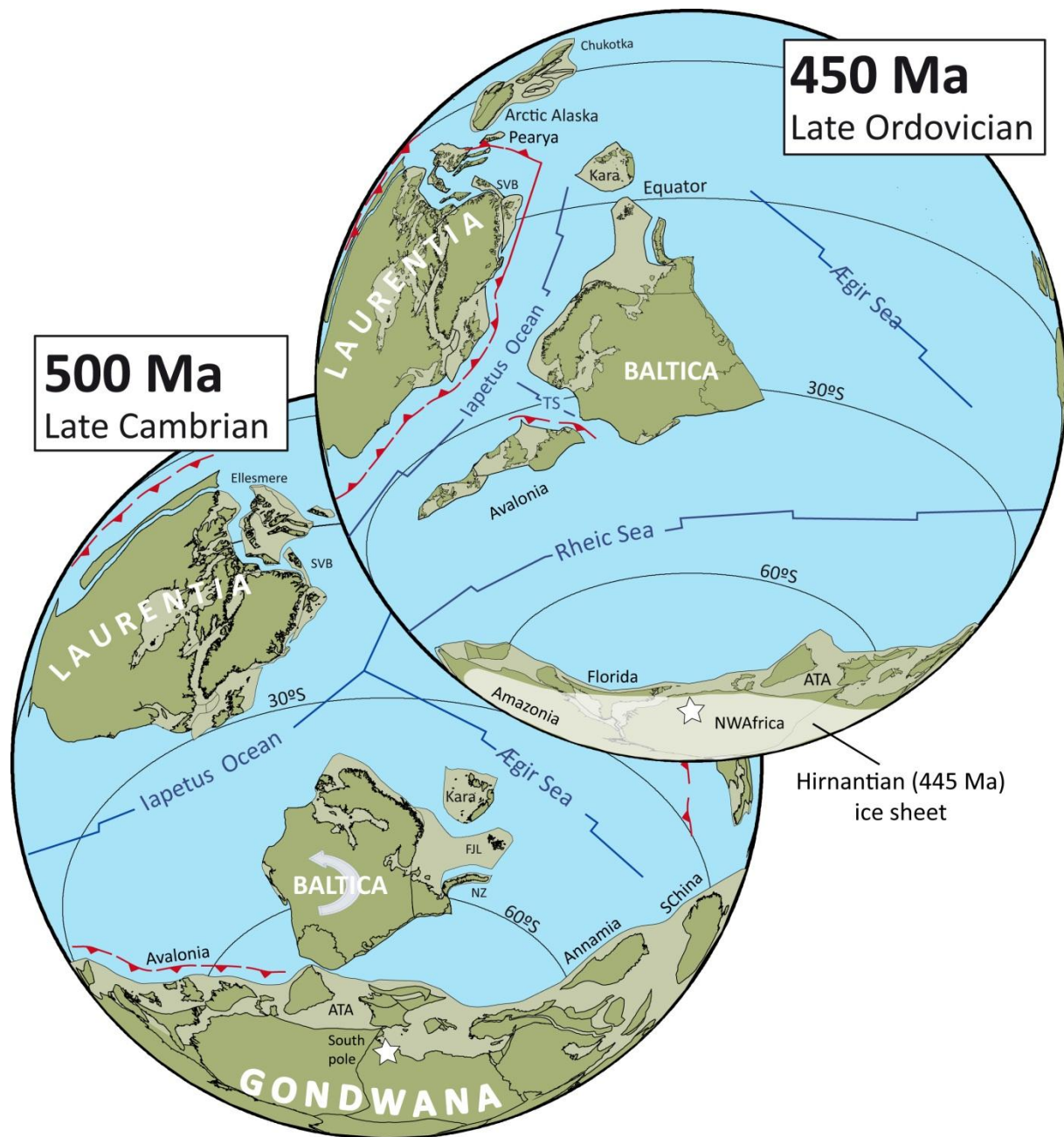


Figure 17 (Torsvik et al. ESR)

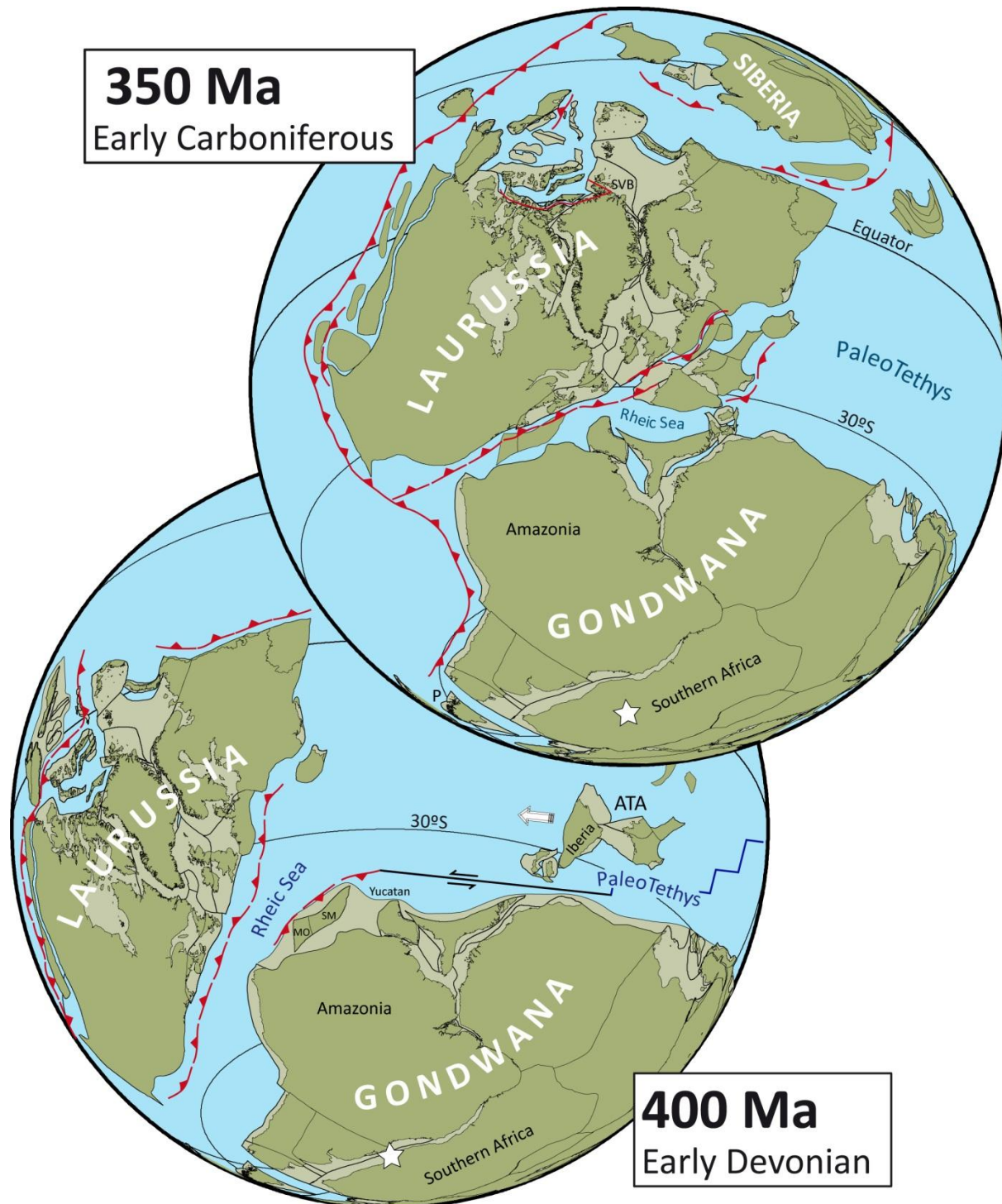


Figure 18 (Torsvik et al. ESR)

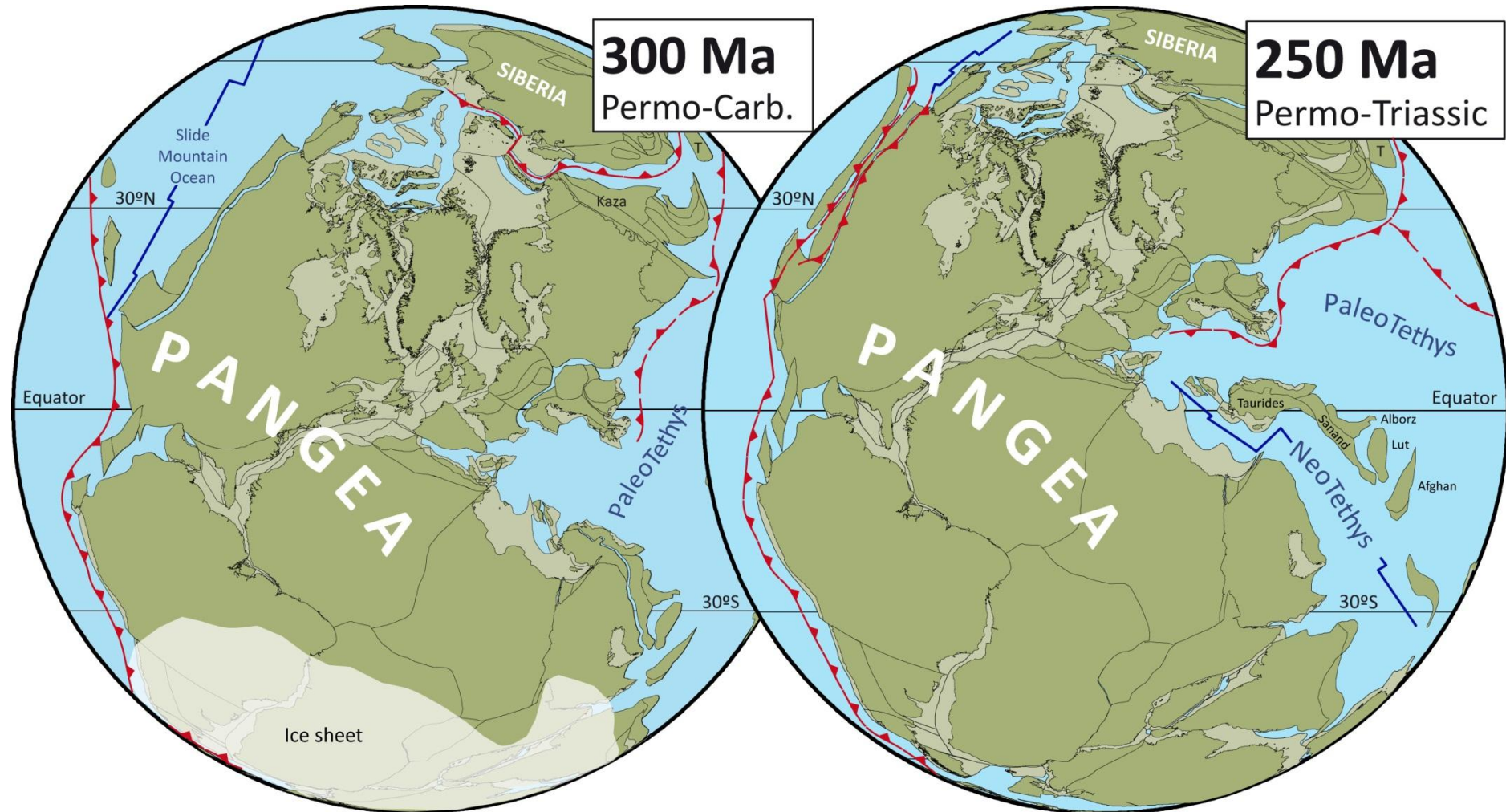


Figure 19 (Torsvik et al. ESR)

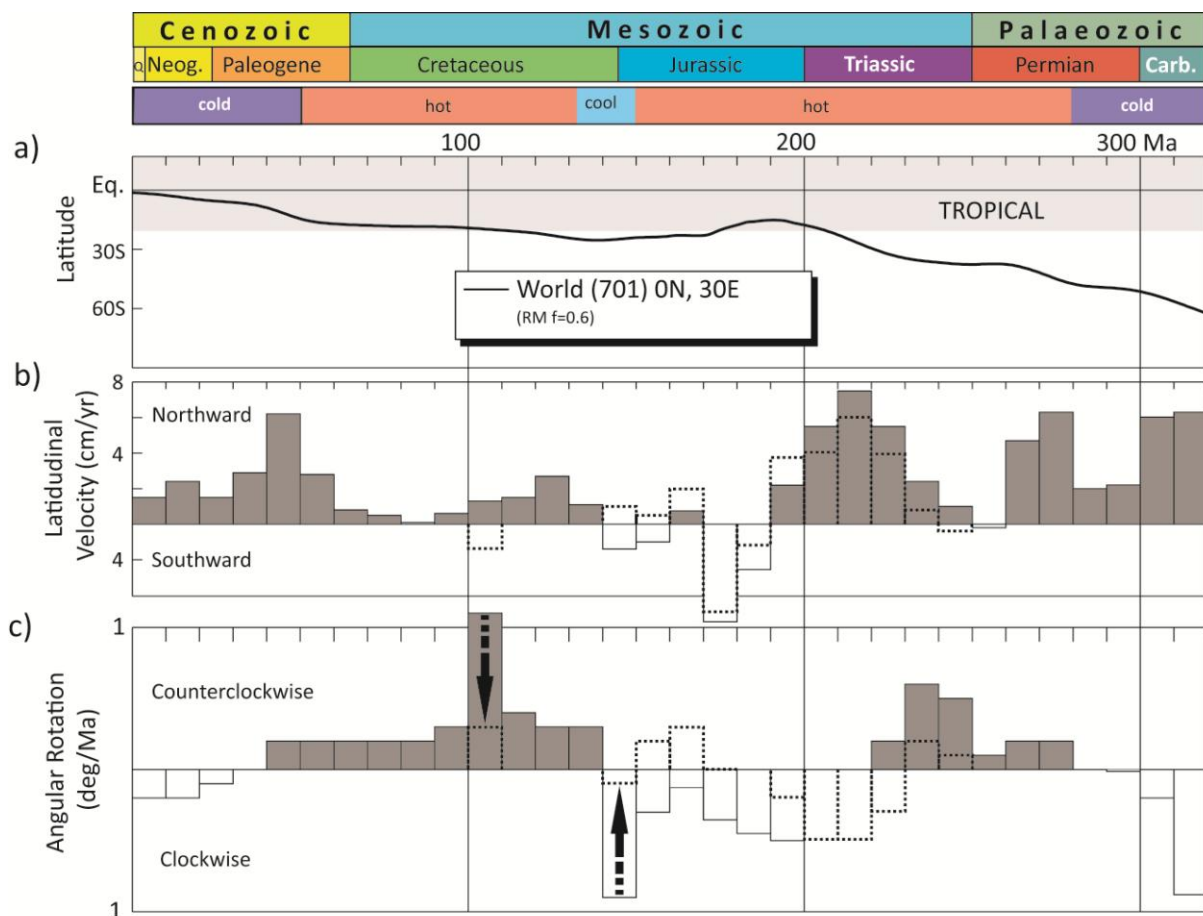


Figure 20 (Torsvik et al. ESR)

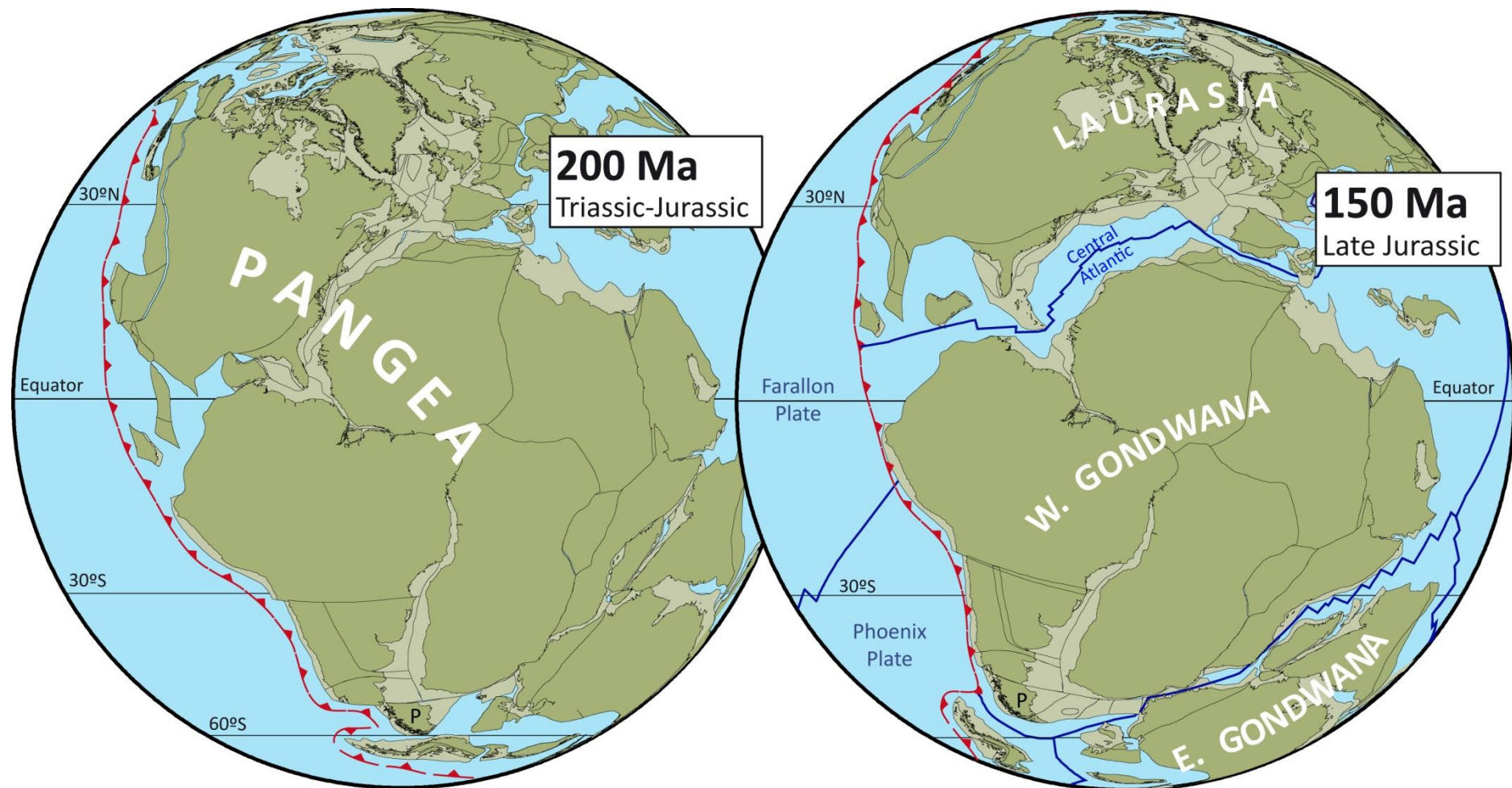


Figure 21 (Torsvik et al. ESR)

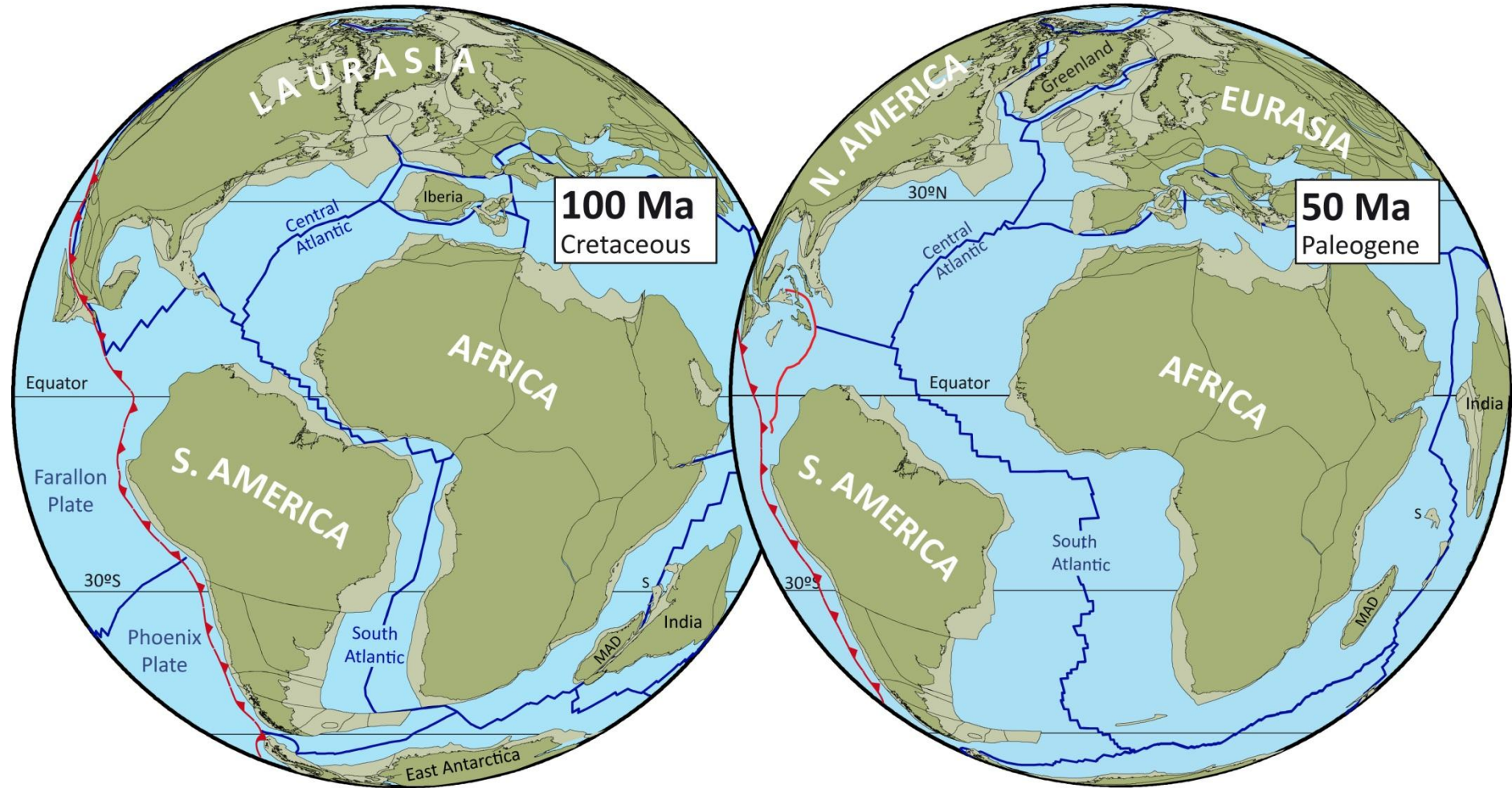


Figure 22 (Torsvik et al. ESR)

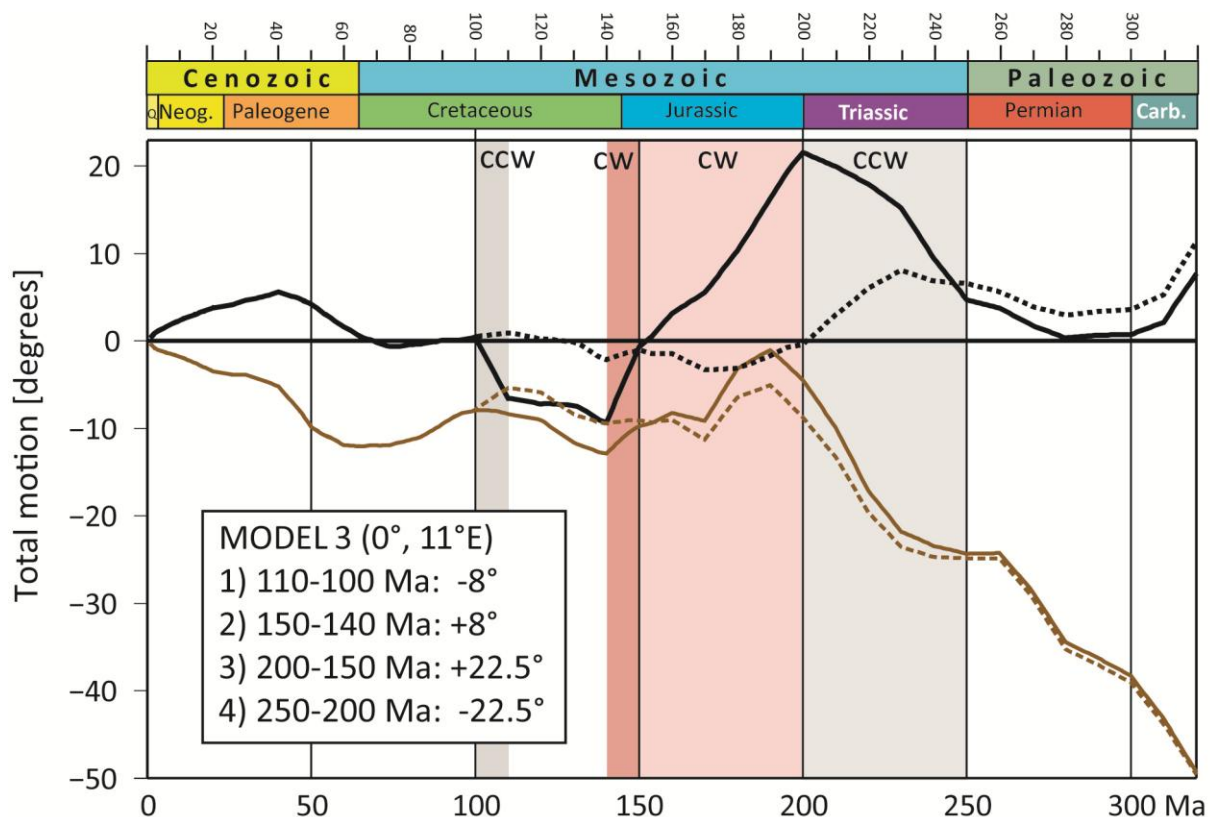


Figure 23 (Torsvik et al. ESR)

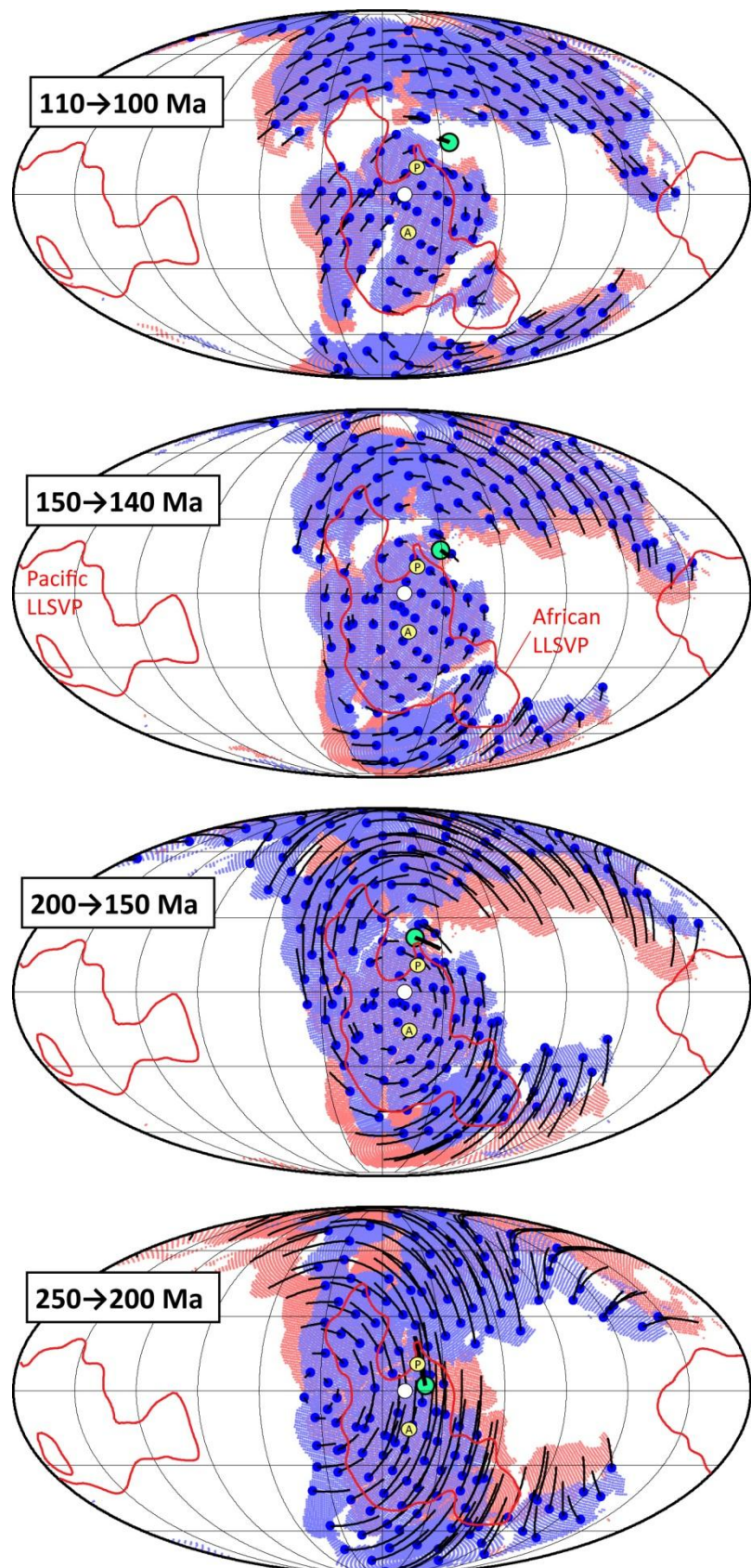
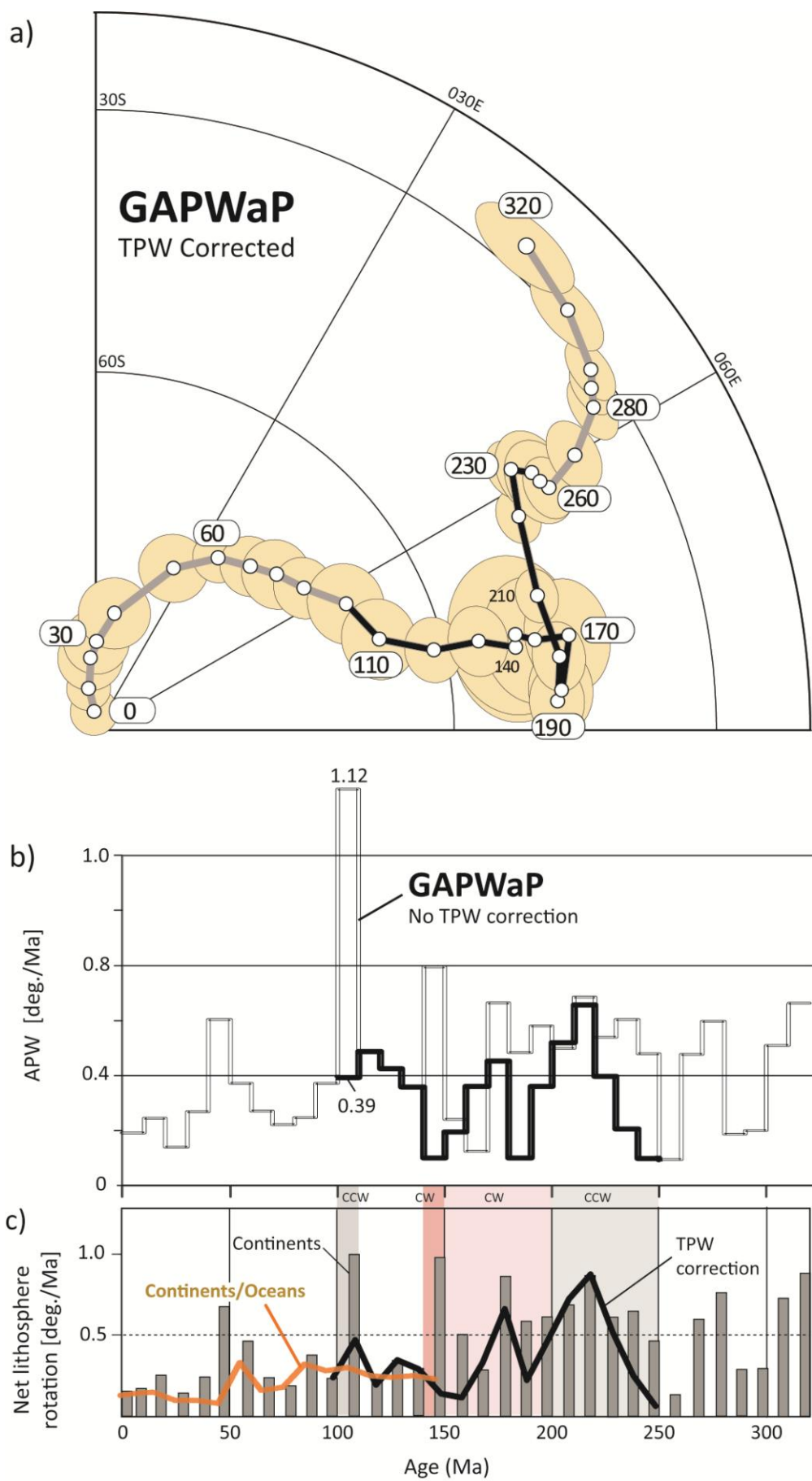


Figure 24 (Torsvik et al. ESR)



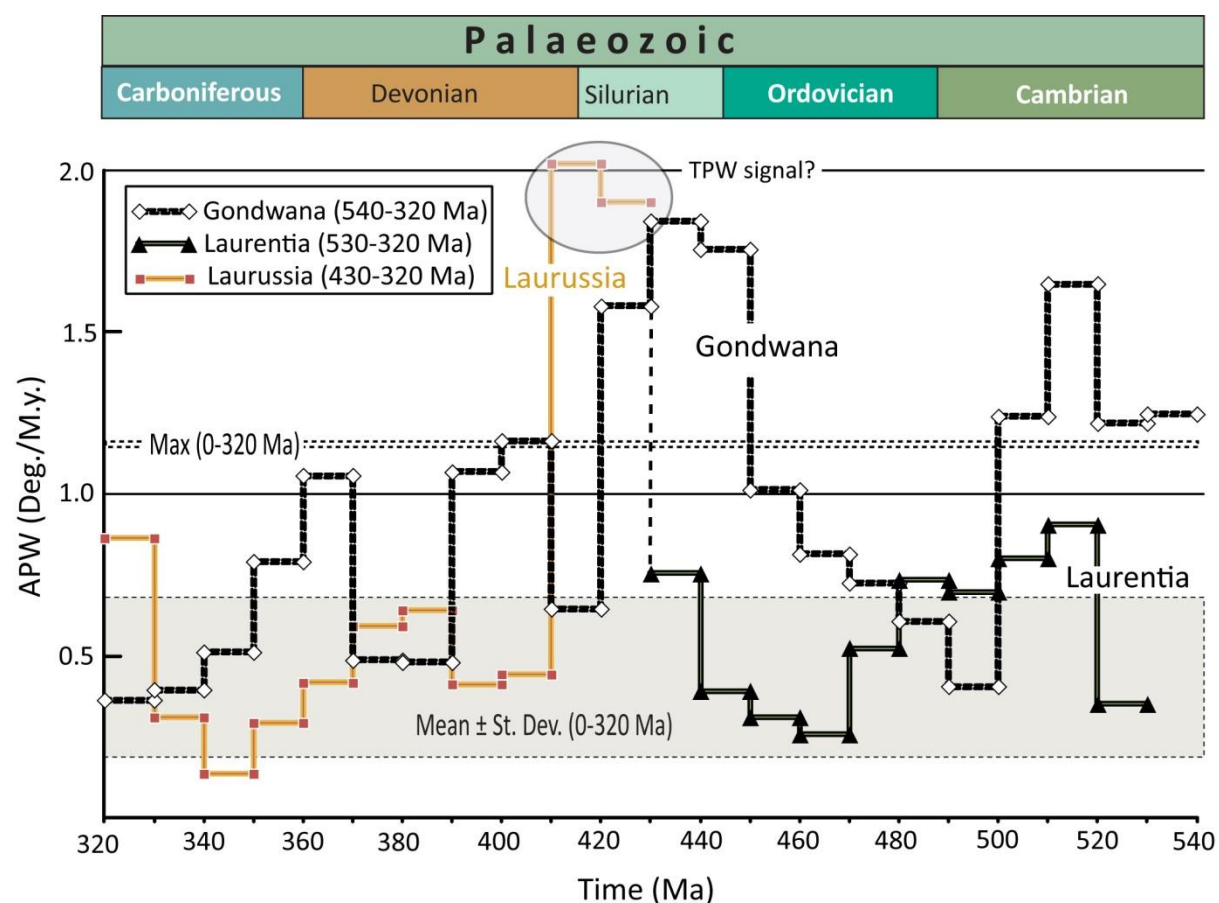


Figure 26 (Torsvik et al. ESR)

Table 1 Global palaeomagnetic compilation. Q=Quality Factor (Van der Voo 1990, 1993); α_{95} = 95 percent confidence oval (or A95 if bold and underlined); Com=Comments; I=Inclination corrected using the inclination-elongation (I/E) method of Tauxe and Kent (2004) or the anisotropy of magnetic susceptibility information (Kodama 2009) [I**, I/E corrected]; #=corrected for counterclockwise Colorado Plateau rotation of 5.4° (Bryan and Gordon, 1990). Lat/Lon=Pole Latitude/Longitude; CLat/CLon=Pole Latitude/Longitude corrected for inclination shallowing with f=0.6 (only for clastic sediments); Rlat/Rlon=Pole rotated to Southern Africa frame; EULER=Rotation latitude, longitude and angle; Age in Ma; GPDB RefNo/Reference= T=Listed in Torsvik *et al.* (2008); TV=Listed in Torsvik and Van der Voo (2002); T96=Listed in Torsvik *et al.* (1996). *Note that numerically assigned pole ages can differ substantially from original sources or the GPDB due to different time-scales* (if stratigraphically dated; in this paper we use Gradstein *et al.* 2004) *or new isotopic ages*.

Q	α_{95}	Com	Formation	Lat	Lon	CLat	CLon	RLat	RLon	EULER	Age	GPDB RefNo/Reference
			LAURUSSIA									
			NORTH AMERICA (101)									
5	4.8		USGS SW North America composite	-86.3	5.7						0.5	Mankinen (2008)
5	9.1		Michoacan Guanajuato volcanic field	-86.4	8.4			-86.4	9.2	(79.2/ 23/ .2)	0.8	Maciel Peña <i>et al.</i> (2009)
5	7.1		Tequila volcanic fields	-85.3	265.9			-85.3	-94.1	(79.9/ 22.7/ .3)	1	Ceja <i>et al.</i> (2006)
5	8.7		Meseta Lago Buenos Aires	-88.4	225.5			-88.4	-135.7	(79.9/ 22.7/ .3)	1	Brown <i>et al.</i> (2004)
5	4.3		Trans Mexican Volcanic Belt	-88.9	285			-88.9	-75.1	(79.9/ 22.7/ .3)	1	Ruiz-Martinez <i>et al.</i> 2010
3	4.9		Katherine Creek sediments	-77.9	303.7	-80	3.5	-80	4.2	(80.8/ 22.8/ .4)	1.5	3060, T
3	7		Banks Island deposits	-85.7	122.7	81.2	73.9	-81.1	74.5	(80.8/ 22.8/ .4)	1.5	3206, T
5	5.7		USGS SW North America composite	-84.5	241			-84.5	-119.1	(80.8/ 22.8/ .4)	1.5	Mankinen (2008)
5	6.2		Trans-Mexican Volcanic Belt	-89.5	214.8			-89.5	-157.9	(80.8/ 22.9/ .8)	3	Mejia <i>et al.</i> (2005)

5	4.1		Trans Mexican Volcanic Belt	-84.6	332.3			-84.8	-25.6	(80.9/ 22.8/ 1)	4	Ruiz-Martinez et al. (2010)
5	6.7		Eastern Alkaline Province	-87.9	275.9			-88	-84.4	(80.9/ 22.8/ 1)	4	Goguitchaichvili et al. (2007)
5	5		Snake River Plain	-85.5	197.4			-85.5	-163.9	(80.9/ 22.8/ 1.3)	5	Tauxe et al. (2004)
5	5		USGS SW North America composite	-85.3	262.1			-85.5	-97.9	(80.9/ 22.8/ 1.8)	7	Mankinen (2008)
5	6.9		Trans Mexican Volcanic Belt	-85.9	357.7			-86	3.9	(80.9/ 22.8/ 2)	8	Ruiz-Martinez et al. (2010)
5	7.8		USGS SW North America composite	-82.9	309.1			-83.3	-47.3	(80.9/ 22.9/ 2.6)	10	Mankinen (2008)
3	12.9		Hepburn's Mesa Formation	-81.1	225.3	83.1	93.2	-82.4	98.8	(80.9/ 23.2/ 4.2)	15.5	2288, T
5	3.7		Stoddard Mountain laccolith	-82.9	346.2			-83.5	-1.3	(80.3/ 25.4/ 5.8)	21	Petronis et al. (2004)
5	9.8		Dinan Bay lavas	-82.7	301.7			-83.7	-51	(80.2/ 26/ 6)	21.7	Irving et al. (2000)
4	6.7		Younger plutons	-87.1	189.5			-86.7	177.4	(80/ 26.6/ 6.2)	22.5	1402, T
3	8.4		Lake City Caldera	-76.4	30.3			-76.2	41	(79.9/ 26.9/ 6.3)	23	1300, T
4	5.2		Latir volcanics	-80.9	331.2			-81.8	-17.8	(79.8/ 27.3/ 6.4)	23.5	1299, T
4	6.8		Conejos and Hinsdale Formation	-79.7	342.8			-80.5	-4.3	(79.3/ 27.5/ 7.1)	26	3130, T
4	5.4		Latir extrusives, sediments	-80.2	315.4			-81.4	-32.9	(78.8/ 22.7/ 7.5)	27	1299, T
3	5		Mongollon-Datil volcanics	-82.8	316.2			-84.2	-24	(77.4/ 12.5/ 8.6)	30	2631, T
4	4.4		Mongollon-Datil volcanics	-81.9	323.6			-83.1	-16.9	(77.4/ 12.5/ 8.6)	30	1315, T
6	6.2		Tuzantlán-Copalillo basin	-80.6	22.1			-79.5	43.5	(76/ 6.1/ 9.7)	33	Molina-Garza & Ortega-Rivera (2006)
4	4.3		Mariscal Mountain Gabbro	-79.8	5.9			-78.9	31.9	(74.9/ 1.4/ 11.4)	37	2943, T
5	7		Ramsay Island lavas	-78.2	297.5			-80.7	-40.3	(74.5/ .1/ 12)	38.5	Irving et al. (2000)
3	2.4		Mistastin Lake Impact	-85.2	296.6			-87.2	-9.1	(74.5/-1.1/ 12.6)	40	562, T

6	3		Beaver River alkalic complex	-79.2	326.4			-80.1	-1.7	(74.4/-2.5/ 13.4)	42	Symons et al. (2003)
5	7.7		East Fork Washakia Basin	-83.7	323.7	76.7	50.4	-73.2	70.3	(74.3/-3.7/ 14.2)	44	1632, T
5	8		Absaroka flows	-82.7	333.6			-82.6	19.8	(74.2/-4.9/ 15)	46	1117, T
4	<u>9.6</u>		Rattlesnake Hills volcanics	-79.3	324.3			-80.2	0.8	(74.2/-4.9/ 15)	46	1712, T
4	10.1		Monterey intrusives	-85.2	62			-81.2	84	(74.5/-4.8/ 15.3)	47	1865, T
6	5.6		Bitterroot Dome dike swarm	-72	343.4			-71.9	10.7	(74.5/-4.8/ 15.3)	47	2560, T
5	4		Robinson Anticline intrusives	-77.1	325.8			-78.1	-0.9	(75.9/-3.5/ 16.2)	50	1348, T
6	6.2		Absorako volcanics	-83.1	326.3			-83.5	15.9	(75.9/-3.5/ 16.2)	50	Harlan & Morgan (2010)
6	4.9		Wasatch and Green River Formation	-77.6	309.1	78.3	22.7	-75.8	51.7	(76.5/-2.8/ 16.5)	51	3150, T
6	2.6		Combined Eocene intrusives	-82.7	347.2			-81.8	31.2	(76.5/-2.8/ 16.5)	51	1270, T
6	4.4		Bighorn Basin	-81.4	347.7	73.9	48.8	-71.3	71.7	(79.8/ 4.1/ 17.6)	55	Clyde et al. (2007)
5	14		Rhyolite intrusion and contact	-68.1	9.4			-67.3	34.2	(80.9/ 6.2/ 18.2)	57	504, T
6	3		Nacimiento formation	-75.9	326.4	74.9	24.7	-73.4	52	(81.8/ 4.8/ 19.4)	61	1033, T
4	1.1		Gringo Gulch volcanics	-77.1	21.3			-75.6	50.6	(82.2/ 4/ 20)	63	1710, T
4	6.6		Edmonton Group, Alberta	-72	5.3	-68	38.1	-66.1	62.3	(82.2/ 4/ 20)	63	1914, T
6	3.7		Combined Paleocene intrusions	-81.9	350.6			-81.7	29.2	(82.2/ 4/ 20)	63	1270, T
5	3.9		Alkalic intrusives	-80.5	359.4			-79.9	34.6	(82.4/ 3.6/ 20.4)	64	1711, T
5	5.8	#	Tombstone volcanics and intrusions	-71.8	28.3			-69.2	56.8	(81.4/-8.2/ 22.7)	71	2806, T
5	6.2	#	Roskruge volcanics	-69.8	354.9			-68.6	26.4	(81.3/-9.2/ 23.1)	72	1240, T
6	4.6		Adel Mountain volcanics	-83.7	15.4			-80.7	58.1	(80.7/-12.3/24.3)	74.5	2370, T
6	9		Doherty Mountain sills	-80.8	358.1			-78	43.4	(79.5/-15.9/25.7)	77	Harlan et al (2008)
5	9.6		Niobrara Formation	-59.8	17.7	-	41.8	-52.8	70.3	(78.7/-18.1/26.9)	79	Shive & Frerichs (1974)

6	6.2		Maudlow Formation welded tuffs	-70.5	27.6	57.8			-65.5	60.8 (78.2/-18.8/27.5)	80 2397, T
7	6.6		Elkhorn Mountains	-81.8	7.8			-77.2	55.4 (77.8/-19.4/28.1)	81 2382, T	
5	4.4		Magnet Cove and other intrusions	-73.6	11.1			-61.2	65.2 (69.4/-23.5/40.5)	100 1322, T	
5	8.3		Cuttingsville	-72.4	20.7			-59.3	70 (69.4/-23.5/40.5)	100 3087, T	
5	4		Randall Mountain	-76.4	319.4			-69.4	45.2 (68.8/-23.1/42.6)	103 3087, T	
5	4.4		Little Rattlesnake Complex	-71.5	2.4			-56	67.6 (67.3/-22/48.2)	111 3087, T	
5	6.5		Pleasant Mountain	-77.4	5.9			-60.7	74.5 (67.2/-21.8/48.9)	112 3087, T	
5	5.6		Burnt Meadow Mountains	-75.7	29.1			-57.1	84.1 (67/-21.7/ 49.6)	113 3087, T	
5	3.6		Alfred Complex	-74.2	30.3			-53.1	88.2 (66/-20.6/ 54.2)	120 3036, T	
5	5.3		Cape Nedick	-74.8	354.8			-56.5	73.9 (65.8/-20.2/54.8)	121 3036, T	
5	4.6		Tatnic Complex	-65.9	27.8			-44.4	86.2 (65.7/-19.8/55.3)	122 3036, T	
6	2.4		Monteregian Hills intrusives	-72	11.2			-51.7	79.7 (65.7/-19.8/55.3)	122 1853, T	
5	3.3		White Mountains igneous complex	-71.3	7.5			-51.5	77.6 (65.7/-19.8/55.3)	122 2644, T	
5	7.5		Lebanon diorite	-71	16.9			-49.4	83.7 (65.4/-18.9/56.8)	125 3036, T	
5	3.6		Notre Dame Bay dikes	-67.2	30.8			-43.6	91.6 (64.9/-17.7/58.7)	129 1854, T	
7	2.6		Kimberlite dikes	-58	23.1			-33.4	89.2 (64.9/-16.7/63.2)	144 2717, T	
6	4.1	#	Morrison Formation, Brushy Basin Member	-64.2	338.8	65.5	12.5	-41.3	86.4 (64.8/-16.8/64.4)	148 2870, T	
5	3.6	#	Upper Morrison Formation	-63.4	344.8	-64	17.5	-39.3	89.3 (65.1/-16.1/64.9)	150 787, T	
6	7	#	Canelo Hills volcanics	-58.7	315.1			-49.8	50.8 (65.3/-15.7/65.2)	151 1256, T	
5	5.3	#	Lower Morrison Formation	-57.4	327.5	62.5	351	-42.6	76.4 (65.8/-14.2/66.8)	156 787, T	
6	6	#	Summerville Formation, Trujillo	-56.8	328.1	58.1	350.6	-37.8	76.3 (65.8/-13.5/69.6)	163 Steiner (2003)	

6	7.4	#	Summerville Formation	-52.6	318.2	58.6	334.6	-42	69.4	(65.9/-13/ 71.5)	168	2419, T
5	4.3	#	Summerville sandstone	-64	299	71.4	321.9	-54.9	77	(65.9/-13/ 71.5)	168	1121, T
4	7.4		Moat volcanics	-78.7	270.3			-68.5	87.8	(65.9/-12.9/71.9)	169	Van Fossen & Kent (1990)
5	7.8	#	Corral Canyon rocks	-58	303.8			-51.9	53	(65.6/-12.9/72.9)	172	1294, T
4	<u>1.4</u>		Newark volcanics II	-63.2	283.2			-61.7	54.7	(64.8/-13.4/75)	180	1702, T
3	1		Anticosti dikes	-75.7	264.7			-67.6	85	(64.4/-13.6/75.7)	183	Larochelle (1971)
6	3.3	#	Kayenta Formation	-58.8	256.4	-62	257.2	-72	47.8	(64.1/-13.8/76.5)	186	2380, T
5	7	#	Kayenta Formation	-61.3	264.8	67.8	268.3	-67.4	64.9	(64.1/-13.8/76.5)	186	Steiner & Helsley (1974)
4	9.8	#	Kayenta Formation	-58.7	277.8	64.4	283	-61	59.4	(64.1/-13.8/76.5)	186	Johnson & Nairn (1972)
3	7.2	#	Sil Nakya Formation	-73.1	275.4			-64.1	78.6	(63.8/-14/ 77.3)	189	T, Kluger-Cohen et al. (1986)
5	3.1		Combined dikes	-72.8	268.1			-66.1	79.2	(63.7/-14/ 77.6)	190	1932, T
5	8.9		Piedmont dikes	-66	266			-66.7	63.8	(63.3/-14.2/78.6)	194	1796, T
4	2.3		Newark volcanics I	-63	263.1			-67.6	56.7	(63.2/-14.2/ 79)	197	1702, T
4	11.1		Connecticut Valley volcanics	-65.5	267.5			-65.9	63.2	(63.2/-14.2/ 79)	197	477, T
6	2.8	#,I	Moenave Formation	-62.5	251			-73.2	55.4	(63.2/-14.2/ 79)	197	Donohoo-Hurley et al. (2010)
5	4		Hartford Newark basalts and volcanics	-68	268.5			-65.4	69.2	(63.2/-14.2/ 79)	197	2278, T
5	6.2		Watchung basalts	-63.6	268.7			-65.2	58.6	(63.2/-14.2/ 79)	197	1339, T
5	6		Hettangian Newark red beds	-55.6	274.6	59.8	273.3	-62.2	51.5	(63.2/-14.2/79.1)	198	2312, T
5	7.9		Piedmont dikes	-61.5	234			-81	61.6	(63.2/-14.2/79.2)	199	1809, T
6	10.7		North Mountain basalt	-66.4	252			-71.9	68.2	(63.2/-14.1/79.2)	200	1932, T

7	3.2	I	Hartford basin	-66.6	268.2			-65.5	66.3	(63.2/-14.1/79.3)	201	Kent and Olsen (2008)
6	5	I	Newark Martinsville core	-67.8	275.8			-62.5	69.5	(63.2/-14/ 79.5)	204	Kent & Tauxe (2005)
5	8		Chinle Group, Redonda Formation	-58.5	256.9	61.2	257.1	-70.3	51.8	(63.2/-14/ 79.5)	204	2979, T
6	10.7	#	Chinle Formation	-58.7	250.9	62.8	251.2	-73	57.3	(63.2/-14/ 79.5)	204	2800, T
6	4.2		Chinle Formation, Redonda Member	-57.8	259.3	59.6	259.5	-68.9	47.8	(63.2/-14/ 79.5)	204	152, T
6	6.5	I	Newark Martinsville core	-64.9	276.6			-61.9	63.3	(63.2/-14/ 79.5)	204	Tan et al. (2007)
6	2.5	I	Newark Weston core	-58.1	271.8			-62.3	48.4	(63.2/-13.9/79.7)	207	Tan et al. (2007)
6	5	I	Newark Westonville	-66.9	267.2			-65.8	67.6	(63.2/-13.9/79.7)	207	Kent & Tauxe (2005)
6	4.7		Passaic Formation, baked sediments	-65.5	255.1			-70.7	65.7	(63.2/-13.9/79.9)	211	2791, T
7	5.6		Passaic Formation, C component	-55.6	274.6	59.9	273.3	-62.1	52.8	(63.2/-13.9/79.9)	211	2312, T
6	3.4	#	Chinle Formation	-56.6	255.9	58.6	256.2	-70.3	45	(63.2/-13.9/79.9)	211	2380, T
6	4	I	Newark Somerset core	-61.7	274.7			-61.9	57	(63.2/-13.9/79.9)	211	Kent & Tauxe (2005)
5	3		Newark Basin both polarities	-57.6	269.6	63.3	266.9	-65.7	59	(63.2/-13.9/79.9)	211	1339, T
4	<u>5.2</u>		Taylor Mountain batholith	-61.4	282.2			-58.4	58.5	(63.2/-13.9/79.9)	212	Symons et al (2009)
6	3.1	I	Newark Rutgers core	-60.1	277.1			-60.3	54.5	(63.2/-13.9/79.9)	214	Kent & Tauxe (2005)
4	7		Manicouagan Stucture, Quebec	-60.1	271.8			-62.9	52.7	(63.2/-13.9/79.9)	215	434, T
3	10		Manicouagan Stucture, Quebec	-59	267.6			-64.6	49	(63.2/-13.9/79.9)	215	443, T
3	14		Popo Agie Formation, Chugwater	-56.1	276	62.4	280.5	-59.5	59.9	(63.2/-13.9/79.9)	215	1134, T

7	7.8		Ankareh Formation	-50.5	267.6	53.4	268.7	-62.1	37.9	(63.2/-13.9/79.9)	215	Weil et al. (2010)
6	5.6		Chinle Formation, Bull Canyon Member	-57.4	267.7	59.3	268.4	-64.3	50	(63.2/-13.9/79.9)	216	2380, T
6	3.2	I	Newark Titusville core	-59.9	279.4			-59.2	54.9	(63.2/-13.9/79.9)	217	Kent & Tauxe (2005)
6	5.1	#	Chinle, Sangre de Cristo	-52.9	282	53.5	282.5	-54.9	45.6	(63.2/-13.9/79.9)	218	2979, T
6	7.7		Dockum Group, Trujillo and Tecovas Formations	-56.4	276.8	-58	277.6	-59.4	50.7	(63.2/-13.9/79.9)	218	2944, T
7	5	#	Shinarump Member, Chinle Formation	-59.6	277.5	63.5	280.6	-59.7	61.9	(63.2/-13.9/79.9)	220	2489, T
6	5		Newark Basin, Lower redbeds	-53.4	281.7	55.9	281.5	-56.6	48.9	(63.2/-13.9/79.9)	220	2331, T
6	2	I	Dan River-Danville Basin	-58.5	279.5			-58.6	52.4	(63.2/-13.9/79.9)	221	Kent & Tauxe (2005)
5	5	I	Newark Nursery core	-60.5	281.6			-58.4	56.7	(63.2/-13.9/79.9)	221	Kent & Tauxe (2005)
4	3.9		Abbott Pluton	-48.3	272.3			-57.6	31.5	(63.2/-13.9/79.9)	221	1831, T
6	5		Upper Red Peak Formation	-49.1	285.1	52.7	287.8	-51.7	47.3	(63.2/-13.9/79.9)	225	1134, T
6	4	I	Newark Princeton core	-54.1	285.2			-53.8	47.9	(63.2/-13.9/79.9)	227	Kent & Tauxe (2005)
6	3.2		Agamenticus Pluton	-48.4	278.5			-54.2	35.8	(63.2/-13.9/79.9)	228	1831, T
5	2.5	#	Upper Moenkopi drillcore	-54.1	288.3	58.6	293.1	-52.3	58	(63.2/-13.9/79.9)	230	160, T
6	4		Chugwater Formation	-45.2	295.4	49.1	299	-44	49.4	(63.2/-13.9/79.9)	230	1266, T
5	3.1	#	Upper Moenkopi Formation	-52.5	290.7	56.6	295	-50.4	56.1	(63.2/-13.9/79.9)	230	159, T
6	4.5	#	Moenkopi Formation (upper)	-56.5	283.2	59.8	286.6	-55.8	57.3	(63.2/-13.9/79.9)	230	2808, T
6	3.3		Chugwater Formation	-46.1	293.6	49.8	296.9	-45.5	48.9	(63.2/-13.9/79.9)	230	1271, T

7	3.4	#	Moenkopi Formation	-55.5	287.9	58.2	290.7	-53.2	56.5	(63.2/-13.9/79.9)	234	2489, T
7	5	#	Moenkopi Formation (Gray Mountain)	-54.6	284.5	57.8	287.8	-54.4	54.5	(63.2/-13.9/79.9)	234	1221, T
6	4.9	#	Moenkopi Formation, Anton Chico Member	-44.7	301.4	44.9	301.7	-39.8	46.9	(63.2/-13.9/79.9)	234	2979, T
5	4.9	#	Moenkopi Formation	-55.6	285.8	60.5	290.9	-54.2	59.9	(63.2/-13.9/79.9)	234	2489, T
4	5.3	#	Moenkopi Formation	-41.1	305.6	40.8	305.2	-35	45.7	(63.2/-13.9/79.9)	234	2632, T
5	7		Lower Red Peak Formation	-46.1	301	50.6	306.1	-41.5	55.1	(63.2/-13.9/79.9)	235	1134, T
6	7.2		Lower Fundy Group	-44.3	271.6	45.5	271.1	-56.6	26.5	(63.2/-13.9/79.9)	246	Symons et al. (1989)
6	5		Dewey Lake Formation	-51	306.5	53.8	310.3	-41.8	60.5	(63.2/-13.9/79.9)	250	2303, T
4	8	#	Bernal Formation	-49.9	298.1	51.6	300	-45.1	52.6	(63.2/-13.9/79.9)	255	2489, T
4	15		Ochoan red beds	-54.8	299.3	57.3	302.2	-47.6	60.4	(63.2/-13.9/79.9)	258	688, T
5	5		Guadalupian red beds	-51.5	306.7	54.8	311.6	-41.9	62.2	(63.2/-13.9/79.9)	263	688, T
5	<u>3.8</u>		Intrusions Southern Illinois	-56.3	302.9			-46.6	59.5	(63.2/-13.9/79.9)	270	Domeier 2011a
4	3.8		Downey Bluff sill	-53	308.7			-42	58.9	(63.2/-13.9/79.9)	272	Reynolds et al. (1997)
4	8.6		Hicks Dome breccia	-54.8	292.1			-50.8	52.3	(63.2/-13.9/79.9)	272	Reynolds et al. (1997)
3	10	#	Toroweap Formation	-51.9	303	56.5	311	-43.2	63.6	(63.2/-13.9/79.9)	277	688, T
3	5		Leonardian subset	-51.7	302.1	53.7	304	-44.5	57.1	(63.2/-13.9/79.9)	277	688, T
7	3.6		Artinskian Pictou red beds	-42.1	306.5	-	306.4	-34.9	46.9	(63.2/-13.9/79.9)	280	2281, T

5	16.3		Churchland pluton	-33.5	306.3			-29	40.8	(63.2/-13.9/79.9)	282	1264, T
4	13.1	#	Fountain and Lykins Formations	-44.6	305.3	47.8	308.8	-38.3	54	(63.2/-13.9/79.9)	283	504
5	2.1	#	Abo Formation	-46.8	304	48.3	305.9	-40.1	52.7	(63.2/-13.9/79.9)	285	1311, T
3	10.2		Piedmont Mafic intrusions	-38.9	300.8			-35.9	41	(63.2/-13.9/79.9)	289	1527
5	1.5		Upper Casper Formation	-50.5	303	56.2	310.3	-43.4	63	(63.2/-13.9/79.9)	291	1455, T
4	5	#	Elephant Canyon Formation	-37.5	296.6	35.8	295.2	-36.7	34.4	(63.2/-13.9/79.9)	292	671, T
5	7.1	#	Cutler Formation, Lisbon Valley	-40.1	307.7	42.1	310.1	-33.5	50	(63.2/-13.9/79.9)	292	1341, T
5	2	#	Ingelside Formation	-43.1	307.9	46.5	311.7	-36	54.6	(63.2/-13.9/79.9)	292	1142,T
4	2	#	Cutler Formation	-41.6	300.4	42.6	301.5	-38.3	44.7	(63.2/-13.9/79.9)	292	671,T
4	2.8	#	Minturn and Maroon Formations	-40.1	300.5	40.3	300.8	-37	42.2	(63.2/-13.9/79.9)	298	1685,T
4	12.8	#	Upper Maroon Formation	-55.3	279.8	60.6	285.1	-56.8	58	(63.2/-13.9/79.9)	299	504, T
5	3.9		Dunkard Formation	-44.1	301.5	41.5	300.4	-38	43	(63.2/-13.9/79.9)	300	302, T
5	2.1		Laborcita Formation	-42.1	312.1	-43	313.4	-32.7	52.9	(63.2/-13.9/79.9)	301	1311, T
5	3.4	#	Wescogame Formation	-44.1	303.9	46.3	306.8	-38.2	51.4	(63.2/-13.9/79.9)	301	1311,T
6	3.1	I	Glenshaw Formation	-28.6	299.9			-28.6	32.4	(63.2/-13.9/79.9)	303	Kodama (2009)
5	1.8		Lower Casper Formation	-45.7	308.6	50.5	314.6	-37.6	59.8	(63.2/-13.9/79.9)	303	1455,T
5	6		Riversdale Group	-36	302	-	301.5	-29	34.8	(63.2/-13.9/79.9)	310	1110, T

7	7.7	I	Shepody Formation, Nova Scotia	-27.2	298.3		30.2		-28.4	30.2	(63.2/-13.9/79.9)	317	Bilardello & Kodama (2010a)
6	8.3	I	Mauch Chunk	-22.6	294.4				-26.9	23.8	(63.2/-13.9/79.9)	320	Bilardello & Kodama (2010a)
7	15.3	I	Maringouin Formation, Nova Scotia	-27.9	297.2				-29.5	29.8	(63.2/-13.9/79.9)	322	Bilardello & Kodama (2010a)
4	6.5		New Brunswick volcanics I and redbeds	-19.5	315.8				-12.6	39.2	(63.2/-13.9/79.9)	330	Seguin et al. (1985)
6	8		Jeffreys Village Member	-27	311	17.8	309.8					333	1534,T
7	9	I**	Deer Lake Formation	-18.6	304.2							335	Billardello & Kodama (2010b)
3	16		Catskill Formation South	-27.4	303	16.6	299.6					370	1693
4	9		Andreas red beds	-13	285	1.5	284.8					415	1388, T96
7	5.3		Wabash Reef	-17	305							420	1277, T96
6	5.8		Rose Hill Formation	-19.1	308.3							425	1218
4	7.3		Ringgold Gap sediments	-24	326.6	16.9	321.7					438	1689
4	3.9		Tablehead Group limestone Mean	-13.4	329.3							470	2257, 1931, T96 (recalculated)
4	4.3		St. George Group limestone	-17.5	332.4							480	1928, T96
6	11.9		Oneota Dolomite	-10.3	346.5							490	1283, T96
5	8.5		Moore Hollow sediments	0.6	343	3.1	338.9					495	2383, T96
5	9.7		Morgan Creek	-10.6	338	-8.4	334.6					495	2376, T96
5	9		Point Peak	-5.2	345.8	-4.7	345					495	801, T96
5	7.1		Taum Sauk limestone	3.4	355.1							500	1284, T96

6	4.3		Royer Dolomite	-12.6	337.3						500	2289 ,T96
6	10		Florida Mountains	5.4	348.7						503	2375,T96
5	3.3		Tapeats Sandstone	-0.6	341.1	-1.7	342.6				508	1044, T96
5	6.2		Mont Rigaud and Chatham-Grenville	11.9	4.5						532	McCausland et al. 2007
			GREENLAND (102)									
6	7.4		Talerua Member lavas	-76.3	21.5			-75	44.1	(72.8/ 9.1/ 11.2)	39	Schmidt et al. (2005)
5	6.3		Nuussuaq lavas, Kanisut Member	-74.6	339.4			-77.6	11.6	(71.1/ 30.9/ 16)	54	Rissager et al. (2003b)
4	6		Kangerdlugsuaq dykes, Irminger	-63	0			-64.6	25.6	(71.4/ 30.2/ 16.4)	54.5	1604
4	15		Scoresby Sund lavas	-63	354			-65	19.8	(71.7/ 29.6/ 16.8)	55	450
3	4.2		Skaergaard Intrusion	-61	345			-63.8	9.9	(72/ 29/ 17.2)	55.5	1432
4	8.9		Kangerdlugssuaq Lavas	-63.4	5.1			-64.4	32	(72/ 29/ 17.2)	55.5	1844
6	3		Jacobsen Fjord dykes	-68	358			-69.6	28	(72/ 30.1/ 17.5)	59	1604
5	9		Jacobsen Fjord basalts	-56	3			-57.4	27.7	(71.9/ 30.3/ 17.5)	59.5	1604
6	3.2		Disko Island lavas combined	-67.5	15			-67.6	44.9	(71.8/ 30.8/ 17.5)	60.5	103
5	6		Svartenhuk lavas, Vaigat Formation	-76.2	37.9			-73.9	73.2	(71.8/ 30.8/ 17.5)	60.5	Rissager et al. (2003b)
5	6.9		Nuusuaq and Disko lavas, Vaigat Formation	-64.8	321.5			-69.4	-14.9	(71.8/ 30.8/ 17.5)	60.5	Riisager et al. (2003a)
6	5	I	Gipsdalen and Fleming Fjord Formations	-52.7	278.7			-67.9	36.6	(60.5/ 1.4/ 69.3)	209	Kent & Tauxe (2005)
3	11		Kap Stanton Formation	1	302						400	2301
			STABLE "EUROPE" (301, 302, 401 from 250 Myr)									

4	3.6	West Eifel volcanics	-80.6	267.5			-80.6	-92.3	(18.3/-47/ .1)	0.5	1513,T
4	4.4	East Eifel volcanics	-86.4	296.1			-86.4	-63.1	(18.3/-47/ .1)	0.5	1505,T
3	12.9	Volcanics NW Germany	-84.3	357.7			-83.9	5.8	(18/-26.7/ 1)	8	56,T
5	1.8	Prado section, Teruel, Spain	-78.9	328.3			-78.9	-25.8	(17.9/-26.4/ 1.1)	9.5	Abels et al. (2009)
5	3.5	Cascante, Spain	-77.4	314.2			-77.7	-40.4	(18.5/-26.3/ 1.2)	10	Abdul Aziz et al. (2004)
5	6.9	Velay Oriental volcanics	-84.1	351.2			-83.6	3	(19.7/-25.7/ 1.4)	11.5	3324,T
5	1.5	Orera, Spain	-72.4	352			-71.9	-3.5	(19.6/-25.5/ 1.5)	12	Abdul Aziz et al. (2000)
4	4.4	Volcanics Germany	-77.8	310.8			-78.9	-36.2	(20/-19.7/ 2.9)	24	3282,T
3	3.4	Hochefel volcanics	-80.8	2			-78	26.5	(26.8/-19.5/ 5.5)	34	1506,T
5	6.8	Lower Paleogene mudstone	-63.7	358.6	76.7	357.2	-72.2	30.6	(30.5/-15.7/10.3)	52	3534
5	1.5	Lundy island dikes, Wales	-83	335			-78.2	41.3	(34.5/-15.7/12.4)	59	755
5	3.5	Vaternish dyke swarm, Scotland	-76	340			-72.9	22.7	(34.5/-15.7/12.4)	59	85,T
5	1.2	Arran dikes, Scotland	-81.7	359.8			-74.9	46.3	(34.6/-15.7/12.5)	59.4	1041,T
5	2.8	Arran intrusives and extrusives	-80.2	339.6			-76	33.2	(34.6/-15.7/12.5)	59.5	6090
4	1.5	Sleat dikes, Scotland	-82.5	338			-77.6	40.6	(34.7/-15.7/12.5)	59.8	1174,T
5	5.7	Sky lavas, Scotland	-77.7	325.4			-76.2	18	(34.7/-15.7/12.5)	59.8	Rousse, Ganerød, Torsvik (paper in prep.)
4	2.7	Ardnamurchan complex, Scotland	-77	355			-71.5	34.4	(34.8/-15.7/12.6)	60	1377,T
6	4.5	Faeroe flood volcanics	-71.4	334.7			-69.8	11.3	(34.8/-15.7/12.6)	60.1	3494,T
6	2.4	Rhum and Canna igneous, Scotland	-81	359			-74.3	44.8	(34.9/-15.7/12.7)	60.7	1169,T
6	4.7	Mull lavas, Scotland	-73.3	346.2			-69.5	23.1	(35/-15.7/ 12.8)	60.9	Ganerød et al. (2008)
5	4.7	Antrim Lava, Ireland	-78.9	347			-74	34.1	(35/-15.7/ 12.8)	61	Ganerød et al. (2010)
5	2.7	Muck and Eigg igneous	-74	351			-69.4	27.5	(35.1/-15.7/12.8)	61.2	1204,T

6	3.4		Aix-en-Provence, France	-79.1	344.5	84.9	-	222.9	-82.4	95.9	(35.8/-16/ 14.6)	68	Cojan & Moreau (2006)
7	8		Aix-en-Provence sediments, France	-73	336				-69.8	21.1	(35.4/-15.7/15.2)	74	2394,T
5	3		Dagestan limestones, Caucasus	-74	341				-67.7	35.4	(37.5/-14/ 19.5)	86	3037,T
5	3		Dagestan limestones, Caucasus	-74	328				-70.4	28.7	(37.5/-14/ 19.5)	86	3037,T
4	5		Munsterland Turonian, Germany	-68	329				-65.1	22.3	(39.2/-13.6/21.8)	89.5	1507,T
5	4		Munster Basin limestone	-76	1				-62.9	54.7	(39.4/-13.7/24.2)	93	1495,T
6	<u>2.5</u>		Mongolia/Siberia Cretaceous Volcanics	-80.8	338.4				-63.2	70.6	(41.6/-10.1/34.1)	108	van Hinsbergen et al. (2008)
6	2.9		Berriasian limestones	-74	3				-48	82.4	(45.9/-3.4/ 48.4)	140	1397,T
5	6		Jura Blue limestone, Switzerland	-78	328				-56	87.9	(48.4/-1.1/ 52.8)	156.5	1337,T
3	3.9		Oxfordian sediments	-70	327				-54.5	74.3	(48.5/-1/ 53)	157	616,T
5	7		Terres Noires, France	-78	310				-59.5	88.7	(48.6/-.9/ 53.4)	158	3156,T
4	4		Subtartic Nappe sediments, Poland	-72	312				-59.3	77.2	(48.7/-8/ 53.8)	159	1948,T
6	7.3		Limestones, Krakow-Czestochowa Upland	-72	330				-53.9	78.9	(48.7/-8/ 53.8)	160	1948,T
7	6.3		Jurassic sediments	-63	300				-62.2	62.5	(49.8/.3/ 57)	168	1514,T
6	6.8		Scania basalts (179±6 Ma)	-69	283				-65.8	82.6	(49.4/.2/ 60.3)	179	2729,T
6	12		Thouars and Airvault Sections, France	-71	276				-65.6	90.9	(49.2/ 0/ 61.8)	184	1427,T
5	5.1		Paris Basin drillcore	-66	295.2				-60.6	75.2	(49.1/-1/ 62.3)	186	3554
4	3		Liassic sediments	-77	315				-52.1	94.8	(48.7/ 0/ 63.6)	192	1467,T
5	7.5		Kerforne dykes, France	-61	259				-76	88.7	(48.1/.7/ 63.1)	198	2743,T

6	9	Hettangian-Sinemurian limestone	-55	280			-69.1	54	(47.8/ 1.1/ 62.5)	201	3141,T
7	3	Paris Basin sediments	-51	285			-65.8	44.1	(47.8/ 1.1/ 62.5)	201	3029,T
6	4.5	Andesites, Ukraine	-50	286.4			-65.3	41.7	(47.6/ 1.6/ 61.9)	204.2	Yuan <i>et al.</i> (2011)
6	8	Rhaetian sediments, Germany, France	-50	292	-58	272.9	-73.6	65.6	(47.3/ 2.2/ 61.1)	208	3141,T
5	5.1	Merci mudstone, Somerset	-50	308	58.2	298.2	-61.7	60.7	(46.6/ 3.2/ 59.5)	215	3311,T
5	4.6	Sunnhordland dike	-50	305			-56.9	45.8	(46/ 3.9/ 58.2)	221	T, Walderhaug (1993)
6	6	Gipskeuper sediments	-49	311			-52.9	46.9	(46/ 3.9/ 58.2)	226	3141,T
5	2.9	Taimyr Sills, Siberia	-47.1	301.6			-57.8	39.2	(46/ 3.9/ 58.2)	228	Walderhaug <i>et al.</i> (2005)
6	3	Heming limestone, France	-54	321			-49.4	58.3	(46/ 3.9/ 58.2)	234	2411,T
6	12	Musschelkalk carbonates, Poland	-53	303			-59.1	50.4	(46/ 3.9/ 58.2)	234	3253,T
5	15	Bunter and Musschelkalk, Germany	-49	326	56.5	318.6	-51.6	61.2	(46/ 3.9/ 58.2)	239	158,T
6	5	Upper Buntsandstein, France	-43	326	47.8	322.2	-45.8	50.6	(46/ 3.9/ 58.2)	243	1028,T
6	3.8	Volpriehausen Formation, Germany	-49	348.2	-57	344.7	-39.2	71.2	(46/ 3.9/ 58.2)	246	Szurlies (2004)
6	7.8	Taimyr basalts, Siberia	-59.3	325.8			-49	67.4	(46/ 3.9/ 58.2)	248	Walderhaug <i>et al.</i> (2005)
7	3.3	German Trias, Lower Buntstein	-50.6	345.6	58.8	341	-41.8	71.7	(46/ 3.9/ 58.2)	249	T, Szurlies <i>et al.</i> (2003)
3	10	Taimyr Siberian Traps, Siberia	-59	330			-46.9	68.2	(46/ 3.9/ 58.2)	250	2832
6	3.3	Siberian Traps, Siberia	-56.2	326			-47.7	63.2	(46/ 3.9/ 58.2)	251	Gurevitch <i>et al.</i> (2004)
3	13.9	Kotuy River Siberian Traps, Siberia	-52.7	328.4			-44.8	59.6	(46/ 3.9/ 58.2)	251	Pavlov <i>et al.</i> (2007)
5	2.1	Siberian Traps NSP1 pole	-56.4	321.7			-49.9	62	(46/ 3.9/ 58.2)	251	Pavlov <i>et al.</i> (2007)

6	5		Sudetes sediments, Poland	-50	343	59.3	336.5	-44.1	70.7	(46/ 3.9/ 58.2)	251	3161,T
3	5.3		Stolbovaya River Siberian Traps, Siberia	-53.3	330.2	-		-44.2	61.1	(46/ 3.9/ 58.2)	251	Pavlov <i>et al.</i> (2007)
3	5		Big Nirundaiver intrusion and sediments, Siberia	-54.3	323	-		-48.4	59.5	(46/ 3.9/ 58.2)	251	Pavlov <i>et al.</i> (2007)
3	2.7		Moyero River Siberian Traps, Siberia	-58.5	314.5	-		-54.3	63.2	(46/ 3.9/ 58.2)	251	Gallet & Pavlov (1996); Pavlov <i>et al.</i> (2007)
6	9.7		Siberian Traps Mean recalculated, Siberia	-52.8	334.4	-		-41.8	62.3	(46/ 3.9/ 58.2)	251	Kravchinsky <i>et al.</i> (2002), recalculated
5	2.7		Dome de Barrot red beds, France	-46	327	-50	324.7	-45.5	54.7	(46/ 3.9/ 58.2)	255	652,T
6	4		Massif des Maures, France	-51	341	55.4	338.1	-41.4	66.8	(46/ 3.9/ 58.2)	255	1408,T
5	3.5		Late Permian sediments, Urals	-45.6	350.2	54.9	338.2	-41	66.2	(46/ 3.9/ 58.2)	260	Bazhenov <i>et al.</i> (2008)
5	5		Esterel sediments, France	-47	331	50.6	327.7	-44.2	56.7	(46/ 3.9/ 58.2)	261	165,T
6	4		Brive Basin sediments, France	-49	343	52.6	341.7	-38	65.3	(46/ 3.9/ 58.2)	261	3144,T
4	0		Permian red beds, Lodeve, France	-53	331	58.6	326.4	-48.5	66.5	(46/ 3.9/ 58.2)	264	1207,T
5	1.5		Lodeve Basin, France	-49	334	52.5	331.5	-43.1	60.7	(46/ 3.9/ 58.2)	264	1813,T
3	4.6		Upper Lodeve sandstone, France	-47	336	49.3	334.7	-39.6	58.5	(46/ 3.9/ 58.2)	264	168,T
5	4		Saxonian red sandstone, France	-51	324	56.4	318.8	-51.4	61	(46/ 3.9/ 58.2)	264	2361,T
5	6.1		Esterel extrusives, France	-51.5	322	-		-47.7	55.3	(46/ 3.9/ 58.2)	264	165,T

4	4.1		Cracow volcanics B	-50	344			-35.3	63.8	(46/ 3.9/ 58.2)	269	Nawrocki <i>et al.</i> (2008)
5	<u>2.5</u>		Lunner dikes, Norway	-51	343			-36.4	64.3	(46/ 3.9/ 58.2)	271	Dominguez <i>et al.</i> (2011)
5	5.9		Lunner dikes, Norway	-53	344			-37.1	66.7	(46/ 3.9/ 58.2)	271	3188,T (redated)
4	8.6		Bohuslan dikes combined, Sweden	-51	345			-35.4	65.3	(46/ 3.9/ 58.2)	275	1155, T
4	11		Scania melaphyre dikes, Sweden	-54	352			-34.1	71.4	(46/ 3.9/ 58.2)	279	2222,T
4	7		Bohemian quartz porphyry, Germany	-37	341			-28.3	50.6	(46/ 3.9/ 58.2)	280	3145,T
3	14		Mauchline lavas, Scotland	-47	337			-37.1	57.3	(46/ 3.9/ 58.2)	280	3093,T
5	10		Bohemian Massif igneous, Germany	-42	346			-29	57.8	(46/ 3.9/ 58.2)	280	2356,T
5	1		Oslo volcanics, Norway	-47	337			-37.1	57.3	(46/ 3.9/ 58.2)	281	915,T
4	13.4		Ringerike lavas, Norway	-44.6	337.4			-35.4	55.2	(46/ 3.9/ 58.2)	281	1830
4	6.9		Sarna alkaline intrusion, Sweden	-38	346			-26.2	54.6	(46/ 3.9/ 58.2)	281	1735,T
5	6.5		Trachytes, Ukraine	-49.4	359.7			-27.4	71.4	(46/ 3.9/ 58.2)	282.6	Yuan <i>et al.</i> (2011)
4	6.7		Moissey volcanics, France	-41	352			-25.1	60.6	(46/ 3.9/ 58.2)	285	1205,T
5	3.2		Intrasudetic Basin volcanics, Poland	-43	352			-26.5	62.1	(46/ 3.9/ 58.2)	285	3161,T
5	5.1		North Sudetic Basin sediments, Poland	-44	4	48.6	4.1	-24.9	73.2	(46/ 3.9/ 58.2)	285	3161,T
5	2		Krkonose Basin oil shales, Czech Republic	-40	346	42.4	345.2	-29.6	57.7	(46/ 3.9/ 58.2)	285	2444,T
3	7.7		Lower Lodeve sandstone	-44	350	39.8	-9.4	-25	58.8	(46/ 3.9/ 58.2)	285	168,T
5	6.3		Mount Hunneberg Sill, Sweden	-38	346			-26.2	54.6	(46/ 3.9/ 58.2)	285	2211,T

4	8.1		North Sudetic Basin volcanics, Poland	-42	354			-24.8	62.5	(46/ 3.9/ 58.2)	285	3161,T	
5	2		Lodeve Basin, France	-42	349	40.5	-	-9.8	-25.7	59	(46/ 3.9/ 58.2)	285	1813,T
4	17		Lodeve B Component, France	-49	342	52.5	-	340.1	-38.7	64.5	(46/ 3.9/ 58.2)	285	2454,T
4	6.8		Intrasudetic basin sediments, Poland	-37	340	38.5	-	339.4	-30.2	50.9	(46/ 3.9/ 58.2)	285	3161,T
4	7.9		Krakow volcanics, Poland	-43	345				-30.2	58.1	(46/ 3.9/ 58.2)	285	275,T
5	4		Bohemian red beds, Czech Republic	-41	345	-44	343.5	-31.6	58.1	(46/ 3.9/ 58.2)	285	167,T	
3	13.2		Lower Silesia volcanics, Poland	-40	352			-24.3	59.8	(46/ 3.9/ 58.2)	285	465, T (recalculated)	
5	4		Exeter Lavas, UK	-50	330			-42.6	57.1	(46/ 3.9/ 58.2)	286	165,T	
4	5.9		Black Forest volcanics, Germany	-49	356			-28.8	69.1	(46/ 3.9/ 58.2)	286	170, T (recalculated)	
4	10		Exeter Lavas, UK	-48	343			-34.5	61.4	(46/ 3.9/ 58.2)	286	411, T (recalculated)	
3	1		Black Forest rhyolites, Germany	-42	353			-25.3	61.9	(46/ 3.9/ 58.2)	286	2941,T	
4	5.8		Thuringer Forest sediments, Germany	-41.5	340	45.3	-	338.1	-35.5	56.3	(46/ 3.9/ 58.2)	287	1792,T
4	2.4		Stabben Sill, Norway	-32	354			-17.3	55.4	(46/ 3.9/ 58.2)	291	1540,T	
3	15.9		Saar-Nahe volcanics, Germany	-41	349			-26.7	58.8	(46/ 3.9/ 58.2)	291	712,T	
3	13		Nahe volcanics, Germany	-46	347			-31.2	61.8	(46/ 3.9/ 58.2)	291	940,T	
6	13		Sudetic Mountain granitoids, Poland	-42	346			-29	57.8	(46/ 3.9/ 58.2)	293	2446,T	
4	4.8		Great Whin Sill, UK	-44	339			-34.1	55.5	(46/ 3.9/ 58.2)	294	585,T	

5	3.5		Hadrian's Wall-Pennines Sill and Hett Dike (Whin Sill), UK	-32.9	347.1			-21.9	51.4	(46/ 3.9/ 58.2)	294	T, Liss <i>et al.</i> (2004)	
5	6.3		Holy Island Sill and Dyke (Whin Sill), UK	-35.4	346.8			-23.9	53.1	(46/ 3.9/ 58.2)	294	T, Liss <i>et al.</i> (2004)	
4	4		Nideck-Donon volcanics, France	-47	348			-31.3	63.2	(46/ 3.9/ 58.2)	294	1010,T	
3	19		Lower Nideck volcanics, France	-42	348			-27.9	59	(46/ 3.9/ 58.2)	294	174,T	
4	4.8		Cracow volcanics A, Poland	-44	355			-25.7	64.6	(46/ 3.9/ 58.2)	294	Nawrocki <i>et al.</i> (2008)	
5	8.1		Alnwick Sill, High Green and St. Oswalds Chapel Dyke (Whin Sill), UK	-47.1	337.1			-37.1	57.5	(46/ 3.9/ 58.2)	294	T, Liss <i>et al.</i> (2004)	
5	6.5		Scania dolerites, Sweden	-38	348			-25.1	55.8	(46/ 3.9/ 58.2)	294	2222,T	
5	11		Scania dolerite dikes, Sweden	-37	354			-21.1	58.9	(46/ 3.9/ 58.2)	294	2211,T	
4	7.1		Thuringer Forest volcanics, Germany	-37.1	350			-23.3	56.4	(46/ 3.9/ 58.2)	295	1792,T	
4	13.6		Silesia volcanics, Poland	-43	354			-25.5	63.3	(46/ 3.9/ 58.2)	296	465,T	
3	7.1		Arendal diabase dykes, Norway	-42.5	339.6			-32.8	54.5	(46/ 3.9/ 58.2)	297	175,T	
4	2.9		Ny-Hellesund sills, Norway	-39	341			-29.7	52.3	(46/ 3.9/ 58.2)	297	626,T	
5	1.3		Peterhead dyke, Scotland	-41	342			-30.5	54.6	(46/ 3.9/ 58.2)	297	1535,T	
6	3		Donets basin, Ukraine	-43	345	49.9	337.3	-38.6	60.4	(46/ 3.9/ 58.2)	297	Iosifidi <i>et al.</i> (2010)	
5	2.4		Svedlodarsk, Karamыш Formation, Donbas	-48.4	349.8	-	56.1	341.2	-40.3	68.8	(46/ 3.9/ 58.2)	299	Meijers <i>et al.</i> (2010)
5	4		Mount Billinger sill, Sweden	-31	354			-16.6	54.7	(46/ 3.9/ 58.2)	299	2211,T	
5	2.2		Svetlodarsk, Kartamыш Formation, Donbas	-48.2	348.3	55.9	-	339.4	-41	67.9	(46/ 3.9/ 58.2)	299	Meijers <i>et al.</i> (2010)

6	4		Donets basin, Ukraine	-42	359	- 45.7	356.5	-26.3	66.8	(46/ 3.9/ 58.2)	301	Iosifidi <i>et al.</i> (2010)
5	2		Debaltsevo Donbas, Ukraine	-48.2	342.3			-35	61.3	(46/ 3.9/ 58.2)	303	Meijers <i>et al.</i> (2010)
3	3		Wackerfield dyke, England	-49	349			-32.2	65.4	(46/ 3.9/ 58.2)	303	180,T
5	5.2		Queensferry sill, Scotland	-38.3	354			-22	59.8	(46/ 3.9/ 58.2)	305	2447,T
5	9		Westphalian-Stephanian red beds, Czech Republic	-38	343	- 40.3	341.5	-30.3	53.7	(46/ 3.9/ 58.2)	305	167,T
5	2.9		Tashkovska Donbas, Ukraine	-38.4	339.5			-30.1	50.9	(46/ 3.9/ 58.2)	312	Meijers <i>et al.</i> (2010)
6	7		Burntisland-Kinghorn lavas, Scotland	-14	332						332	2447, T96 (redated)
6	8.2		Derbyshire Lavas, England	-14.3	335.9						335	2440,T
6	11		Cheviot Hills igneous, England	4	323						396	190,T96
6	7		Old Red Sandstone lavas and sediments, Scotland	-5	320						410	194,T96
7	3		Strathmore lavas, Scotland	2	318						410	1536,T96
6	7.3		Devonian sediments, Podolia, Ukraine	3.7	325.5						411	2664
5	6		Lorne Plateau lavas, Scotland	2	321						412	193, T96
4	2.5		Glenbervie ignimbrite, Scotland	-8	335						415	2565 ,T96
4	4.3		Lintrathen ignimbrite, Scotland	-1	325						415	2565,T96
4	4.9		Middle Silurian limestone, Dniester basin, Ukraine	-17	350						419	Jelenska <i>et al.</i> (2005)
7	9.1		Ringerike sandstone, Oslo, Norway	-19	344	- 13.6	-16				421	1830, T96
3	5.7		Foyers granite, Scotland	-27	346						421	1530, T96
3	8		Gotland Medby limestone	-23	351						422	1734 ,T96

4	4.6		Yaruga limestone and dolomite, Dniester basin, Ukraine	-15	350					424	Jelenska et al. (2005)
5	7.9		Ratagen Complex, Scotland	-15	347					425	1200,T96
3	6		Gotland Follingbo limestone, Sweden	-21	344					425	1734 ,T96
4	2		Gotland Dacker limestone, Sweden	-19	349					426	1734,T96
5	5.1		Gotland Visby limestone, Sweden	-19	352					427	2363, T96
3	5		Strontian granite, Scotland	-21	344					430	1530,T96
4	5.2		Peterhead granite, Scotland	-21	358					432	1535 ,T96
5	13.4		Swedish Limestone I(N)	3	35					458	2362, T96
6	4.8		Vestergotland (N3), Sweden	5	34					459	2362 ,T96
5	4.9		Llandeilian limestone, St.Petersburg, Russia	12	41.9					463	Pavlov et al 2008 EPSL
6	4.4		Vestergotland (N1-N2 and R13), Sweden	14	49					466	2362,T96
4	6.7		Dapingian-Darriwilian limestone, Estonia	11.3	39.1					467	Plado et al. 2010 GJI 180
6	9.2		Komstad Limestone, Sweden	19	51					471	Torsvik & Rehnström (2003a)
6	6.8		Gullhøgen (R1+R2), Sweden	18.7	54					472	2959, T96
4	7.1		Florian limestone, Estonia	25	50.9					472	Plado et al. 2010 GJI 180
5	9		Swedish Limestones	30	55					475	2541 , T96
6	5.1		Swedish Limestones I(R)	18	46					475	2438, T96
6	4		Narva Ordovician limestone, Russia	18	55					477	Khramov & Iosifidi (2009)

5	3.6		St Petersburg Limestone, Russia	34.7	59.1						478	3179
5	5		Narva Cambrian sandstone, Russia	22	87	34.2	79.8				500	Khramov & Iosifidi (2009)
3	6.8		Andrarum limestone, Sweden	52	111						500.1	3425
4	6.9		Tornetrask Formation/Divald Group, Sweden	58.4	122.5	68.7	102.2				535	Rehnström & Torsvik (2003)
			West GONDWANA									
			AMAZONIA (S AMERICA, 201)									
3	10		El Loa Formation and associated ignimbrites, Chile	-85.4	303.8			-85.5	-37.4	(62.1/-40.5/ 2.8)	8.5	3323,T
3	10		Lipiyoc Formation, Puna, Argentina	-85.7	80.5			-84.6	75.6	(62.1/-40.5/ 2.8)	8.5	3027,T
5	11.4		Remedios, Sao Jose formations, Fernando de Noronha, Brazil	-84.5	316			-84.4	-26.3	(62/-40.6/ 3.1)	9.5	1404,T
5	5.9		Itatiaia and Passa Quatro Complexes, Brazil	-79.5	0			-69.6	46.8	(63.5/-33.4/26.2)	70.5	3261,T
6	2.6		Pocos de Caldas Alkaline Complex, Brazil	-83.2	320.1			-71.8	48.8	(61.6/-34.3/33.8)	84	3261,T
5	4.2		Sao Sebastiao Island Intrusions, Brazil	-79.4	331.9			-67.5	44.3	(61.2/-34.3/34.4)	85	3261,T

3	4.8		Intrusives, Cabo de Santo Agostinho, Brazil	-87.6	315.1			-69.5	65.2	(58.2/-34.6/38.7)	92	1448,T
4	3		Cabo Magmatic Province, Brazil	-87.9	335.9			-63.5	69.8	(54.9/-34.8/44.9)	102	Font et al. (2009)
4	2.8		East Maranhao intrusives, Brazil	-83.6	81			-53.7	84.1	(51.8/-35/ 52.4)	118	1431,T
6	2.6		Florianopolis dyke swarm, Santa Catarina Island, Brazil	-89.1	3.3			-56.3	76.3	(51/-34.3/ 53.6)	123.5	3190,T
6	2		Ponta Grossa dykes, Brazil	-82.4	30.3			-48.1	77.9	(50.1/-32.8/54.8)	130	2958,T
6	2.4		Northeast Parana Magmatic Province Combined, Brazil	-83	71.4			-49.6	85.6	(50/-32.5/ 55.1)	132	3422
4	14.1		Dykes, Rio Grande do Norte, Brazil	-80.6	275			-59.3	63.3	(50/-32.5/ 55.1)	146	1509,T
3	9.3		West Maranhao Basalts, Brazil	-85.3	262.5			-58.5	72.7	(50/-32.5/ 55.1)	175	1431,T
5	3.8		Anari and Tapirapua Formations, Brazil	-65.5	250.3			-70.6	34.3	(50/-32.5/ 55.1)	196.6	3316,T
5	4		French Guyana dikes, Brazil	-81.2	235.1			-63.6	72.7	(50/-32.5/ 55.1)	198	3378
4	4.9		Bolivar dykes, Venezuela	-66.9	245.6			-71.9	40.3	(50/-32.5/ 55.1)	202.5	150,T
4	10		Dolerite dykes, Suriname	-82	320			-52.7	66.4	(50/-32.5/ 55.1)	232	701,T
6	6		Mitu Group red beds, Peru	-71.4	303.6	-60	294.1	-50.4	29.1	(50/-32.5/ 55.1)	248.5	3524,T
6	6.6		Independencia Group	-80.7	7	70.7	325.5	-45.5	52.9	(50/-32.5/ 55.1)	260	Rapalini et al. (2006)
4	4.5		Copacabana Group sediments, Peru	-68.2	321.3	56.1	305.2	-43.4	29.2	(50/-32.5/ 55.1)	280	Rakotosolofo et al. (2006)
4	4.1		Santa Fe Group, Brazil	-65.7	330.9	53.2	324	-33.7	36	(50/-32.5/ 55.1)	300	Brandt et al. (2009)
3	11.2		Itarare Subgroup, Tubarao Group, Brazil	-57	357	48.3	338.2	-24.3	41.3	(50/-32.5/ 55.1)	310	798,T

			PARANA (S AMERICA, 202)								
3	6		Rio de Los Molinos dykes 1, Cordoba, Argentina	-77	18		-66.8	52.3	(63.9/-33.6/24.7)	65.5	102,T
4	3.7		Serra Geral basalts, Brazil	-84.6	115.4		-57	86.1	(51.7/-35/ 52.6)	119	765,T
3	10.4		Vulcanitas Cerro Colorado Formation, Cordoba, Argentina	-81	14		-49.2	71.8	(51.5/-34.9/53)	121	123,T
5	5.9		El Salto-Almafuerte lavas, Cordoba, Argentina	-72	25		-39.1	73.6	(50.9/-34.2/53.7)	124	1087,T
3	11		Rio de Los Molinos dykes 2, Cordoba, Argentina	-79	8		-43	71.3	(47.5/-33.3/56.1)	139.5	102,T
3	18.1		Sierra de las Animas volcanic Complex, Uruguay	5.9	338.1		24.1	12.1	(47.6/-33.3/56.2)	510	3513
			COLORADO (S AMERICA, 290)								
4	8		Piragua basalts and red beds, Argentina	-85	222		-73	71.4	(56.9/-34.7/40.9)	95.5	1131,T
5	8.7		Marifil Formation, North Patagonia, Argentina	-83	138		-53.3	90.1	(47.5/-33.3/57.3)	183	3535,T
6	4.5		Mendoza-Neuquen sediments and volcanics	-74	67		-38.1	89.4	(47.5/-33.3/57.3)	183	Iglesia-Lhanos et al. (2006)
5	<u>6.8</u>		Lepa-Osta Arena Formation	-75.5	129.4		-51	102	(47.5/-33.3/57.3)	187	3314
6	4.5		Mendoza sediments and volcanics	-51	223		-84.7	-21.3	(47.5/-33.3/57.3)	195	Iglesia- Llanos et al. (2006)
4	7.6		Los Colorados Mendoza	-81.8	298.3		-52.4	65.2	(47.5/-33.3/57.3)	216	Vizan et al. (2004)
4	7		Amana Formation, Paganzo Group, Argentina	-83	317	-	298.5	-49.7	45.5 (47.5/-33.3/57.3)	240	1132,T

6	<u>6.4</u>	Puesto Viejo Formation Volcanics, Mendoza	-76	313.4			-48.1	57.7	(47.5/-33.3/57.3)	240	Domeier et al. (2011c)
6	<u>4.9</u>	Puesto Viejo Formation Sediments, Mendoza	-89.2	346.1	75.1	293.5	-52.6	54.2	(47.5/-33.3/57.3)	240	Domeier et al. (2011c)
6	3.3	Sierra Chica, La Pampa	-80.1	348.6			-44.9	68.6	(47.5/-33.3/57.3)	263	Domeier et al. (2011b)
6	<u>4.1</u>	Upper Choiyoi Group, Mendoza	-75.7	326			-45.3	59.5	(47.5/-33.3/57.3)	264	Domeier et al. (2011c)
4	5.2	Tambillos, Uspallate Basin, Argentina	-80.6	308.3			-50.7	63.7	(47.5/-33.3/57.3)	267	2475
4	2.8	La Colina Formation, Paganzo	-80.6	268.8	66.7	285.5	-53.7	39.6	(47.5/-33.3/57.3)	283	Geuna & Escosteguy (2004)
3	2.5	Middle Paganzo II, Los Colorados Lower Beds, Argentina	-59.5	357.5	55.2	332.3	-29.2	43.2	(47.5/-33.3/57.3)	283	620,T
3	3.1	La Colina Formation, Los Colorados 1, Argentina	-74	313	60.9	301.3	-45.1	35.2	(47.5/-33.3/57.3)	283	166,T
4	4.9	Rio del Penon Formation sediments, Argentina	-76.8	293.7	62.4	292.2	-49.6	34.4	(47.5/-33.3/57.3)	290	Geuna & Escosteguy (2004)
4	7	Punta del Agua Formation volcanics, Argentina	-73.1	272.4			-58.4	50.8	(47.5/-33.3/57.3)	290	Geuna & Escosteguy (2004)
3	5	La Colina basalt, Argentina	-66	348			-33.4	57.8	(47.5/-33.3/57.3)	300	178,T
4	5.7	La Tabla Formation, Chile	-51	347			-20.8	48.8	(47.5/-33.3/57.3)	310	1420,T
6	5	La Colina Formation, Argentina	-49	343	45.4	323.6	-25.1	31.5	(47.5/-33.3/57.3)	310	1144,T
6	9.6	Pular and Cas formations, Chile	-57	350			-25.2	53.6	(47.5/-33.3/57.3)	310	1420,T
		PATAGONIA (S AMERICA,									

			291)									
5	<u>5.7</u>		Eocene volcanics Patagonia	-81	337.4		-74.4	33.2	(57.2/-31.2/19.4)	47	Somoza (2007)	
6	4.3		Patagonian Plateau basalts, Chile, Argentina	-78.7	358.4		-68.8	45.5	(63.4/-33.4/26.5)	71.5	2374,T	
5	2		San Bernardo, Patagonia	-86.8	35.2		-66.7	71.5	(58.2/-34.6/38.7)	92	Somoza & Zaffarana (2008)	
4	<u>3.8</u>		Cerro Barcino sediments, Argentina	-87	159	77.5	283.2	-60.9	51.4	(52/-35/ 52.1)	116	Geuna et al. (2000)
5	5.5		Posadas and Sierra Colorado ignimbrites, Argentina	-81	172		-57.9	90.4	(47.5/-33.3/ 58)	156.5	3535	
4	4.9		Chon Aike Formation, combined result, Argentina	-85	197		-55.8	82	(47.5/-33.3/59.2)	167	133,T	
			SOUTHERN AFRICA (701)									
5	<u>5.2</u>		Cretaceous Kimberlites 1, South Africa, Lesotho	-64.1	46.1					90.5	2293,T	
6	<u>9.7</u>		Cretaceous Kimberlites 2, South Africa	-47.6	89.9					129	2293,T	
5	3.1		Kaoko lavas, Namibia	-48.3	86.6					132	126,T	
4	13.3		Batoka basalts, northern Zimbabwe	-64	80.6					180	T, Jones et al. (2001)	
3	15.8		Hoachanas lavas, Namibia	-61.9	71.9					183	126,T	
5	3.2		Stormberg lavas (Lesotho basalts), South Africa	-71.6	93.5					183	3090,T	
4	11		Stormberg lavas, Sani Pass and Maseru, Lesotho	-70.5	88.7					183	984,T	

3	7	Karoo lavas, Central Africa, Zimbabwe, Mozambique	-57	84						183	635,T
5	9.5	Karoo dolerites combined, South Africa, Zimbabwe	-65.4	75.1						183	317,T
5	8.7	Marangudzi Ring Complex, Zimbabwe	-70.7	106.7						186	470,T
3	4.6	Red sandstone Formation, Zambia	-68	50.5	54.7	39.5				221.5	323,T
3	6	Cassanje Series, Angola	-54	80	-49	62.6				248.5	1960,T
5	7.6	Karoo Basin	-50.9	86.3	-48	63.8				251	Kock & Kirschvink (2004)
6	5.6	K1 Dwyka Varves, Zimbabwe, Zambia, Tanzania	-26.5	26.5	21.6	27.7				281.5	435,T
6	12	Dwyka Group combined	-25	67	25.2	53.6				315	3489,T
4	7	Bokkeveld Group, Cape Province, South Africa	10	15	-3.3	16				398.5	1416,TV
5	18	Pakhuis, Cedarberg Formations, Cape Province, South Africa	25	343	17	-11				446.5	1416,TV
6	9	Graafwater Formation, Cape Province, South Africa	28	14	13.9	13.8				482.5	1416,TV
		MESETA (707)									
4	14	Intrusives, Beni Mellal, Morocco	-46	78						120	1859,T
6	9	Beni Mellal volcanics, Morocco	-44	71			-42.6	73.6 (33.6/ 26/ 2.3)		173.5	148,TV
4	11	Beni Mellal basalts, Morocco	-45	68			-43.7	70.7 (33.6/ 26/ 2.3)		173.5	1859,T

5	6		Argana Flows, Morocco	-69.2	55.5			-68.2	61	(33.6/ 26/ 2.3)	201	Ruiz-Martinez, Torsvik, van Hinsbergen, Gaina (paper in prep.)
3	7		Moroccan Intrusives, Morocco	-71	36			-70.5	42.7	(33.6/ 26/ 2.3)	201	148,T
5	<u>19</u>		Central Atlantic Magmatic Province, Morocco	-73	61.3			-71.8	67.4	(33.6/ 26/ 2.3)	201	T, Knight et al. (2004)
3	4.6		Taztot Trachyandesite, Morocco	-38.7	56.8			-37.7	59.4	(33.6/ 26/ 2.3)	273	723,T
5	4.7		Chougrane red beds, Morocco	-32.2	64.1	33.4	66	-32.1	68.3	(33.6/ 26/ 2.3)	273	723,T
3	7.8		Djebel Tarhat red beds, Morocco	-24	63.8	23.3	62.3	-22.1	64.3	(33.6/ 26/ 2.3)	273	1080,T
3	20.9		Volcanics, Mechra ben Abou and Chougrane, Morocco	-36	58			-34.9	60.5	(33.6/ 26/ 2.3)	280.5	1859,T
			SOMALIA (709)									
3	4.1		Afar Stratoid Series, Ethiopia	-87.5	359.3			-87.5	-2.3	(52.4/ 6.3/-1)	1	3336,T
3	5.7		Stratoid Basalts, Ethiopian Afar, Ethiopia	-87.2	37.1			-87.3	34.3	(50.2/ 6.5/-2)	2	3559,T
3	4.1		Gamarri section lavas, Afar Depression, Ethiopia	-79.7	350.2			-79.6	-11	(50.3/ 6.4/-3)	2.5	3234,T
5	3.8		Ngorora Formation, Kenya	-85.7	75.8	84.4	65.5	-85.1	59.6	(50.4/ 6.4/-1.3)	11.5	3111,T
4	8.8		East African volcanics, Kenya and Tanzania	-86.5	6.6			-86.4	-7.5	(50.4/ 6.4/-1.3)	12	774,T
3	10		Volcanics, Kenya	-80.1	214.2			-79.7	-142.7	(50.3/ 6.4/-1.3)	13.5	1517,T
5	3.1		Turkana Lavas, Kenya	-84.6	343.3			-84.2	-25.5	(50.4/ 6.4/-1.3)	17	774,T
4	8.4		Southern Plateau volcanics, Ethiopia	-75.1	350.3			-74.8	-14.2	(50.3/ 6.4/-1.5)	34	2764,T

4	3	Lupata series volcanics, Mozambique	-61.8	79.5			-62.7	77.8	(50.3/ 6.4/-1.5)	111	992,T
3	9.3	Mlanje Massif syenite, Malawi	-60	82			-60.9	80.4	(50.3/ 6.4/-1.5)	124.5	401,T
3	5	K3 beds, Galula coalfield, Tanzania	-46	40	33.3	36.9	-33.7	35.2	(50.3/ 6.4/-1.5)	257	324,T
5	1.9	Ntonya Ring Structure, Malawi	27.5	344.8			27.8	-15.9	(50.3/ 6.4/-1.5)	522	404,TV
4	5	Sinyai dolerite, Kenya	-28.4	319.1			-27.7	-42.4	(50.3/ 6.4/-1.5)	547	3106,TV
		NORTHWEST AFRICA (714)									
4	6.7	Famara Volcanics, Canary Islands	-87.5	358.2						7.5	2938,T
3	5.2	Basalt Series II, Canary Islands	-77.8	326.2						8	1493,T
4	4.1	Miocene volcanics, Canary Islands	-81.9	294.4						13	25,T
3	2.3	Massif de Cavallo, Algeria	-86.8	202.9						13	555,T
5	8	Basalt Series I, Canary Islands	-72	71.2						81	1493,T
6	6.3	Upper Jurassic sediments, Tunisia	-65.2	20.3			-65.3	25.8	(33.6/ 26/ 2.3)	152.5	1167,T
3	19.2	Intrusive rocks, Nigeria	-62.5	61.6			-61.3	65.8	(33.6/ 26/ 2.3)	160	1081,T
5	7.4	Diabase dykes and sills, Liberia	-68.5	62.4			-67.3	67.4	(33.6/ 26/ 2.3)	185.5	140,T
4	4.1	Hank volcanics, North Mauritania	-69.4	52			-68.5	57.7	(33.6/ 26/ 2.3)	187	3259,T
4	6.1	Hodh volcanics, South Mauritania	-71.4	60.2			-70.2	66	(33.6/ 26/ 2.3)	187	3260,T

4	6.2		Freetown Complex, Sierra Leone	-82.9	32.7			-82.4	48.7	(33.6/ 26/ 2.3)	193	3287,T
5	<u>4.1</u>		Ighrem and Foum Zguid dykes, Morocco	-73	64.7			-71.7	70.6	(33.6/ 26/ 2.3)	200	Palencia-Ortas et al. (2011)
6	2.6		Zarzaitine Formation, Algeria	-70.9	55.1	76.2	78.9	-74.6	84.4	(33.6/ 26/ 2.3)	206.5	2932,T
5	6		Serie d'Abadla, Upper Unit, Morocco	-29	60	26.8	56.5	-25.7	58.6	(33.6/ 26/ 2.3)	273	1459,T
5	3.6		Abadla Formation, Lower Unit, Algeria	-29.1	57.8	26.3	54.2	-25.4	56.3	(33.6/ 26/ 2.3)	275	3275,T
5	2.8		Upper El Adeb Larache Formation, Algeria	-38.5	57.5	33.7	52.4	-32.8	54.8	(33.6/ 26/ 2.3)	286.5	2540,T
4	4.1		Lower Tiguentourine Formation, Algeria	-33.8	61.4	-29	55.5	-28	57.7	(33.6/ 26/ 2.3)	290	2728,T
5	3.5		Lower El Adeb Larache Formation, Algeria	-28.7	55.8	20.9	48.3	-20.1	50.3	(33.6/ 26/ 2.3)	307	2540,T
6	4.6		Illizi Basin sediments, Algeria	-28.3	58.9	21.1	51.5	-20.2	53.4	(33.6/ 26/ 2.3)	309	3484,T
5	2.6		Reggane Basin, Harsi Bachir Formation, Algeria	-32.8	55.7	27.8	49.9	-27	52.1	(33.6/ 26/ 2.3)	310	Derder et al. (2009)
4	4.5		Oubarakat and El-Adeb Larache Formations, Algeria	-28.2	55.5	20.3	47.8	-19.6	49.8	(33.6/ 26/ 2.3)	317	3481,T
7	5.3		Reggane Basin, Algeria	-26.6	44.7	17.5	36.2	-17.1	38.1	(33.6/ 26/ 2.3)	320	3402,T
5	5.9		Tin Serranine Basin intrusions	-18.8	31.2			-18.6	33.2	(33.6/ 26/ 2.3)	348	Derder et al. (2006).
5	3.7		Griotte limestones, Algeria	-21	19.9			-21.2	21.9	(33.6/ 26/ 2.3)	365	2725,TV
6	3.7		Ben-Zireg limestones, Algeria	-19.2	19.8			-19.4	21.8	(33.6/ 26/ 2.3)	365	2521, TV
5	6.6		Air intrusives, Niger	-43.4	8.6			-43.9	11.7	(33.6/ 26/ 2.3)	409	1364,TV

NORTHEAST AFRICA (715)											
5	2.5	Main Ethiopian Rift basalts	-87.6	346.9						1.5	Kidane et al. (2006)
5	3.1	Hadar Basin, Ethiopia	-84.9	127.9						3	Dupont-Nivet et al. (2008a)
5	7.4	South Holhol-Djibouti	-86.1	336.5						4	Audin et al. (2004)
5	11.2	Volcanics, Jebel Soda, Libya	-69	4						11.5	60,T
5	8.3	Volcanics, Jebel Soda, Libya	-78.4	16.1						11.5	50,T
5	2.6	Blue Clay Formation, Malta	-73	0.5	-	83.2	341.7			13.5	Abels et al. (2005)
4	12.7	Ethiopian Flood basalts, Abbay and Kessen gorges, Ethiopia	-83	13.3						26.5	3496,T
6	6	Qatrani Formation, Egypt	-79.6	332.2	-	79.5	258.6			29	3280,T
5	5.4	Ethiopian Traps, Ethiopia	-77.9	32.8						30	3209,T
5	6.4	Iron ores combined, Baharia Oasis, Egypt	-83.5	318.6						37	1500,T
6	4	Fayum Province, Egypt	-71	340	-	76.5	308.4			37.5	Lotfy & van der Voo (2007)
6	4.2	Mokattam limestone, Egypt	-78.1	342.8						42.5	3280,T
6	6	Fayum Province, Egypt	-68	338	-	73	314.8			44.5	Lotfy & van der Voo (2007)
3	5.8	Basalts, Wadi Abu Tereifiya, Egypt	-69.4	9.4						44.5	1141,T
5	8.5	Wadi Natash volcanics, Egypt	-69.3	78.1		-69.4	78.3 (39.9/-61.4/-2)			93	1500,T
3	18.1	Wadi Natash volcanics, Egypt	-75.7	48.3		-75.9	48.4 (40.1/-61.4/-2)			94.5	3260,T

3	11.5		Upper Triassic Sediments, Southern Tunisia	-54.9	43.3	59.7	-	27	-60.2	26.5	(40.5/-61.4/-7)	221.5	3020,T
4	5.5		Al Azizia Formation, Kaf Bates, Libya	-54.5	45.8				-55	45.6	(40.5/-61.4/-7)	231	3408,T
5	3.8		Al Azizia Formation, Al Azizia, Libya	-59.3	34.1				-59.8	33.7	(40.5/-61.4/-7)	231	3408,T
4	6		Jebel Nehoud Ring Complex, Kordofan, Sudan	-40.8	71.3				-41.2	71.2	(40.4/-61.4/-7)	280	3504,T
3	10.8		Gilif Hills volcanics, Bayuda Desert, Sudan	25.9	11.6				25.4	11.2	(40.4/-61.4/-7)	377	2189,TV
6	9.2		Salala Ring Complex, Sudan	39.6	329.5				39.3	-30.6	(40.4/-61.4/-7)	463	2715,TV
			East GONDWANA										
			INDIA-PAKISTAN (501)										
4	5.4		Mount Pavagarh Traps, Gujarat, India	-39.2	105.6				-73.4	66.6	(18.8/ 22.6/-39.2)	64	94,T
6	<u>5.7</u>		Mahabeleshwar Plateau lavas	-39	100.8				-72	54.5	(19/ 21.9/-40.2)	65	Jay et al. (2009)
4	6.7		Deccan Traps, Mahabaleshwar, India	-40	96				-70.6	42.6	(19.2/ 21.5/-40.7)	65.5	107,T
6	5.9		Deccan Traps, Nagpur to Bombay traverse, India	-38.4	102.4				-72.7	57.9	(19.2/ 21.5/-40.7)	65.5	393,T
3	3.8		Deccan Traps, Western Ghats, India	-34.5	103.6				-69.8	66.8	(19.2/ 21.5/-40.7)	65.5	705,T
5	9.4		Deccan dyke swarms, western India	-37.2	100.5				-70.8	56.2	(19.2/ 21.5/-40.7)	65.5	3094,T

3	3.8		Deccan Traps, Jalna, India	-39	99			-71.5	49.9	(19.2/ 21.5/-40.7)	65.5	686,T
4	10.1		Central Kerala dykes, India	-34.6	94			-67.6	42.9	(20.2/ 19.3/-43.8)	69	2754,T
4	12		Central Kerala gabbro dyke, India	-21.6	119.4			-74.9	73.7	(19.8/ 27.2/-59.2)	88	2754,T
5	7.5		St. Mary Islands, western India	-14.2	117.8			-66.7	79.4	(20.2/ 27.6/-58.5)	91.2	T, Torsvik et al. (2000)
3	4		Rajmahal Traps, West Bengal and Bihar, India	-3	118			-49.8	86.8	(23.4/ 31.3/-53.8)	116	633,T
6	3.5		Rajmahal Traps, Bihar, India	-7	117			-53.3	83.2	(23.4/ 31.3/-53.8)	116	678,T
6	8.3		Rajmahal Traps, West Bengal, India	-9.3	124.8			-57.6	95.2	(23.4/ 31.3/-53.8)	116	2977,T
4	5.5		Rajamahal Traps, North Rajmahal Hills, India	-6.5	120.2			-53.8	88.5	(23.4/ 31.3/-53.8)	116	T, Tarduno et al. (2001)
3	7		Sylhet Traps, Khasi Hills, India	-16	121			-63	84.4	(23.5/ 31.4/-53.7)	116.5	985,T
5	2.4		Rajmahal Traps, Bihar, India	-9.4	116.6			-55.1	81.1	(23.5/ 31.5/-53.6)	117	3095,T
5	4.6		Pachmarhi beds, Central India	-10.1	130.1	-2.4	118.5	-45.1	71.3	(29.8/ 42.1/-60.5)	206.5	593,T
4	4.6		Mangli Beds, Central India	7.3	124.3	12.2	110.9	-28.7	73.5	(29.8/ 42.1/-60.5)	243	593,T
5	6		Panchet clays, Karanpura Coalfields, India	7.5	120.5	13.4	109.1	-26.7	72.5	(29.8/ 42.1/-60.5)	248.5	162,T
6	4.3		Wargal and Chidru Formations, Salt Range, Pakistan	2.2	125.8			-44.6	83.5	(29.8/ 42.1/-60.5)	250.5	2467,T
3	1.8		Kamthi beds, Tadoba, India	4.1	102.8	10.2	94.5	-20.3	58.1	(29.8/ 42.1/-60.5)	250.5	593,T
6	6.5		Kamthi red beds, Wardha Valley, Central India	4	129	9.5	115.1	-33.2	75.8	(29.8/ 42.1/-60.5)	250.5	163,T
3	12.1		Alozai Formation, Baluchistan, Pakistan	18.1	111			-23.8	77	(29.8/ 42.1/-60.5)	289.5	1236,T

			ARABIA (503)								
5	4.1		Volcanics, Syria	-82.4	62.2		-82.9	57.8	(36.5/ 18/-8.)	2.5	Abou-Deeb et al. (1999); Abou-Deeb & Tarling (2005)
5	3.4		Volcanics, Syria	-76	13.5		-75.2	-3.1	(36.5/ 18/-4.5)	19	Abou-Deeb et al. (1999); Abou-Deeb & Tarling (2005)
5	<u>3.6</u>		Afro-Arabian flood volcanic province, Yemen	-74.2	69.1		-77.7	46.7	(35.7/ 20.4/-7.1)	29	Riisager et al. (2005)
3	7.2		Abu Durba sediments, SW Sinai, Egypt	-25.6	64	13.4	58.4	-17.7	51.5 (37.1/ 17.1/-8.9)	306.5	2784,T
			MADAGASCAR (702)								
5	4.4		Antanimena and Mailaka volcanics	-74	43.7					86.5	3481,T
4	7.6		Volcanics, Massif d'Androy Andria	-64	63					87	547,T
4	4.9		Volcanics, Antanimena Andria	-66.1	49.7					87	708,T
4	4.4		Volcanics, Southeast Coast Andria	-65.8	35.6					87	708,T
4	8.9		Volcanics, Mangoky-Anilahy Andria	-73.7	73.1					87	708,T
5	4.3		Dolerites, east Madagascar	-65.5	38					87	3211,T
4	6.9		Volcanics, Mailaka Andria	-70.3	63.1					87	708,T
5	2.4		Volcanics, Southwest Madagascar	-76.8	68.2					87	3210,T
5	10.7		d'Analava complex	-66.7	43.5					91	T, Meert & Tamrat (2006)

3	5.9		Isalo Group	-74	97.1	65.2	70.8	-50.9	59.5	(14.8/137.5/-15.4)	206.5	147,T
3	7.6		Combined Sakamena Rakotosolofo et al. 1999	-76.7	110.8	68.4	73.5	-54.3	60.4	(14.8/137.5/-15.4)	250.5	T, 3329
3	9.5		Combined Sakoa Rakotosolofo et al. 1999	-51.3	72.6	42.5	60.2	-27.8	54.4	(14.8/ 137.5/-15.4)	305	3329, T
5	11		Carion Granite	-6.8	1			3.1	-2.6	(14.8/ 137.5/-15.4)	509	3405,TV
4	14		Stratoid Granites	-6.8	352.7			1.6	-10.7	(14.8/ 137.5/-15.4)	521	Meert et al. (2003)
			AUSTRALIA (801)									
5	1.8		Tarakohe Quarry, New Zealand (Australian Plate)	-78.4	103.1	70.3	148.6	-80.2	155.3	(12/ 48.8/-10.4)	17.5	Turner et al. (2007)
5	3.6		Barrington Volcano, New South Wales	-70.5	125.6			-80.2	19	(14.1/57/-24.4)	53	592
5	1.8		Otway Group sediments	-48.9	148.7	45.1	146.8	-56.4	93.9	(17.2/103.2/-36)	112	1201
5	3.7		Prospect dolerite, Sydney Basin	-53	179.6			-59.2	64.5	(19.5/ 117.8/-56.2)	168	1177
4	6		Garrawilla volcanics and Nombi extrusives, New South Wales	-46.1	175.2			-57.3	78.3	(19.5/ 117.8/-56.2)	180	780
5	2.9		Tasmanian dolerite	-50.7	174.5			-56.6	69.9	(19.5/ 117.8/-56.2)	183	1113
6	5.1		Newcastle range volcanics	-63.8	124.5			-31.5	48.8	(19.5/ 117.8/-56.2)	321	3561

6	6	Brewer Conglomerate, Northern Territory	-47.1	41	- 49.3	54.7	2.2	28.5	(19.5/ 117.8/- 56.2)	367	2726,TV
6	7.8	Reef Complex, Canning Basin	-49.1	38			3.6	17.7	(19.5/ 117.8/- 56.2)	370	1345,TV
6	15.2	Canning Basin Reef Complexes, Western Australia	-62	23.2			-10	10.7	(19.5/ 117.8/- 56.2)	370	2942,TV
5	5	Canning basin, Upper Frasnian	-63	38.6			-10.3	18	(19.5/ 117.8/- 56.2)	376	Tohver et al (in review)
5	3	Tumblagooda Sandstone, Carnarvon Basin	-26.7	33.7	- 30.4	46	21.9	25.2	(19.5/ 117.8/- 56.2)	465	206,TV
4	13	Jinduckin Formation, Northern Territory	-13	25			38.3	1.5	(19.5/ 117.8/- 56.2)	493	202,TV
6	7.4	Chatswood limestone and Ninmaroo Formation, Western Queensland	3.1	54.1			52.7	45	(19.5/ 117.8/- 56.2)	495	3082,TV
3	3.8	Black Hill Norite, South Australia	-37.5	34.4			15.2	14.8	(19.5/ 117.8/- 56.2)	500	2971,TV
6	10	Hugh River shale, Jay Creek limestone	-19.3	39.1			33.4	19	(19.5/ 117.8/- 56.2)	510	Mitchell et al. (2010)
3	10.1	Lake Frome Group Combined, Flinders Ranges, South Australia	-31.4	26.9	- 31.3	26.7	20.6	7.4	(19.5/ 117.8/- 56.2)	510	1769,TV
3	10.4	Giles Creek dolomite, Ross River, Amadeus Basin	-38.3	24.5			13.4	6.9	(19.5/ 117.8/- 56.2)	510	1769,TV
3	12.3	Cambrian sediments, Kangaroo Island, South Australia	-33.8	15.1	- 32.8	13.9	16.4	-3.2	(19.5/ 117.8/- 56.2)	515	1769,TV

7	6.7		Todd River dolomite, Northern Territory	-43.2	339.9			-6.2	-20.8	(19.5/ 117.8/- 56.2)	522	1070,TV
6	14.4		Billy Creek Formation, Aroona Creek and Wirrealpa limestone, Flinders Ranges	-37.4	20.1			13.5	3.2	(19.5/ 117.8/- 56.2)	523	1769,TV
6	7.3		Pertaoorta Group, Areyonga Gorge, Amadeus Basin	-32.7	11.5	28.7	5.7	17.4	-11.7	(19.5/ 117.8/- 56.2)	525	1769,TV
6	4.1		Upper Arumbera sandstone, Northern Territory	-46.6	337.3	37.4	331.7	-6.5	-29.4	(19.5/ 117.8/- 56.2)	534	1070,TV
5	11.4		Hawker Group, Flinders Ranges, South Australia	-21.3	14.9			27.5	-6.6	(19.5/ 117.8/- 56.2)	535	1769,TV
6	16		Brachina Formation, Adelaide Geosyncline, South Australia	-33	328	20.2	326.5	1.6	-45.3	(19.5/ 117.8/- 56.2)	550	1648,TV
			EAST ANTARCTICA (802)									
5	4		McMurdo Sound volcanics	-85.5	143.6			-85.5	141.7	(8.3/-49.4/ .2)	1	Tauxe et al. (2004)
5	<u>6.3</u>		McMurdo volcanics combined	-87.3	137.3			-87.3	130.8	(8.2/-49.4/ .3)	2	1319,T
5	7		James Ross Island volcanics	-86.4	28.5			-85.7	30.7	(8.2/-49.4/ .8)	5	Kristjansson et al. (2005)
5	<u>2.3</u>		Kerguelen islands (Antarctic Plate)	-85.5	9.3			-81.7	25.3	(11.6/-48.2/ 4.2)	27	Camps et al. (2007)
5	4.4		Lavas and dykes, Vestfjella	-51.4	203.4			-55	98.6	(10.5/148.8/- 58.2)	164	1548,T
4	3.4		Ferrar dolerites, Northern Prince Albert Mountains	-47.8	225.5			-69.3	91.3	(10.5/ 148.8/- 58.2)	183	2721,T
3	3.3		Ferrar dolerite sill, Mount Cerberus	-57.8	224.3			-61.5	75.7	(10.5/ 148.8/- 58.2)	183	1838,T
5	2.4		Ferrar dolerites, Wright Valley	-45.3	208			-59.4	108.3	(10.5/ 148.8/- 58.2)	183	1599,T

5	10.2		Ferrar dolerite, McMurdo Sound	-50.5	211.4			-60	97.1	(10.5/ 148.8/- 58.2)	183	1657,T
4	6.9		Storm Peak Lavas, Queen Alexandra Range	-44.1	231.5			-74.9	91.3	(10.5/ 148.8/- 58.2)	193	808,T
5	3.8		Vestfjella lavas and dykes	-41.8	226.5			-73.2	105.8	(10.5/ 148.8/- 58.2)	195	1154,T
5	5.2		Vanda lamprophyre and porphyry, Wright Valley	-2.5	23.8			37.8	-2.5	(10.5/ 148.8/- 58.2)	471.5	1599,TV
5	7.6		South Victoria Land intrusives	-3.5	22.7			36.3	-2.7	(10.5/ 148.8/- 58.2)	475	2966,TV
5	7.2		Teall Nunatak, Victoria Land	-11	21			29.6	2	(10.5/ 148.8/- 58.2)	479	3187,TV
4	10.9		Lamprophyre dykes, Taylor Valley	-9.3	26.7			34.5	5.7	(10.5/ 148.8/- 58.2)	484	1079,TV
4	12		Killer Ridge/Mount Lok	-7	21.4			32.8	-0.9	(10.5/ 148.8/- 58.2)	499	3298,TV
4	8.1		Granitic rocks, Wright Valley	-5.4	18.5			32	-4.6	(10.5/ 148.8/- 58.2)	500	1599, TV
3	4.5		Sør Rondane intrusives, Queen Maud Land	-28.5	9.5			9.5	6.1	(10.5/ 148.8/- 58.2)	515	546,TV

Table 2 Relative fits of Greenland/Europe vs. North America and Europe vs. Greenland

	Greenland vs. North America			Europe vs. Greenland			Europe vs. North America		
Age	Lat	Long	Angle	Lat	Long	Angle	Lat	Long	Angle
220				65.1	126.1	-18.9	78.6	161.9	-31.0
215				62.2	126.8	-17.8	77.4	160.3	-29.7
210				58.9	127.3	-16.8	76.0	159.0	-28.5
205				55.1	127.9	-15.8	74.5	157.7	-27.2
200				50.9	128.4	-14.9	72.8	156.6	-26.0
195				46.2	128.8	-14.1	71.0	155.6	-24.8
190				40.9	129.2	-13.3	69.0	154.8	-23.6
185				40.9	129.2	-13.3	69.0	154.8	-23.6
180				40.9	129.2	-13.3	69.0	154.8	-23.6
175				40.9	129.2	-13.3	69.0	154.8	-23.6
170				40.7	129.1	-13.3	69.0	154.8	-23.5
165				40.5	129.0	-13.2	69.0	154.8	-23.4
160				40.3	128.9	-13.1	69.0	154.8	-23.3
155				40.1	128.8	-13.0	69.0	154.8	-23.2
150				39.9	128.6	-12.9	69.0	154.8	-23.1
145				39.7	128.5	-12.8	69.0	154.8	-23.1
140				39.7	128.5	-12.8	69.0	154.8	-23.1
135				39.7	128.5	-12.8	69.0	154.8	-23.0
130				39.7	128.5	-12.8	69.0	154.8	-23.0
125	67.5	-118.5	-14.0	39.7	128.5	-12.8	69.0	154.8	-23.0
120	67.5	-118.5	-13.8	40.3	128.8	-12.9	69.0	154.7	-23.1
115	67.4	-118.6	-13.6	39.6	128.7	-12.8	68.5	154.2	-22.7
110	67.2	-118.8	-13.3	38.2	128.4	-12.6	67.7	153.3	-22.1
105	67.1	-119.0	-13.0	36.6	128.1	-12.5	66.8	152.3	-21.5
100	66.9	-119.2	-12.7	36.6	127.3	-12.3	66.8	151.6	-21.1
95	66.7	-119.4	-12.4	36.6	126.4	-12.1	66.7	150.8	-20.6
90	66.3	-120.2	-11.9	37.4	125.5	-12.0	66.6	149.9	-20.2
85	65.6	-121.9	-11.2	39.4	124.5	-12.1	66.6	149.2	-19.8
80	63.5	-125.3	-9.8	39.7	124.3	-12.1	64.1	148.0	-18.7
75	60.1	-129.8	-8.2	39.4	125.0	-12.1	60.2	147.5	-17.4
70	54.7	-135.0	-6.7	39.2	125.8	-12.1	55.7	147.1	-16.2
65	47.7	-136.8	-5.2	43.1	125.4	-12.1	54.9	146.6	-15.1
60	36.4	-137.5	-3.9	48.3	124.5	-12.2	55.6	145.8	-14.1
55	28.7	-130.8	-3.1	52.4	123.5	-12.0	58.6	144.8	-13.1
50	53.3	-109.3	-3.0	53.2	126.1	-10.0	64.4	141.0	-11.7
45	62.8	-99.1	-2.3	56.3	128.9	-8.9	65.8	137.5	-10.3
40	62.8	-99.1	-1.3	60.9	129.5	-8.3	66.7	135.6	-9.2
35	63.1	-99.1	-0.4	66.1	130.8	-7.8	67.7	132.9	-8.1

30				68.3	131.7	-7.0	68.3	131.7	-7.0
25				68.6	132.0	-6.1	68.6	132.0	-6.1
20				68.9	132.5	-5.1	68.9	132.5	-5.1
15				67.9	132.7	-3.7	67.9	132.7	-3.7
10				66.4	133.0	-2.3	66.4	133.0	-2.3
5				66.4	133.0	-1.2	66.4	133.0	-1.2

Table 3 APWP for Laurentia (North America and Greenland corrected for pre-drift position and seafloor spreading). APWP's are listed without correction for inclination shallowing in clastic sedimentary rocks (RM), corrected for inclination shallowing using a flattening factor of 0.6 (RM f=0.6). The latter APWP is also calculated using the spherical spline method using a moderate smoothing factor (300) and input poles were weighed by their Q-factor (Spline 300 Q f=0.6). N=number of input poles (*Note*: If N=1 then we report α_{95} for that single study; If N=0 then we have linearly interpolated the pole); A₉₅ = 95-percent confidence circle; Plat/Plon=Pole latitude/longitude; GCD=Great Circle Distance between the RM f=0.6 model and the spherical spline path. RM=Running Mean path with 20 Myr sliding window. Age in million years. The recommended APWP is shown with **bold** numbers.

Age	N	RM			RM f=0.6			Spline 300 Q f=0.6		
		A₉₅	Plat	Plon	A₉₅	Plat	Plon	Plat	Plon	GCD
0	15	2.2	-87.5	295.4	2.3	-88.0	322.8	-88.5	305.0	0.8
10	16	2.2	-87.4	283.7	2.4	-88.4	334.3	-86.7	314.2	1.9
20	11	3.7	-84.0	325.4	3.6	-84.1	338.1	-84.7	332.6	0.8
30	14	3.1	-82.8	341.9	3.1	-82.8	341.9	-82.4	346.5	0.8
40	15	2.8	-81.7	338.1	3.2	-81.8	344.8	-81.3	350.3	0.9
50	20	4.0	-76.0	349.6	4.2	-75.7	358.4	-77.4	2.7	2.0
60	21	3.8	-74.2	355.6	3.9	-73.8	5.0	-73.2	9.1	1.3
70	14	4.6	-75.3	7.5	4.9	-75.0	18.0	-75.7	15.0	1.1
80	7	7.0	-74.4	14.6	7.9	-74.5	21.3	-75.9	22.8	1.4
90	4	6.3	-74.7	18.6	6.3	-74.7	18.6	-75.7	17.2	1.0
100	3	13.1	-75.6	0.7	13.1	-75.6	0.7	-75.0	5.2	1.3
110	7	4.7	-75.4	10.0	4.7	-75.4	10.0	-74.2	5.4	1.8
120	10	3.2	-72.5	16.6	3.2	-72.5	16.6	-72.7	15.1	0.5
130	7	4.0	-71.3	18.2	4.0	-71.3	18.2	-71.3	19.2	0.3
140	3	18.3	-63.3	357.1	7.1	-62.6	18.2	-67.8	15.8	5.3
150	5	12.5	-62.4	341.4	12.9	-64.1	359.8	-66.2	357.6	2.2
160	7	9.2	-62.7	319.3	10.6	-66.8	337.9	-62.7	342.6	4.6
170	6	10.6	-63.3	305.4	12.4	-67.0	316.1	-65.9	317.0	1.1
180	8	6.8	-65.9	275.3	6.0	-67.8	277.2	-67.0	283.4	2.5
190	16	3.5	-65.2	264.6	3.2	-66.5	264.9	-66.6	264.5	0.2
200	19	2.8	-63.5	262.8	2.6	-64.2	262.8	-64.7	260.9	1.0
210	27	2.3	-59.8	269.7	2.1	-61.3	270.0	-61.1	267.0	1.4
220	28	2.5	-56.0	278.2	2.5	-58.0	279.2	-57.3	279.6	0.8
230	19	3.3	-52.1	288.0	3.5	-54.5	290.1	-53.9	291.6	1.1
240	13	4.4	-50.2	292.4	4.7	-53.2	295.3	-52.3	292.8	1.8
250	4	12.5	-50.8	293.2	13.6	-53.1	294.8	-53.0	295.8	0.6
260	5	3.5	-52.8	302.7	3.5	-54.9	305.4	-55.1	303.9	0.9
270	7	4.2	-51.7	303.3	4.9	-53.1	305.3	-53.0	305.1	0.1
280	10	4.8	-47.4	303.4	5.2	-48.5	304.8	-45.9	306.1	2.8
290	13	3.9	-43.1	302.0	4.6	-44.4	303.6	-45.1	305.9	1.8

300	13	4.4	-42.4	302.2	5.5	-43.6	304.0	-42.9	304.1	0.7
310	8	7.0	-36.4	302.1	8.0	-36.4	302.9	-33.4	300.3	3.7
320	5	9.4	-26.9	301.6	8.2	-25.7	301.5	-25.8	298.7	2.6
330	5	8.8	-23.3	304.6	8.7	-21.5	304.4	-20.1	305.1	1.4
340	3	11.0	-21.8	310.3	8.5	-18.7	309.9	-17.7	305.7	4.2
350			-23.2	308.5		-18.1	306.5	-16.3	303.3	3.5
360			-24.6	306.8		-17.4	303.0	-14.9	301.0	3.1
370	1	16.0	-27.4	303.0	16.0	-16.6	299.6	-13.1	298.6	3.6
380			-19.5	297.9		-12.2	296.0	-9.7	293.7	3.3
390			-11.4	293.3		-7.8	292.4	-5.8	289.5	3.5
400	1	11.0	-3.3	289.0	11.0	-3.3	289.0	-4.2	288.3	1.1
410	3	19.2	-11.2	292.9	21.9	-6.3	292.7	-9.2	295.0	3.7
420	3	19.3	-16.6	299.4	26.2	-11.7	299.2	-14.2	301.9	3.6
430	3	17.5	-20.3	313.1	13.0	-17.8	311.7	-18.8	313.2	1.8
440	1	7.3	-24.0	326.6	7.3	-16.9	321.7	-18.8	321.2	1.9
450			-21.1	328.1		-16.5	324.8	-17.8	325.2	1.4
460			-18.3	329.5		-16.0	327.8	-16.8	328.3	0.9
470	2	11.1	-15.4	330.8	11.1	-15.4	330.8	-15.7	330.7	0.3
480	3	14.7	-13.8	336.1	14.7	-13.8	336.1	-13.9	335.8	0.3
490	7	7.9	-7.5	342.7	8.3	-6.8	341.5	-8.5	340.9	1.8
500	8	6.2	-3.8	344.5	6.6	-3.3	343.6	-2.4	344.2	1.1
510	4	12.9	-1.1	345.6	12.7	-1.4	346.0	3.8	349.4	6.2
520			5.5	354.9		5.3	355.1	9.1	356.7	4.1
530	1	6.2	11.9	4.5	6.2	11.9	4.5	9.4	0.3	4.9

Table 4 APWP for Stable Europe/Baltica (Siberia after 251 Ma). The recommended APWP is shown with **bold** numbers. See Table 3 for more information.

Age	N	RM			RM f=0.6			Spline 300 Q f=0.6		
		A95	Plat	Plon	A95	Plat	Plon	Plat	Plon	GCD
0	5	5.5	-82.5	312.2	5.5	-82.5	312.2	-83.7	290.3	2.9
10	7	5.2	-81.8	327.2	5.2	-81.8	327.2	-80.2	331.1	1.7
20	4	7.6	-78.6	331.6	7.6	-78.6	331.6	-78.0	336.9	1.2
30	2	21.1	-80.3	332.6	21.1	-80.3	332.6	-78.9	340.6	2.0
40	1	3.4	-80.8	2.0	3.4	-80.8	2.0	-79.2	346.6	3.1
50	8	4.7	-78.0	346.2	2.5	-79.6	344.2	-78.9	349.8	1.2
60	13	3.0	-77.2	346.1	2.2	-78.1	345.0	-77.7	344.1	0.5
70	7	3.1	-75.7	345.5	3.1	-75.7	345.5	-74.7	338.3	2.1
80	4	3.9	-72.3	333.2	3.9	-72.3	333.2	-73.5	336.7	1.6
90	4	6.2	-73.4	338.1	6.2	-73.4	338.1	-74.2	339.0	0.9
100	2	14.3	-78.6	352.0	14.3	-78.6	352.0	-77.6	343.2	2.1
110	1	2.5	-80.8	338.4	2.5	-80.8	338.4	-79.7	348.2	2.0
120			-78.8	349.8	0.0	-78.8	349.8	-78.7	359.0	1.8
130			-76.5	357.5	0.0	-76.5	357.5	-77.1	2.4	1.3
140	1	2.9	-74.0	3.0	2.9	-74.0	3.0	-75.3	1.7	1.3
150	6	5.0	-74.7	328.5	5.0	-74.7	328.5	-75.7	342.3	3.7
160	6	5.7	-72.5	316.5	5.7	-72.5	316.5	-72.9	318.0	0.6
170	3	14.4	-69.0	302.7	14.4	-69.0	302.7	-67.7	297.8	2.2
180	3	6.6	-68.9	285.5	6.6	-68.9	285.5	-68.5	287.2	0.7
190	4	12.2	-69.9	281.7	12.2	-69.9	281.7	-66.6	281.8	3.3
200	6	10.9	-58.0	284.0	10.4	-59.3	280.3	-57.7	279.7	1.7
210	5	6.7	-51.6	290.5	6.1	-54.7	284.5	-53.9	287.4	1.9
220	4	3.4	-49.1	306.4	6.8	-51.2	304.2	-51.8	300.2	2.6
230	6	5.8	-50.7	311.2	5.1	-51.8	309.7	-51.3	309.7	0.5
240	8	7.1	-52.9	328.5	5.8	-56.3	325.2	-54.5	321.8	2.6
250	16	3.7	-52.8	332.8	2.6	-55.6	329.8	-56.3	331.4	1.1
260	20	2.8	-52.0	332.2	2.2	-54.5	329.8	-54.1	332.2	1.4
270	16	3.3	-48.9	339.1	3.6	-51.1	337.4	-51.5	338.5	0.8
280	29	2.4	-44.7	346.5	2.4	-45.1	346.3	-46.0	345.4	1.1
290	47	1.7	-42.3	347.0	1.9	-43.1	346.5	-42.3	347.3	1.0
300	27	2.3	-41.5	347.9	2.7	-42.6	347.0	-44.2	346.6	1.6
310	6	6.3	-42.5	347.8	5.9	-43.5	347.0	-39.7	343.1	4.8
320			-28.5	339.9	0.0	-29.0	339.6	-29.6	337.9	1.6
330	2	8.3	-14.2	334.0	8.3	-14.2	334.0	-18.2	334.6	4.1
340	2	8.3	-14.2	334.0	8.3	-14.2	334.0	-9.3	333.1	4.9
350			-10.6	331.7	0.0	-10.6	331.7	-2.5	331.5	8.1
360			-6.9	329.5	0.0	-6.9	329.5	2.0	329.7	8.9
370			-3.3	327.3	0.0	-3.3	327.3	4.6	327.3	7.9

380			0.4	325.2	0.0	0.4	325.2	5.9	324.6	5.5
390	1	11.0	4.0	323.0	11.0	4.0	323.0	5.9	321.7	2.3
400	3	8.2	0.3	320.3	8.2	0.3	320.3	4.7	319.2	4.5
410	7	10.0	-3.4	327.6	10.0	-3.4	327.6	-0.2	322.5	6.0
420	16	7.3	-13.0	338.6	7.3	-12.6	338.6	-12.9	340.1	1.5
430	10	3.3	-20.1	348.5	3.5	-19.5	348.5	-19.8	355.5	6.6
440			-8.7	12.2	0.0	-8.4	12.2	-17.0	9.7	8.9
450	2	4.9	4.0	34.5	4.9	4.0	34.5	-6.5	24.5	14.5
460	5	7.2	9.1	39.7	7.2	9.1	39.7	7.0	38.1	2.7
470	10	5.8	20.2	49.9	5.8	20.2	49.9	17.8	48.7	2.6
480	7	5.8	23.4	52.9	5.8	23.4	52.9	27.3	58.8	6.6
490	2	86.3	37.6	96.5	66.7	44.2	93.1	34.7	72.0	18.7
500	2	86.3	37.6	96.5	66.7	44.2	93.1	40.3	85.1	7.0
510	2	86.3	37.6	96.5	66.7	44.2	93.1	46.7	93.3	2.6
520			48.7	106.8	0.0	56.5	96.1	54.5	98.6	2.4
530	1	6.9	58.4	122.5	6.9	68.7	102.2	63.5	102.0	5.1

Table 5 APWP for Laurussia/Laurasia (<251 Ma). The recommended APWP is shown with **bold** numbers. See Table 3 for more information.

Age	N	RM			RM f=0.6			Spline 300 Q f=0.6			GCD
		A95	Plat	Plon	A95	Plat	Plon	Plat	Plon		
0	20	2.1	-86.3	300.7	2.3	-86.6	313.4	-87.9	289.1	1.7	
10	23	2.4	-85.9	305.8	2.4	-86.4	325.5	-83.8	326.2	2.6	
20	15	3.3	-82.8	319.7	3.3	-83.1	327.3	-83.0	327.2	0.2	
30	16	2.9	-83.4	328.5	2.9	-83.4	328.5	-83.0	333.1	0.7	
40	16	2.8	-82.5	322.8	3.1	-83.0	329.0	-82.9	339.0	1.2	
50	28	2.9	-78.1	339.9	2.9	-79.0	346.8	-80.7	343.1	1.9	
60	34	2.5	-77.1	343.0	2.4	-78.0	349.7	-77.9	350.3	0.1	
70	21	3.2	-78.5	346.9	3.5	-79.3	355.1	-79.9	347.0	1.6	
80	11	5.1	-77.6	347.0	5.9	-78.5	350.6	-80.3	355.0	2.0	
90	8	5.0	-77.4	349.6	5.0	-77.4	349.6	-76.7	345.9	1.1	
100	5	6.2	-78.7	348.2	6.2	-78.7	348.2	-78.0	345.6	0.9	
110	8	4.1	-80.0	355.0	4.1	-80.0	355.0	-78.5	359.0	1.8	
120	10	3.2	-78.0	14.0	3.2	-78.0	14.0	-78.3	12.7	0.4	
130	8	3.6	-76.8	16.3	3.6	-76.8	16.3	-74.3	26.5	3.5	
140	4	11.8	-68.7	2.6	6.8	-70.3	22.7	-70.7	22.7	0.4	
150	11	6.5	-70.0	339.1	6.7	-72.5	348.1	-70.2	359.3	4.3	
160	13	6.0	-66.4	322.6	6.2	-70.2	330.4	-69.7	335.7	1.9	
170	9	7.8	-62.9	310.5	8.5	-66.3	315.0	-65.2	313.1	1.3	
180	11	5.5	-61.8	287.2	4.8	-63.3	287.7	-64.6	290.6	1.8	
190	20	3.7	-60.4	281.1	3.4	-61.4	281.0	-62.6	280.6	1.2	
200	25	3.0	-57.0	282.6	2.8	-57.8	281.6	-56.5	279.3	1.8	
210	32	2.2	-53.7	291.9	2.1	-55.5	290.9	-55.2	288.8	1.2	
220	32	2.3	-50.9	302.9	2.4	-53.0	303.0	-52.4	303.8	0.8	
230	25	2.8	-48.7	312.5	2.8	-51.0	313.3	-50.2	314.6	1.1	
240	21	4.0	-49.1	321.3	3.7	-52.3	321.5	-52.4	321.1	0.2	
250	20	3.9	-51.9	329.5	3.2	-54.5	327.5	-55.1	328.7	0.9	
260	25	2.3	-51.6	331.0	1.9	-54.0	329.5	-54.0	331.6	1.2	
270	23	2.8	-49.1	335.5	2.9	-51.0	334.8	-51.6	334.0	0.8	
280	39	2.6	-45.0	341.8	2.6	-45.6	342.0	-45.0	340.9	1.0	
290	60	2.1	-42.2	342.7	2.2	-43.1	342.6	-42.7	343.5	0.7	
300	40	2.9	-41.3	341.3	3.0	-42.4	341.2	-43.2	340.2	1.1	
310	14	6.2	-37.9	336.4	6.4	-38.3	336.5	-33.7	332.8	5.5	
320	6	9.3	-26.6	331.0	8.9	-25.6	331.0	-23.5	327.4	3.9	
330	7	6.3	-19.0	333.1	6.0	-17.7	333.1	-16.7	333.0	0.9	
340	5	6.2	-17.6	336.7	4.8	-15.8	336.7	-14.4	335.1	2.0	
350			-20.6	334.8		-15.6	333.9	-13.0	335.4	2.5	
360			-22.5	332.8		-14.5	331.2	-11.4	332.9	3.5	
370	1	16.0	-24.8	330.8	16.0	-13.8	328.6	-8.4	329.9	5.6	
380			-11.4	325.8		-5.8	324.9	-3.8	326.1	2.3	
390	2	10.9	2.2	321.3	10.9	2.2	321.3	1.4	322.5	1.4	

400	4	5.0	0.4	320.1	5.0	0.4	320.1	3.9	319.2	3.7
410	10	7.7	-4.7	326.2	7.8	-3.2	326.3	0.3	321.8	5.8
420	19	6.5	-13.1	337.1	6.7	-12.0	337.1	-12.4	337.6	0.6
430	13	4.9	-19.6	348.3	4.6	-18.7	348.0	-22.2	354.7	7.2

Table 6a Relative fits for Gondwana (South Africa is fixed). Fits at 160 Ma is used back to 550 Ma.

	NW Africa			NE Africa			Somalia			Madagascar			India			Arabia		
AGE	Lat	Long	Angle	Lat	Long	Angle	Lat	Long	Angle	Lat	Long	Angle	Lat	Long	Angle	Lat	Long	Angle
160	33.6	26.0	2.3	40.5	-61.4	-0.7	9.9	143.0	-0.2	14.7	137.6	-15.6	29.9	42.3	-60.5	37.1	17.2	-8.9
155	33.6	26.0	2.3	40.5	-61.4	-0.7	9.9	143.0	-0.2	10.7	130.3	-13.2	27.1	41.4	-61.6	37.1	17.2	-8.9
150	33.6	26.0	2.3	40.5	-61.4	-0.7	9.9	143.0	-0.2	4.6	120.2	-11.1	24.3	40.6	-62.8	37.1	17.2	-8.9
145	33.6	26.0	2.3	40.5	-61.4	-0.7	9.9	143.0	-0.2	0.8	118.8	-9.1	22.8	39.2	-62.5	37.1	17.2	-8.9
140	33.6	26.0	2.3	40.5	-61.4	-0.7	9.9	143.0	-0.2	0.6	-55.4	7.4	22.1	37.7	-61.4	37.1	17.2	-8.9
135	33.6	26.0	2.3	40.5	-61.4	-0.7	9.9	143.0	-0.2	1.1	-56.9	5.9	21.3	36.4	-61.5	37.1	17.2	-8.9
130	33.7	26.0	2.0	40.5	-61.4	-0.7	9.9	143.0	-0.2	2.6	-63.3	3.9	21.4	36.4	-60.0	37.1	17.2	-8.9
125	33.6	26.0	1.0	40.5	-61.4	-0.7	9.9	143.0	-0.2	2.6	-63.3	1.8	23.5	35.0	-55.2	37.1	17.2	-8.9
120	0.0	0.0	0.0	40.5	-61.4	-0.7	9.9	143.0	-0.2	0.0	0.0	24.0	32.0	-53.1	37.1	17.2	-8.9	
115				40.5	-61.4	-0.6	9.9	143.0	-0.2			23.3	31.1	-54.0	36.9	17.8	-8.8	
110				40.5	-61.4	-0.5	9.9	143.0	-0.2			22.6	30.3	-54.9	36.6	18.4	-8.8	
105				40.5	-61.4	-0.4	9.9	143.0	-0.2			21.9	29.6	-55.9	36.4	19.0	-8.7	
100				40.5	-61.4	-0.3	9.9	143.0	-0.2			21.3	28.8	-56.8	36.1	19.6	-8.7	
95				40.6	-61.4	-0.2	9.9	143.0	-0.2			20.7	28.1	-57.8	35.9	20.2	-8.6	
90				39.5	-61.4	-0.1	9.9	143.0	-0.2			20.0	27.5	-58.8	35.6	20.8	-8.6	
85				27.7	-61.4	0.0	9.9	143.0	-0.2			22.2	22.5	-53.9	35.4	21.3	-8.5	
80				0.0	0.0	0.0	9.9	143.0	-0.2			21.1	21.2	-51.2	35.3	21.6	-8.5	
75							9.9	143.0	-0.2			19.9	22.0	-48.8	35.3	21.6	-8.5	
70							9.9	143.0	-0.2			19.1	23.0	-45.6	35.3	21.6	-8.5	
65							9.9	143.0	-0.2			16.2	27.3	-42.7	35.3	21.6	-8.5	
60							9.9	143.0	-0.2			16.1	31.5	-37.2	35.3	21.6	-8.5	
55							9.9	143.0	-0.2			18.5	33.8	-30.8	35.3	21.6	-8.5	
50							9.9	143.0	-0.2			20.3	39.9	-24.8	35.3	21.6	-8.5	

45							9.9	143.0	-0.2				21.1	43.9	-21.5	35.3	21.6	-8.5
40							9.9	143.0	-0.2				20.7	45.1	-19.5	35.3	21.6	-8.5
35							9.9	143.0	-0.2				20.7	43.9	-17.0	35.3	21.6	-8.5
30							9.9	143.0	-0.2				21.7	41.8	-14.2	35.6	20.8	-7.4
25							9.9	143.0	-0.2				23.6	38.2	-11.2	36.3	18.6	-5.6
20							9.9	143.0	-0.2				26.5	32.2	-8.3	36.5	18.0	-4.7
15							9.9	143.0	-0.2				25.4	31.3	-5.9	36.5	18.0	-4.0
10							14.9	150.2	-0.2				25.0	33.0	-3.9	36.5	18.0	-3.3
5							34.9	-165.7	-0.3				28.1	32.9	-2.0	36.5	18.0	-1.7

Table 6b Relative fits for Gondwana (South Africa is fixed) continued (fits at 190 Ma is used back to 550 Ma).

AGE	Australia			East Antarctica			Amazonia (SAM)			Parana (SAM)			Colorado (SAM)			Patagonia (SAM)		
	Lat	Long	Angle	Lat	Long	Angle	Lat	Long	Angle	Lat	Long	Angle	Lat	Long	Angle	Lat	Long	Angle
190	19.6	117.9	-56.4	10.4	148.7	-58.4	50.0	-32.5	55.1	47.5	-33.3	56.2	47.5	-33.3	57.3	47.5	-33.3	63.0
185	19.6	117.9	-56.4	10.4	148.7	-58.4	50.0	-32.5	55.1	47.5	-33.3	56.2	47.5	-33.3	57.3	47.5	-33.3	62.2
180	19.6	117.9	-56.4	10.4	148.7	-58.4	50.0	-32.5	55.1	47.5	-33.3	56.2	47.5	-33.3	57.3	47.5	-33.3	61.3
175	19.6	117.9	-56.4	10.4	148.7	-58.4	50.0	-32.5	55.1	47.5	-33.3	56.2	47.5	-33.3	57.3	47.5	-33.3	60.5
170	19.6	117.9	-56.4	10.4	148.7	-58.4	50.0	-32.5	55.1	47.5	-33.3	56.2	47.5	-33.3	57.3	47.5	-33.3	59.7
165	19.6	117.9	-56.4	10.4	148.7	-58.4	50.0	-32.5	55.1	47.5	-33.3	56.2	47.5	-33.3	57.3	47.5	-33.3	58.8
160	19.6	117.9	-56.4	10.4	148.7	-58.4	50.0	-32.5	55.1	47.5	-33.3	56.2	47.5	-33.3	57.3	47.5	-33.3	58.0
155	17.6	115.8	-54.5	9.0	148.0	-55.6	50.0	-32.5	55.1	47.5	-33.3	56.2	47.5	-33.3	57.3	47.5	-33.3	58.0
150	15.5	113.6	-52.7	7.4	147.1	-52.8	50.0	-32.5	55.1	47.5	-33.3	56.2	47.5	-33.3	57.3	47.5	-33.3	58.0
145	15.1	113.2	-50.7	7.3	148.0	-50.9	50.0	-32.5	55.1	47.5	-33.3	56.1	47.5	-33.3	57.2	47.5	-33.3	57.7
140	15.7	113.8	-48.5	8.0	150.1	-49.5	50.0	-32.5	55.1	47.5	-33.3	56.1	47.5	-33.3	57.1	47.5	-33.3	57.5
135	16.0	113.2	-46.7	8.6	150.9	-47.8	50.0	-32.5	55.1	47.5	-33.3	56.0	47.5	-33.3	57.1	47.5	-33.3	57.2

130	15.9	111.7	-44.6	9.0	151.5	-45.5	50.1	-32.8	54.8		48.5	-33.4	55.4		48.5	-33.4	56.1		48.5	-33.4	56.1
125	15.8	110.4	-42.4	9.4	152.4	-43.2	50.8	-33.9	54.0		50.8	-33.9	54.0		50.8	-33.9	54.0		50.8	-33.9	54.0
120	16.4	109.5	-40.5	10.2	153.5	-41.5	51.7	-35.0	52.8		51.7	-35.0	52.8		51.7	-35.0	52.8		51.7	-35.0	52.8
115	16.9	105.8	-37.6	9.0	152.2	-37.8	52.1	-35.0	51.9		52.1	-35.0	51.9		52.1	-35.0	51.9		52.1	-35.0	51.9
110	17.4	101.3	-35.0	7.4	150.7	-34.1	52.9	-35.0	50.0		52.9	-35.0	50.0		52.9	-35.0	50.0		52.9	-35.0	50.0
105	17.9	95.9	-32.7	5.5	148.8	-30.5	54.1	-34.9	46.8		54.1	-34.9	46.8		54.1	-34.9	46.8		54.1	-34.9	46.8
100	18.5	89.7	-30.9	3.1	146.5	-27.0	55.5	-34.8	43.7		55.5	-34.8	43.7		55.5	-34.8	43.7		55.5	-34.8	43.7
95	16.0	86.5	-31.2	2.7	-38.3	26.0	57.1	-34.7	40.6		57.1	-34.7	40.6		57.1	-34.7	40.6		57.1	-34.7	40.6
90	17.8	81.3	-29.0	1.3	-37.1	22.5	59.0	-34.5	37.5		59.0	-34.5	37.5		59.0	-34.5	37.5		59.0	-34.5	37.5
85	19.9	75.1	-27.0	0.7	144.6	-19.0	61.2	-34.3	34.4		61.2	-34.3	34.4		61.2	-34.3	34.4		61.2	-34.3	34.4
80	20.6	69.0	-26.6	2.8	142.7	-16.3	62.7	-34.3	31.5		62.7	-34.3	31.5		62.7	-34.3	31.5		62.7	-34.3	31.5
75	20.0	63.8	-26.7	3.8	139.0	-14.1	63.2	-33.9	28.6		63.2	-33.9	28.6		63.2	-33.9	28.6		63.2	-33.9	28.6
70	17.8	60.9	-26.3	0.4	137.2	-12.5	63.5	-33.4	26.1		63.5	-33.4	26.1		63.5	-33.4	26.1		63.5	-33.4	26.1
65	15.6	60.2	-26.1	4.3	-45.3	11.9	63.7	-33.5	24.6		63.7	-33.5	24.6		63.7	-33.5	24.6		63.7	-33.5	24.6
60	14.2	58.9	-25.7	7.7	-46.1	11.2	62.5	-32.8	23.3		62.5	-32.8	23.3		62.5	-32.8	23.3		62.5	-32.8	23.3
55	13.8	57.7	-24.9	9.5	-44.5	10.5	60.7	-31.9	22.0		60.7	-31.9	22.0		60.7	-31.9	22.0		60.7	-31.9	22.0
50	14.8	56.1	-23.6	8.8	-40.7	9.5	58.2	-31.2	20.5		58.2	-31.2	20.5		58.2	-31.2	20.5		58.2	-31.2	20.5
45	14.3	54.3	-23.0	11.0	-41.8	8.4	57.0	-31.4	18.6		57.0	-31.4	18.6		57.0	-31.4	18.6		57.0	-31.4	18.6
40	14.1	52.1	-22.4	13.1	-43.6	7.2	57.1	-32.6	16.6		57.1	-32.6	16.6		57.1	-32.6	16.6		57.1	-32.6	16.6
35	13.7	51.4	-20.7	12.2	-44.2	6.2	56.5	-33.4	14.3		56.5	-33.4	14.3		56.5	-33.4	14.3		56.5	-33.4	14.3
30	13.0	50.9	-17.8	11.4	-44.8	5.1	56.7	-34.5	11.9		56.7	-34.5	11.9		56.7	-34.5	11.9		56.7	-34.5	11.9
25	13.2	49.4	-14.9	10.6	-45.7	4.0	57.7	-36.4	9.6		57.7	-36.4	9.6		57.7	-36.4	9.6		57.7	-36.4	9.6
20	12.7	49.0	-11.8	9.2	-47.1	3.0	58.5	-37.1	7.5		58.5	-37.1	7.5		58.5	-37.1	7.5		58.5	-37.1	7.5
15	11.8	51.2	-9.0	8.0	-47.4	2.4	59.6	-38.1	5.4		59.6	-38.1	5.4		59.6	-38.1	5.4		59.6	-38.1	5.4
10	11.0	54.6	-6.2	5.5	-47.1	1.7	61.8	-40.3	3.3		61.8	-40.3	3.3		61.8	-40.3	3.3		61.8	-40.3	3.3
5	12.8	56.7	-3.2	2.2	142.7	-0.9	62.1	-40.2	1.6		62.1	-40.2	1.6		62.1	-40.2	1.6		62.1	-40.2	1.6

Table 7 Gondwana APWP in South African co-ordinates. The recommended APWP is shown with **bold** numbers. See Table 3 for more information.

Age	N	RM			RM f=0.6			Spline 500 Q f=0.6		GCD
		A95	Plat	Plon	A95	Plat	Plon	Plat	Plon	
0	15	2.5	-87.1	11.9	2.5	-87.1	11.9	-87.9	65.6	2.4
10	26	2.6	-85.6	3.6	2.6	-86.5	3.4	-85.1	5.1	1.5
20	16	3.9	-82.8	7.2	4.3	-85.0	5.1	-84.6	1.9	0.5
30	8	4.9	-80.0	2.2	6.0	-82.6	353.6	-83.1	346.5	1.1
40	8	5.6	-75.8	356.8	6.0	-77.9	351.4	-79.1	338.3	2.8
50	5	7.9	-75.0	2.5	8.4	-76.7	359.5	-77.6	6.4	1.8
60	10	3.0	-71.0	44.9	3.0	-71.0	44.9	-73.9	35.2	4.2
70	11	1.7	-69.7	46.3	1.7	-69.7	46.3	-69.7	47.0	0.2
80	14	2.9	-70.5	53.2	2.9	-70.5	53.2	-70.1	50.6	1.0
90	20	2.6	-70.3	58.0	2.6	-70.3	58.0	-69.7	58.7	0.6
100	9	4.2	-68.9	63.9	4.2	-68.9	63.9	-66.1	73.0	4.5
110	13	3.2	-56.6	83.7	4.0	-56.7	82.2	-59.9	81.7	3.2
120	18	3.1	-54.1	82.4	3.6	-54.1	81.3	-52.8	82.3	1.4
130	10	4.4	-48.9	79.1	4.4	-48.9	79.1	-49.5	81.1	1.5
140	5	8.1	-49.9	77.4	8.1	-49.9	77.4	-54.5	72.8	5.4
150	4	14.5	-62.8	63.6	14.5	-62.8	63.6	-61.0	64.0	1.8
160	6	10.7	-61.1	74.5	10.7	-61.1	74.5	-60.5	73.0	0.9
170	9	6.0	-55.8	76.7	6.0	-55.7	76.7	-52.8	79.3	3.3
180	22	4.5	-60.6	82.5	4.5	-60.6	82.5	-56.8	83.6	3.9
190	26	4.4	-66.3	82.2	4.4	-66.3	82.2	-70.3	82.9	4.1
200	14	5.0	-72.1	65.0	6.4	-70.8	64.1	-71.4	65.6	0.7
210	9	5.7	-66.6	64.0	8.0	-64.6	63.0	-62.9	60.1	2.1
220	3	15.9	-59.0	53.6	18.0	-56.8	44.9	-58.1	50.8	3.6
230	7	7.2	-55.9	56.4	5.9	-54.7	47.1	-55.0	48.9	2.5
240	9	7.7	-51.1	65.8	9.1	-48.3	56.0	-47.8	57.7	1.2
250	13	6.5	-48.1	71.7	7.8	-42.6	59.7	-43.2	63.5	2.8
260	10	8.0	-47.8	69.4	8.4	-42.6	62.0	-42.3	62.5	0.5
270	11	6.0	-38.5	63.5	7.4	-38.1	59.6	-37.5	59.0	1.6
280	17	6.5	-37.5	59.6	7.4	-36.4	53.1	-35.6	48.8	3.6
290	14	7.3	-40.4	57.4	8.3	-38.7	48.8	-36.9	48.1	1.9
300	14	5.9	-33.3	55.7	6.8	-29.5	48.4	-30.8	48.7	1.7
310	14	3.9	-28.7	55.7	4.4	-24.3	48.0	-24.3	47.9	3.1
320	9	4.9	-26.4	53.5	5.4	-24.4	46.2	-23.3	44.2	2.2
330	2	16.4	-29.7	47.2	41.1	-25.3	42.5	-23.0	40.3	3.0
340			-18.6	33.2		-22.0	37.7	-21.7	36.3	1.6
350	1	5.9	-18.6	33.2	5.9	-18.6	33.2	-19.4	31.4	1.5
360	5	11.9	-10.2	16.5	11.8	-10.8	18.3	-15.2	24.4	7.3

370	7	13.0	-5.7	15.6	13.1	-6.2	16.9		-7.8	16.6	1.3
380	4	21.4	-0.3	12.3	21.4	-0.3	12.3		-4.3	13.2	4.3
390			10.0	15.0	0.0	-12.0	13.2		-9.1	13.3	3.2
400	2	180.0	-17.0	13.6	105.8	-23.6	14.2		-19.8	13.4	4.4
410	1	6.6	-43.9	11.7	6.6	-43.9	11.7		-31.0	9.8	13.0
420			-21.3	0.0		-23.9	2.3		-28.9	2.7	5.3
430			1.9	351.6		-3.5	355.5		-14.7	355.3	11.5
440	1	18.0	25.0	343.0	18.0	17.0	349.0		3.1	350.4	14.0
450	1	18.0	25.0	343.0	18.0	17.0	349.0		20.5	347.8	4.1
460	2	95.6	32.7	351.5	151.4	31.8	358.2		30.5	349.5	8.6
470	5	14.3	34.0	356.0	17.0	33.6	358.6		33.2	358.6	0.6
480	5	7.2	33.5	3.4	11.0	30.7	3.6		31.1	6.8	3.3
490	7	4.2	32.8	7.8	13.4	30.8	7.9		34.3	12.9	5.5
500	10	10.7	25.2	6.5	10.7	25.2	6.5		30.7	10.7	6.7
510	9	7.8	16.9	4.4	7.9	17.0	4.2		19.9	4.0	2.9
520	11	9.2	13.6	357.8	9.4	13.8	357.1		9.3	351.0	7.5
530	7	13.5	7.7	347.0	13.8	8.5	344.7		4.2	339.8	6.5
540	4	30.9	-6.9	332.1	32.4	-3.9	326.8		-1.3	328.6	3.2
550	2	44.7	-18.6	320.7	66.3	-14.7	315.2		-7.5	313.4	7.4

TABLE 8 Updated Siberian APWP (see Cocks & Torsvik 2007 for pole entries and text for changes). Spline path (Q-weighted; smoothing, 300). Clastics corrected for potential I-error ($f=0.6$). See Table 3 for more information.

Age	Plat	Plon
250	-56.1	326.2
260	-54.2	336.2
270	-51.1	343.7
280	-47.1	348.6
290	-42.8	351.2
300	-38.2	352.1
310	-34.0	351.4
320	-29.4	349.2
330	-24.7	346.0
340	-20.1	341.6
350	-15.6	336.1
360	-11.1	329.4
370	-6.8	321.5
380	-2.6	313.2
390	1.3	305.3
400	4.7	298.4

410	7.4	294.1
420	10.0	292.3
430	12.1	294.3
440	13.9	300.9
450	16.5	312.9
460	21.8	328.0
470	31.1	332.1
480	38.0	323.3
490	38.9	317.3
500	39.0	314.4
510	42.3	318.4
520	43.6	322.8
530	45.8	327.8
537	49.1	340.7

Table 9 Relative fits for North America vs. NW Africa (fixed). Fits at 210 Ma is used back to 320 Ma.

AGE	Lat	Long	Angle
210	64.3	-14.7	78.0
205	64.3	-14.9	77.7
200	64.3	-15.0	77.4
195	64.3	-15.2	77.1
190	64.8	-15.0	75.8
185	65.4	-14.7	74.5
180	65.9	-14.5	73.1
175	66.5	-14.2	71.8
170	67.1	-13.9	70.6
165	67.1	-14.4	68.6
160	67.1	-15.1	66.6
155	67.1	-15.7	64.6
150	66.4	-17.8	63.2
145	66.1	-18.6	61.8
140	66.4	-18.2	60.1
135	66.4	-18.5	58.7
130	66.0	-19.2	57.7
125	65.9	-19.8	56.0
120	66.0	-20.6	54.2
115	66.7	-21.4	51.0
110	67.5	-22.1	47.5
105	68.4	-22.9	44.0
100	69.4	-23.5	40.5
95	71.6	-24.2	37.1
90	74.3	-22.7	33.9
85	76.2	-21.2	30.5
80	78.2	-18.8	27.5
75	80.4	-13.1	24.6
70	81.6	-6.5	22.4
65	82.6	3.2	20.7
60	81.6	5.1	19.1
55	79.8	4.1	17.6
50	75.9	-3.5	16.2
45	74.3	-4.3	14.6
40	74.5	-1.1	12.6
35	75.4	3.5	10.5
30	77.4	12.5	8.6
25	79.5	28.1	6.8
20	80.6	24.4	5.5
15	80.9	23.2	4.1

10	80.9	22.9	2.6
5	80.9	22.8	1.3

Table 10 Global APWP in South African co-ordinates. The recommended APWP is shown with **bold** numbers. See Table 3 for more information.

Age	N	RM no correction			RM f=0.6			Spline 300 Q f=0.6		
		A95	Plat	Plon	A95	Plat	Plon	Plat	Plon	GCD
0-5	24	1.9	-88.6	325.9	1.9	-88.5	353.9	-89.4	299.4	1.3
10	49	1.8	-86.3	342.1	1.8	-86.6	350.0	-84.2	349.9	2.4
20	31	2.5	-83.2	354.5	2.6	-84.2	355.6	-84.3	354.7	0.1
30	24	2.5	-82.0	3.2	2.6	-82.9	0.3	-83.3	0.1	0.4
40	24	2.7	-79.8	6.9	2.9	-80.5	9.0	-80.9	359.9	1.5
50	33	2.8	-75.3	20.2	2.8	-75.5	25.6	-77.5	23.9	2.0
60	44	2.1	-73.1	30.9	2.1	-72.9	35.3	-72.7	34.5	0.3
70	32	2.4	-72.0	39.7	2.5	-71.7	43.3	-71.5	44.0	0.3
80	25	2.7	-70.6	47.7	2.9	-70.6	49.2	-71.3	51.5	1.1
90	28	2.5	-69.4	55.6	2.5	-69.4	55.6	-68.9	55.3	0.5
100	14	3.3	-67.0	63.2	3.3	-67.0	63.2	-65.0	65.6	2.2
110	21	3.0	-58.2	79.7	3.3	-58.2	78.7	-59.7	77.8	1.5
120	28	2.4	-53.6	82.0	2.6	-53.6	81.3	-52.9	81.7	0.7
130	18	2.8	-49.3	80.9	2.8	-49.3	80.9	-47.3	84.1	3.0
140	9	5.9	-47.1	77.8	6.0	-45.8	82.1	-44.2	83.1	1.8
150	15	6.1	-54.0	72.7	6.4	-53.1	77.2	-50.2	75.3	3.2
160	19	5.0	-56.5	70.4	5.1	-55.4	75.9	-54.2	76.7	1.3
170	18	4.6	-56.6	70.6	4.6	-55.9	73.9	-53.8	72.4	2.3
180	33	3.6	-62.3	77.6	3.4	-62.1	78.5	-59.6	79.8	2.6
190	46	3.0	-67.0	75.5	2.9	-66.8	76.6	-69.6	77.7	2.8
200	39	2.6	-69.2	60.8	2.8	-69.0	62.2	-70.0	60.1	1.2
210	41	2.1	-64.5	53.2	2.2	-64.6	56.3	-65.1	55.7	0.6
220	35	2.2	-58.0	47.6	2.3	-58.4	50.4	-58.1	49.4	0.6
230	33	2.7	-52.9	49.3	2.5	-53.0	50.0	-52.1	49.8	0.9
240	31	3.8	-48.5	56.1	3.6	-48.3	56.1	-48.4	55.4	0.5
250	34	3.7	-45.7	64.0	3.6	-44.7	60.7	-44.6	63.5	2.0
260	35	2.9	-44.4	62.0	2.6	-44.3	61.8	-44.2	60.8	0.7
270	34	2.7	-39.0	60.2	2.9	-39.8	60.1	-39.6	61.0	0.7
280	56	2.6	-34.5	58.5	2.8	-34.4	57.1	-33.4	54.7	2.2
290	74	2.2	-32.6	56.3	2.4	-32.9	55.4	-32.6	56.2	0.8
300	54	2.6	-31.6	54.8	2.8	-31.3	53.5	-32.4	55.0	1.7
310	28	3.7	-30.2	52.2	3.9	-28.0	48.5	-26.4	47.1	2.0
320	15	5.7	-26.8	46.4	4.9	-25.1	41.8	-24.7	36.3	4.9

Table 11 GAPWaP (as running mean path in Table 10) but here listed in six other co-ordinate frames.

			NORTH AMERICA		EUROPE		INDIA		AMAZONIA		AUSTRALIA		EAST ANTARCTICA	
Age	N	A95	Plat	Plon	Plat	Plon	Plat	Plon	Plat	Plon	Plat	Plon	Plat	Plon
0	24	1.9	-88.5	353.9	-88.5	353.9	-88.5	353.9	-88.5	353.9	-88.5	353.9	-88.5	353.9
10	49	1.8	-86.4	342.2	-86.7	330.0	-87.2	60.4	-87.0	319.8	-86.6	119.3	-87.3	319.7
20	31	2.6	-83.7	343.2	-84.4	332.1	-83.7	74.7	-84.8	308.3	-82.2	113.0	-85.6	325.9
30	24	2.6	-82.1	338.7	-83.1	326.5	-79.7	101.7	-83.2	294.7	-77.1	121.4	-84.9	314.9
40	24	2.9	-80.1	337.2	-81.1	324.3	-74.7	106.8	-81.4	296.2	-72.9	119.5	-84.1	320.0
50	33	2.8	-76.4	354.5	-78.9	344.7	-65.1	98.4	-80.3	320.9	-69.6	109.6	-82.9	351.7
60	44	2.1	-73.6	7.5	-78.2	352.6	-48.5	100.8	-80.2	340.0	-65.5	110.3	-83.6	17.8
70	32	2.5	-73.5	12.6	-79.2	355.7	-36.4	100.7	-80.8	348.7	-63.1	112.6	-84.1	35.4
80	25	2.9	-74.7	10.5	-79.7	357.9	-29.0	103.5	-82.2	342.2	-63.1	118.5	-86.7	34.6
90	28	2.5	-76.8	4.8	-80.4	347.2	-20.9	111.4	-84.4	317.2	-62.7	130.2	-87.9	209.0
100	14	3.3	-78.7	358.4	-80.8	332.3	-19.7	113.0	-85.7	284.7	-60.8	136.4	-84.9	202.0
110	21	3.3	-75.2	21.7	-81.2	13.1	-11.1	115.9	-87.3	73.0	-52.7	140.5	-78.9	172.1
120	28	2.6	-73.7	15.5	-79.0	10.1	-8.6	116.4	-84.8	68.7	-50.2	146.4	-75.9	183.6
130	18	2.8	-70.9	5.4	-75.0	3.4	1.0	117.1	-83.6	47.4	-47.7	146.4	-73.7	178.7
140	9	6.0	-67.9	5.7	-72.4	7.9	5.3	117.9	-80.3	47.4	-44.8	147.6	-70.8	176.8

150	15	6.4	-72.6	339.4	-72.9	334.2	-2.9	122.3	-87.4	6.6	-47.0	160.8	-67.5	201.7
160	19	5.1	-72.0	325.9	-70.5	323.4	-9.7	126.6	-88.0	305.7	-47.4	172.7	-62.3	216.3
170	18	4.6	-70.1	314.8	-67.3	316.4	-10.7	125.8	-86.8	297.0	-48.6	173.3	-62.8	218.9
180	33	3.4	-74.1	290.0	-68.3	293.9	-14.8	131.3	-83.4	219.4	-45.7	182.3	-56.4	223.2
190	46	2.9	-71.6	266.4	-64.1	278.8	-19.3	133.1	-78.5	221.4	-45.9	189.2	-53.1	229.4
200	39	2.8	-64.9	259.9	-57.9	279.3	-24.4	130.0	-74.4	238.7	-50.1	195.1	-53.3	239.0
210	41	2.2	-62.0	269.0	-56.1	290.8	-23.0	124.8	-75.4	257.5	-54.3	190.8	-58.0	241.9
220	35	2.3	-57.4	279.2	-52.8	304.1	-21.0	117.7	-74.1	283.2	-60.0	183.6	-64.2	247.7
230	33	2.5	-54.8	287.6	-50.7	312.1	-17.6	113.2	-72.8	301.7	-62.6	173.8	-69.6	249.6
240	31	3.6	-55.5	298.1	-52.2	321.5	-11.6	112.5	-74.2	322.6	-60.0	162.4	-74.1	236.8
250	34	3.6	-55.8	306.6	-53.4	329.2	-6.8	112.5	-74.1	340.2	-57.0	155.2	-76.5	220.3
260	35	2.6	-56.1	308.0	-53.8	330.5	-6.0	112.7	-74.2	343.3	-56.3	154.4	-76.5	216.5
270	34	2.9	-52.2	312.4	-50.4	335.6	-3.4	108.9	-69.9	348.6	-57.0	146.1	-80.8	207.7
280	56	2.8	-46.6	315.5	-45.1	339.8	-0.9	103.5	-64.0	350.4	-58.2	135.2	-86.2	182.5
290	74	2.4	-44.6	315.4	-43.1	340.2	-0.8	101.4	-62.0	349.4	-59.1	131.6	-88.0	161.4
300	54	2.8	-42.3	315.2	-40.8	340.4	-0.7	99.2	-59.8	348.1	-60.0	127.6	-88.5	83.6
310	28	3.9	-37.0	313.4	-35.4	339.6	-1.5	93.8	-54.8	344.1	-62.7	117.6	-84.0	23.4
320	15	5.0	-31.0	309.9	-29.1	337.0	-4.1	87.6	-49.2	338.2	-66.3	104.6	-77.7	9.2

Table 12 True Polar Wander correction for the past 250 Myr in Southern Africa co-ordinates (finite reconstruction rotation for the entire Earth relative to spin axis).

EULER POLE				
Age	Lat	Long	Angle	
0	0	0	0	
100	0	0	0	
110	0	11	-8	
140	0	11	-8	
150	0	11	0	
200	0	11	22.5	
250	0	11	0	

Table 13 GAPWaP corrected for TPW in South African co-ordinates. As running mean path in [Table 10](#) but with added rotations from [Table 12](#) with opposite sense of rotation.

Age	N	A95	Plat	Plon
0-5	24	1.9	-88.5	353.9
10	49	1.8	-86.6	350.0
20	31	2.6	-84.2	355.6
30	24	2.6	-82.9	0.3
40	24	2.9	-80.5	9.0
50	33	2.8	-75.5	25.6
60	44	2.1	-72.9	35.3
70	32	2.5	-71.7	43.3
80	25	2.9	-70.6	49.2
90	28	2.5	-69.4	55.6
100	14	3.3	-67.0	63.2
110	21	3.3	-65.5	72.2
120	28	2.6	-61.0	76.6
130	18	2.8	-56.8	76.9
140	9	6.0	-53.3	78.8
150	15	6.4	-53.1	77.2
160	19	5.1	-51.3	78.4
170	18	4.6	-47.7	78.7
180	33	3.4	-49.3	85.1
190	46	2.9	-49.8	86.4
200	39	2.8	-49.1	81.0
210	41	2.2	-49.9	73.0
220	35	2.3	-48.6	63.2
230	33	2.5	-46.8	57.9

240	31	3.6	-45.1	59.4
250	34	3.6	-44.7	60.7
260	35	2.6	-44.3	61.8
270	34	2.9	-39.8	60.1
280	56	2.8	-34.4	57.1
290	74	2.4	-32.9	55.4
300	54	2.8	-31.3	53.5
310	28	3.9	-28.0	48.5
320	15	4.9	-25.1	41.8